

THESIS

SPATIOTEMPORAL VARIABILITY OF PEROXY ACYL NITRATES (PANS) OVER
MEGACITIES FROM SATELLITE OBSERVATIONS

Submitted by

Madison J. Shogrin

Department of Atmospheric Science

In partial fulfillment of the requirements

For the Degree of Master of Science

Colorado State University

Fort Collins, Colorado

Spring 2023

Master's Committee:

Advisor: Emily V. Fischer

Vivienne H. Payne

Jeffrey Pierce

Steven Miller

Sheryl Magzamen

Copyright by Madison J. Shogrin 2023

All Rights Reserved

ABSTRACT

SPATIOTEMPORAL VARIABILITY OF PEROXY ACYL NITRATES (PANS) OVER MEGACITIES FROM SATELLITE OBSERVATIONS

Peroxy acyl nitrates (PANs) are photochemical pollutants with implications for health and atmospheric oxidation capacity. PANs are formed via the oxidation of non-methane volatile organic compounds (NMVOCs) in the presence of nitrogen oxide radicals ($\text{NO}_x = \text{NO} + \text{NO}_2$). PANs serve as reservoir species and sources for NO_x in outflow regions of megacities, facilitating O_3 production downwind. While urban environments are large sources of PANs, in-situ observations in urban areas are generally limited. Here we use satellite measurements of PANs from the Tropospheric Emission Spectrometer (TES) and the S-NPP Cross-Track Infrared Sounder (CrIS) to evaluate the spatiotemporal variability of PANs over and surrounding 9 megacities: Mexico City, Beijing, Los Angeles, Tokyo, São Paulo, Delhi, Mumbai, Lagos, and Karachi. We use monthly mean values of PANs to determine the seasonal cycle within the urban center of megacities. We find pronounced seasonal cycles of PANs in megacities and seasonal maxima in PANs correspond to seasonal peaks in local photochemical activity. Local fire activity can explain some of the observed interannual variability in PANs over and around megacities. We use S-NPP CrIS data to probe the spatial outflow pattern of PANs produced within urban Mexico City during the month with the largest mixing ratios of PANs (April). Peak outflow in April occurs to the northeast of the city and over the mountains south of the city. Outflow to the northwest appears infrequent. CrIS is used to further explore changes in PANs associated with substantial declines in megacity NO_x in response to the COVID-19 pandemic. We only identify two cities over which PANs changed significantly in response to NO_x perturbations: Beijing and Los Angeles. This work demonstrates that the space-based observations provided by CrIS and TES can increase understanding of the

spatiotemporal variability and sensitivity to precursor emissions of PANs over and around global megacities.

ACKNOWLEDGEMENTS

I would like to thank my graduate advisor Dr. Emily Fischer for her continued insight and mentorship during my time at Colorado State University, as well as Dr. Vivienne Payne, Dr. Jeff Pierce, Dr. Steve Miller, and Dr. Sheryl Magzamen for serving on my committee. Dr. Susan S. Kulawik (Bay Area Environmental Research Institute) and Dr. Kazuyuki Miyazaki (Jet Propulsion Laboratory, California Institute of Technology) have been integral collaborators on the work presented here.

I want to especially recognize and thank Dr. Vivienne Payne at JPL, who has been my mentor since I was an undergraduate student. My intern experience under Dr. Vivienne Payne and Dr. Gregory Osterman have been fundamental in shaping my journey as a scientist. On a more personal note, I would also like to thank my family and friends who have supported me the last two years. Especially Andrey Marsavin for his support and constructive comments throughout this document.

This work is funded under NASA award number 80NSSC20K0947. Part of this work was carried out at the Jet Propulsion Laboratory, California Institute of Technology, under a contract with the National Aeronautics and Space Administration (80NM0018D0004). We acknowledge the use of data and/or imagery from NASA's Fire Information for Resource Management System (FIRMS) (<https://earthdata.nasa.gov/firms>), part of NASA's Earth Observing System Data and Information System (EOSDIS). We thank Isabelle De Smedt and Folkert Boersma for collaborating on the proposal that led to this work and for answering questions regarding the OMI data.

TABLE OF CONTENTS

| | | |
|----------------------------|--|----|
| ABSTRACT | | ii |
| ACKNOWLEDGEMENTS | | iv |
| Chapter 1 | INTRODUCTION | 1 |
| 1.1 | PEROXY ACYL NITRATES (PANs) | 1 |
| 1.1.1 | BRIEF PAN CHEMISTRY: | 3 |
| 1.2 | SATELLITE OBSERVATIONS OF PANs | 3 |
| 1.3 | PANs OVER MEXICO CITY | 5 |
| 1.4 | CHANGES ASSOCIATED WITH COVID-19 | 7 |
| Chapter 2 | METHODS | 8 |
| 2.1 | TES OBSERVATIONS | 8 |
| 2.2 | CrIS OBSERVATIONS | 10 |
| 2.3 | ADDITIONAL DATASETS | 13 |
| 2.3.1 | OZONE MONITORING INSTRUMENT (OMI) OBSERVATIONS | 13 |
| 2.3.2 | SURFACE O ₃ | 14 |
| 2.3.3 | MODIS AND VIIRS FIRE RADIATIVE POWER | 14 |
| 2.3.4 | CHEMICAL REANALYSIS PRODUCT | 15 |
| Chapter 3 | SPATIOTEMPORAL VARIABILITY OF PANs OVER AND AROUND MEXICO CITY | 17 |
| 3.1 | SPATIAL DISTRIBUTION OF PANs OVER MEXICO CITY | 17 |
| 3.2 | SEASONAL CYCLES OF PANs OVER MEXICO CITY | 20 |
| 3.3 | SIMULATIONS OF PAN OVER MEXICO CITY | 23 |
| 3.4 | INTERANNUAL VARIABILITY IN PANs OVER MEXICO CITY | 25 |
| 3.5 | RECENT CHANGES PANs, NO _x , AND HCHO | 27 |
| Chapter 4 | CHANGES TO PANs ASSOCIATED WITH COVID-19 | 30 |
| 4.1 | SEASONAL CYCLES OF PANs, CO, AND HCHO IN MEGACITIES | 30 |
| 4.2 | 2020 NO ₂ ANOMALIES | 33 |
| 4.3 | IMPACT OF COVID-19 NO _x REDUCTIONS ON PANs OVER SELECT MEGACITIES | 35 |
| Chapter 5 | CONCLUSIONS AND FUTURE WORK | 39 |
| 5.1 | CONCLUSIONS | 39 |
| 5.2 | FUTURE WORK | 41 |
| Appendix A | ADDITIONAL FIGURES FOR MEGACITIES | 64 |
| A.1 | MEXICO CITY | 64 |
| A.2 | BEIJING | 65 |
| A.3 | LOS ANGELES | 67 |
| A.4 | TOKYO | 69 |

| | | |
|------------|--|----|
| A.5 | SÃO PAULO | 70 |
| A.6 | DELHI | 71 |
| A.7 | MUMBAI | 72 |
| A.8 | LAGOS | 73 |
| A.9 | KARACHI | 74 |
| Appendix B | SPATIAL EXTENTS FOR MEGACITIES | 75 |

Chapter 1

INTRODUCTION

Megacities are large metropolitan areas with greater than ten million residents (Gurjar and Lelieveld, 2005). As of 2018, roughly 55 percent of the world's population resided in urban areas and this is expected to increase to over 60 percent by 2030 (UN/DESA, 2018). Megacities have become important sources of air pollutants, and these emissions contribute to regional and global trace gas budgets as plumes emitted in megacities are redistributed away from source regions, with implications for regional air quality and photochemistry (Mage et al., 1996; Gurjar and Lelieveld, 2005; Madronich, 2006; Lawrence et al., 2007; Butler and Lawrence, 2009; Molina, 2021).

1.1 PEROXY ACYL NITRATES (PANs)

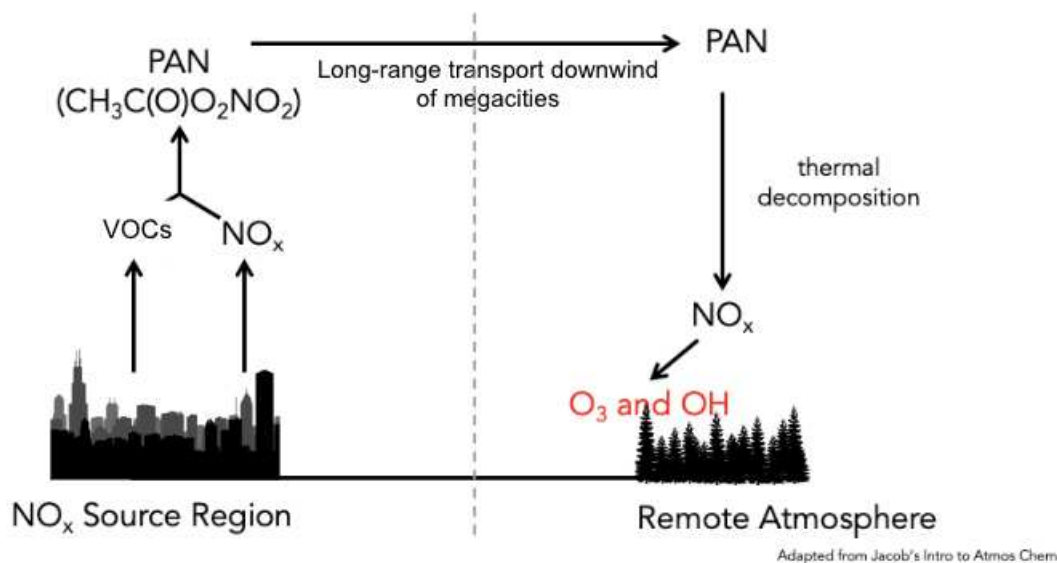


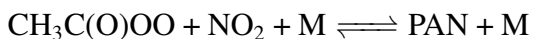
Figure 1.1: PAN is formed in polluted environments and acts as a reservoir for NO_x species in the atmosphere. In this example, we consider the NO_x source region to be a megacity. This figure has been adapted from Daniel Jacob's Introduction to Atmospheric Chemistry.

Peroxy acyl nitrates (PANs) are important photochemically-produced species that are formed alongside ozone (O_3) in polluted environments by the oxidation of non-methane volatile organic compounds (NMVOCs) in the presence of nitrogen oxides ($NO_x = NO + NO_2$) (Figure 1.1) (Singh and Hanst, 1981; Singh et al., 1986; Gaffney et al., 1986; Roberts, 2007; Fischer et al., 2014). PANs cause a suite of health effects. It is a respiratory and eye irritant (Smith, 1965; Altshuller, 1978; Vyskocil et al., 1998), and it acts as a phototoxin (Taylor, 1969; Shepson et al., 1986; Kleindienst et al., 1990). PANs are considered to be a sensitive tracer of photochemistry (e.g., Rappenglück et al., 2003). Formation and decomposition of PANs can impact the production of O_3 (e.g. Steiner et al., 2010), the production of PANs acts as an indicator of regional photochemistry (Sillman and West, 2009), and the concentration of PANs can be used to gauge effectiveness of O_3 -control strategies (Gaffney et al., 1986). PANs respond to precursor emissions non-linearly and have been shown to be differentially more sensitive to changes in NMVOCs than to changes in NO_x (Fischer et al., 2014).

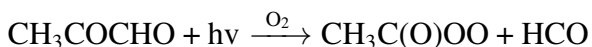
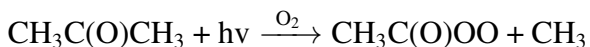
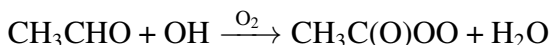
The lifetime of PANs against thermal decomposition is strongly dependent on air mass temperature, where PANs are thermally unstable in the lower troposphere (lifetime on the order of hours at $20^\circ C$), but have a lifetime > 1 month at temperatures characteristic of the mid-troposphere (Honrath et al., 1996). When transported from polluted continental regions to the remote troposphere, PANs serve as the principal reservoir species for NO_x and can contribute to efficient production of downwind O_3 in NO_x limited conditions (Zaveri, 2003; Fischer et al., 2010; Mena-Carrasco et al., 2009; Fischer et al., 2014). The distribution of O_3 in the remote atmosphere would be substantially different without PAN chemistry (e.g., Jiang et al., 2016). There have been major changes in NO_x and VOC emissions in urban areas in the recent decades (Schneider et al., 2015; Borbon et al., 2013; Hilboll et al., 2013; Georgoulas et al., 2019) elevating the need for continued and extended observations of photochemically-relevant species in urban regions. In situ measurements of PANs have been collected for select urban areas for select seasons (Gaffney, 1986; Gaffney, 1999; Lee et al., 2008; Lee et al., 2013; Wang et al., 2014; Zhang et al., 2014; Zhang et al., 2015; Qiu et al., 2019; Qiu et al., 2020a; Qiu et al., 2021), though observations are generally sparse.

1.1.1 BRIEF PAN CHEMISTRY:

PAN is produced by the reversible reaction of the peroxyacetyl (PA) radical ($\text{CH}_3\text{C}(\text{O})\text{OO}$) with NO_2 :



Where M is some third body in the reaction, typically N_2 or O_2 . On a global scale, the dominant sources of the PA radical are the oxidation of acetaldehyde (CH_3CHO) and the photolysis of acetone ($\text{CH}_3\text{C}(\text{O})\text{CH}_3$) and methylglyoxal (CH_3COCHO):



These three precursors are all both directly emitted (primary sources) and produced in the atmosphere via oxidation of primary emissions of NMVOCs (secondary sources). The distribution of primary emission versus secondary formation varies by location and season. Other peroxy acyl nitrates ($\text{RC}(\text{O})\text{OONO}_2$) are similarly formed by the oxidation of NMVOCs, but their yields and abundances are much lower than for PAN, which typically accounts for 75-90% of the total peroxy acyl nitrate species (Fischer et al., 2014; Roberts, 2007; 1998; 2002; Wolfe et al.).

The main sink of PAN is thermal decomposition (reverse of the first reaction). The effective lifetime of PAN depends on whether or not the PA radical reacts with NO_2 to reform PAN, or reacts with another species (typically NO or HO_2), which would lead to a permanent loss of PAN (Fischer et al., 2014). Other loss pathways for PAN include dry deposition and photolysis, however, these account for only 1.2 % and 1.8 % of the global PAN sink, respectively (Fischer et al., 2014).

1.2 SATELLITE OBSERVATIONS OF PANs

PANs have absorption features in the thermal infrared that can be readily measured with spaceborne spectrometers. Limb-sounding satellite observations have provided global-scale information on PAN in the upper troposphere and lower stratosphere with high vertical resolution and sensitivity (Glatthor et al., 2007; Moore and Remedios, 2010; Wiegele et al., 2012; Tereszchuk et al., 2013;

Pope et al., 2016; Ungermann et al., 2016), but the limb-viewing geometry is not well suited to evaluation of urban influences on the free-troposphere. Nadir-viewing observations of PAN have been reported from the Tropospheric Emission Spectrometer (TES) (Payne et al., 2014), the Infrared Atmospheric Sounding Interferometer (IASI) (Franco et al., 2018) and the Cross-Track Infrared Sounder (CrIS) (Payne et al., 2022). These nadir observations have shown large enhancements in PAN associated with fires (Alvarado et al., 2011; Clarisse et al., 2011; Juncosa Calahorrano et al., 2021) and have so far been used to shed new light on the role of fires, PAN precursor emissions, dynamics on the global distribution of PAN, and on long-range transport of O₃ (Zhu et al., 2015; Zhu et al., 2017; Payne et al., 2017; Jiang et al., 2016; Fischer et al., 2018). The TES record includes a set of targeted special observations over megacities between 2013 and 2015 (Cady-Pereira et al., 2017). Further details are provided in Chapter 2. The spatial and temporal coverage routinely provided by the IASI and CrIS meteorological sounders offers rich opportunities for examination of wider spatial context and long-term variation of PAN around megacities.

For various reasons, direct comparisons of the TES, IASI and CrIS products discussed above would be challenging. The three instruments have different noise characteristics, spectral coverage and spectral resolution, which have affected choices made for different algorithms. The TES PAN retrievals utilized the PAN spectral feature centered around 1150 cm⁻¹, while the IASI observations used a larger spectral range that includes multiple PAN spectral features. The CrIS observations have made use of a spectral feature centered around 790 cm⁻¹. This spectral feature appears in the IR spectra of all PANs at essentially the same frequency. Thus, the CrIS measurements reported are for all PANs (i.e., they include propionyl peroxy nitrate (PPN; CH₃CH₂C(O)OONO₂), methacryloyl peroxy nitrate (MPAN; CH₂C(CH₃)C(O)OONO₂), etc.) in addition to peroxy acetyl nitrate (PAN; CH₃C(O)O₂NO₂). The IASI PAN product described by Franco et al. 2018 utilizes a neural network approach to retrieve PAN total column densities, while the TES and CrIS products cited above utilize an optimal estimation approach to retrieve profiles of volume mixing ratio (vmr), which have then been used to calculate free-tropospheric averages. The TES and CrIS PAN products share a common algorithm heritage, though there are some important differences,

as discussed above and in Chapter 2. In this thesis, I use the targeted TES megacity observations to provide a view of PAN over megacities worldwide, and use CrIS observations to focus in on the local metropolitan areas and immediate surroundings. These data sets are further discussed in Chapter 2 below.

1.3 PANs OVER MEXICO CITY

Mexico City is one of the world’s largest megacities with a population greater than 20 million and is well known for its high levels of pollution and reduced visibility (Molina and Molina, 2002). The Mexico City Metropolitan Area (MCMA) is situated at a high altitude in the tropics (2240 m; 19.43° N, 99.13° W), and it is surrounded on three sides by mountains with a wide-open basin to the north and a mountain passage to the southeast (Chalcho passage) (Figure 1.2). The MCMA is particularly prone to poor air quality given the regional topography, frequently weak synoptic forcing, and emissions from a variety of sources (see Molina et al., 2007 and references within).

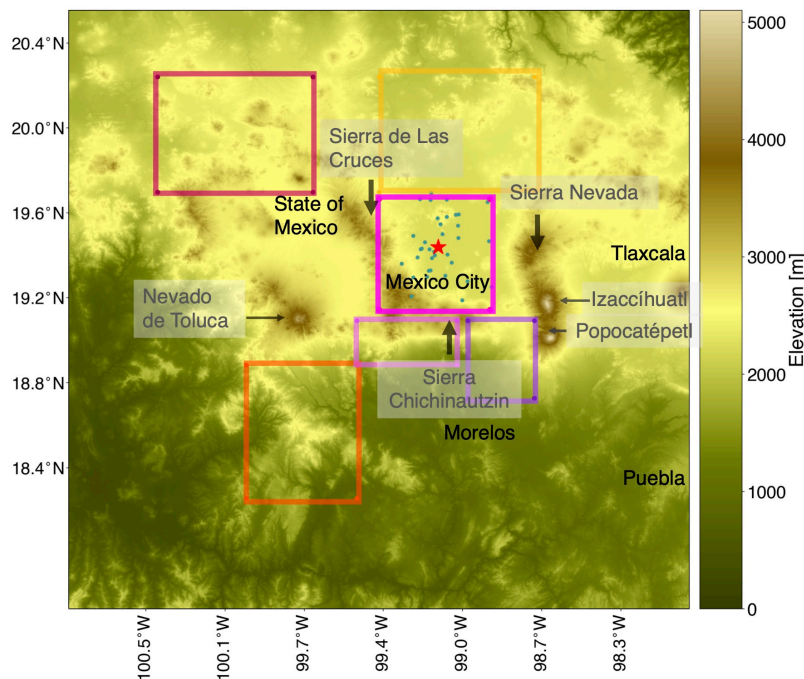


Figure 1.2: Elevation map of the Mexico City region. The red star denotes the center of Mexico City and the pink box represents the area averaged to create monthly means used throughout the analysis. Colored boxes represent regions of potential pollutant outflow further shown in Fig. 4.

During the mid 1980s and 1990s, Mexico City was ranked as the most polluted megacity in the world with all criteria pollutants exceeding air quality standards for human health (UNEP and WHO, 1992). Pollutants of concern include O₃, fine particulate matter (PM), NO_x, and volatile organic compounds (VOCs). In addition to monitoring by the Mexico City atmospheric monitoring system (Sistema de Monitoreo Atmosférico or SIMAT), there have been a number of other efforts to observe and attribute regional photochemistry using in situ measurements. Analysis of field campaign datasets (e.g, MCMA-2003 and MILAGRO-2006; Molina et al., 2007 and Molina et al., 2010) indicate that O₃ formation is often VOC-limited in the urban core and largely NO_x-limited in the surrounding area (Lei et al., 2007; Lei et al., 2008; Tie et al., 2007). The extent of NO_x-versus-VOC limited regions is dependent on meteorological conditions (Lei et al., 2008; Song et al., 2010).

PANs may play an important role in diagnosing aspects of photochemistry within the MCMA and determining the scale over which the MCMA impacts atmospheric composition. The high elevation (Figure 1.2) and tropical latitude of the MCMA makes for intense sunlight to the area year round, supporting efficient production of PANs given an abundance of precursors (Bravo et al., 1989; MARI, 1994; Streit and Guzmán, 1996; Fast and Zhong, 1998; citations from Marley et al., 2007; Lei et al., 2007; Tie et al., 2007; Lei et al., 2008; Emmons et al., 2010). Substantially elevated PANs have been observed within Mexico City (Bravo et al., 1989; MARI, 1994; Streit and Guzmán, 1996; Fast and Zhong, 1998; Gaffney, 1999; Marley et al., 2007; Lei et al., 2007; Tie et al., 2007; Lei et al., 2008; Emmons et al., 2010). For example, maximum daily mixing ratios in 1997 reached 34 ppbv (Gaffney, 1999) and a maximum of 8 ppbv was observed in 2003 (Marley et al., 2007; Molina et al., 2010). O₃ production can continue in outflow regions of the MCMA as PANs act as a reservoir and source of NO_x (Mena-Carrasco et al., 2009). Comparison of field campaign observations from 2003 and 2006 to observations from 2014 and 2019 indicate that there have been major changes in O₃-relevant VOC sources in the MCMA and oxidized nitrogen chemistry since the earlier studies (e.g., Lei et al., 2007; Tie et al., 2007; Lei et al., 2008; Zavala

et al., 2020). This points to a need for continued and expanded observations of photochemically-relevant species in this region, including PANs.

1.4 CHANGES ASSOCIATED WITH COVID-19

To slow the spread of the 2019 novel coronavirus (COVID-19), urban centers across the globe began shutting down as governments began enforcing travel bans and stay-at-home orders (Chinazzi et al., 2020; WHO, 2020). A consequence of this reduced economic activity was a radical decrease in the emissions of many primary air pollutants. Reductions in global and regional particulate matter, NO_x , carbon dioxide (CO_2), and other trace gases associated with the COVID-19 pandemic have been documented (Bauwens et al., 2020; Miyazaki et al., 2020a; Sharma et al., 2020; Shi and Brasseur, 2020; Venter et al., 2020; Liu et al., 2021; Miyazaki et al., 2021; Gough and Anderson, 2022; Odekanle et al., 2022; Zhang et al., 2022a). Less is understood about changes to secondary pollutants as they respond non-linearly to changes in precursor emissions and their production also depends on local photochemical conditions (Kroll et al., 2020). For example, both increases and decreases in surface ozone (O_3) have been documented in urban areas during the COVID-19 pandemic despite decreases in precursor emissions (Le et al., 2020; Sicard et al., 2020; Shi and Brasseur, 2020; Qiu et al., 2020b; Miyazaki et al., 2021).

PANs have been shown to respond non-linearly to precursor emissions (Fischer et al., 2014). We aim to quantify the impacts of substantial reductions in tropospheric NO_2 on the abundance of PANs over 8 megacities: Mexico City, Beijing, Los Angeles, Tokyo, São Paulo, Lagos, and Karachi.

In the following chapters we present the first detailed analysis of the spatiotemporal variability of PANs over and around megacities. Chapter 3 consists of the results from Shogrin et al. 2023 discussing the spatiotemporal variability of PANs in and around the Mexico City metropolitan area. In Chapter 4 we identify seasonal cycles of PANs over 9 different megacities, and we discuss the responses of urban PANs to declines in tropospheric NO_2 associated with COVID. In Chapter 5, we discuss our conclusions from Chapters 3 and 4, as well as discuss some of the potential directions for future work.

Chapter 2

METHODS

2.1 TES OBSERVATIONS

The Tropospheric Emission Spectrometer (TES) is a nadir-viewing Fourier transform spectrometer capable of measuring thermal infrared radiances at high spectral resolution (0.06 cm^{-1}). TES is one of four instruments aboard the NASA Aura satellite, which flies in a sun-synchronous polar orbit in the NASA Afternoon train (A-train) constellation with equatorial overpass times of 01:30 and 13:30 local time (LT). Aura was launched in July 2004, and the TES instrument took science measurements between September 2004 and January 2018.

A full description of the TES PAN retrieval algorithm is provided in Payne et al. [2014] and key details are summarized in Fischer et al. [2018]. We use the publicly available TES v7 Level 2 product ([NASA/LARC/SD/ASDC,2017](#)). On a single footprint basis, TES is sensitive to elevated PAN (detection limit roughly 0.2 ppbv) in the free troposphere with uncertainties between 30-50 %. The peak sensitivity for TES PAN is typically between 400 and 800 hPa (Payne et al., 2014), though TES has some degree of sensitivity to elevated PAN in the boundary layer (Fischer et al., 2018). In general, TES PAN retrievals have about one degree of freedom, meaning that the retrievals do not contain information on the vertical distribution of PAN. The TES PAN retrievals are performed using an optimal estimation approach, with the state vector expressed in log (volume mixing ratio (VMR)). One impact of this is that the degrees of freedom for signal (DOFS) depends on the amount of PAN present. For the analysis presented below, we use a tropospheric average from 825 hPa to 215 hPa for retrievals with $\text{DOF} > 0.6$. This criteria ensures that we only include retrievals dominated by signal in the measurement rather than signal from the prior value. We also only use retrievals where the PANs desert quality flag > 0.95 , as suggested by Payne et al. [2014] to avoid issues with a silicate feature that occurs in the surface emissivity for rocky/sandy surfaces and happens to coincide with the location of the 1150 cm^{-1} PAN spectral feature.

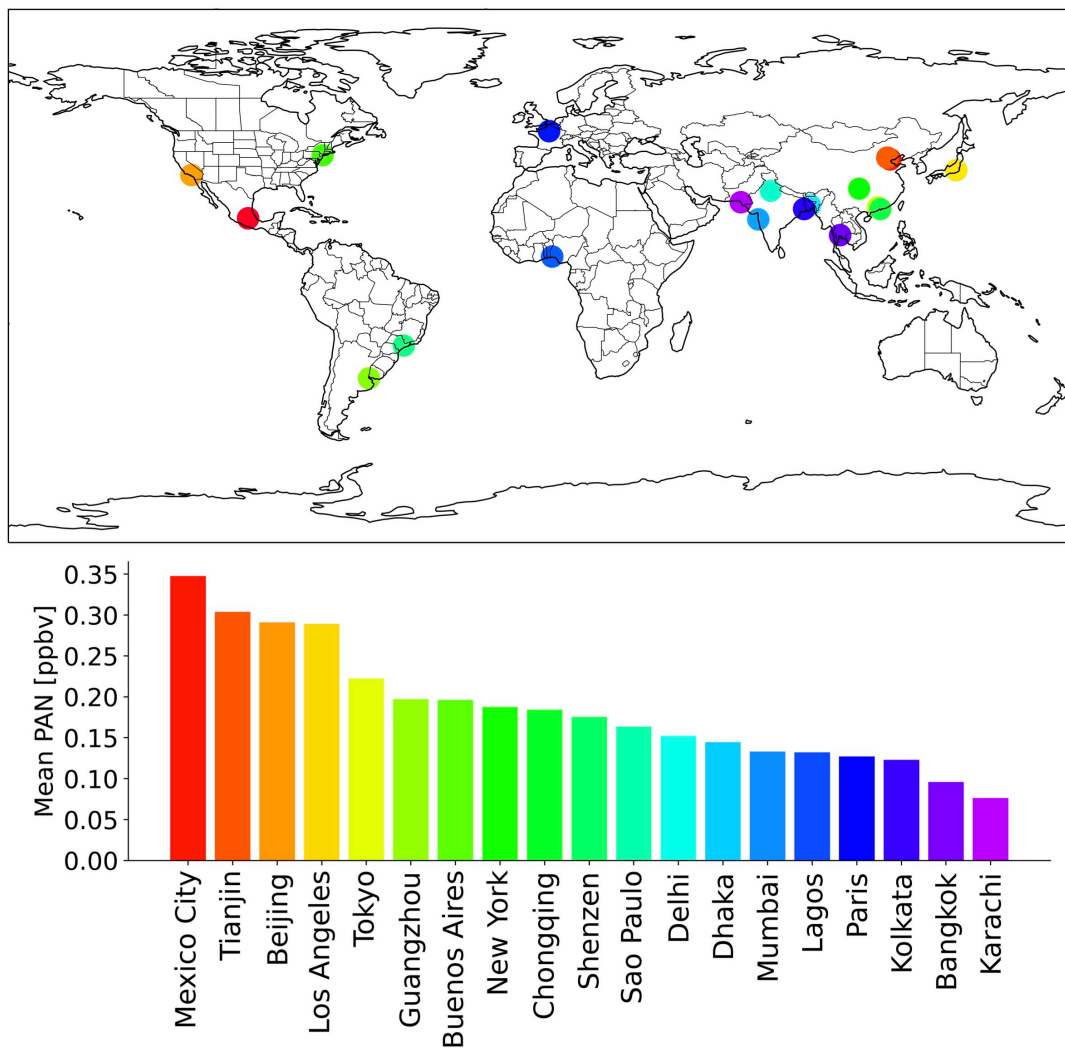


Figure 2.1: Ranked mean PAN in TES megacity transects collected between 2013 and 2015.

Here we use TES “transect” special observations over megacities collected between January 2013 and December 2015. TES has three methods of observation: global survey, step-and-stare mode, and transect mode. Global survey mode is the nominal observation strategy for TES in which the instrument makes periodic observations along the satellite track spaced 200 km apart. In step-and-stare mode the instrument takes nadir measurements every 40 km along the satellite track for a specified latitude range, and in transect mode TES takes 20 consecutive scans spaced roughly 12 km apart. An observation strategy focusing on 19 of the world’s megacities was intro-

duced in January 2013 and operated through December 2015. A special observation strategy was introduced in 2011 in order to preserve the instrument's lifetime and the megacity transect collection used here is a part of these special observations. This sampling strategy reduced the number of sample points globally, but increased the number of retrievals over the selected 19 megacities. Each TES megacity transect consists of 20 footprints, each footprint 5 by 8 km in size, spaced 12 km apart resulting in relatively dense coverage along the orbit track over a limited area, providing a chemical snapshot of each megacity roughly every 2 weeks. For each of these megacities, we calculated the mean tropospheric PAN over all TES transect observations that pass the quality screening criteria over the 2013 to 2015 observation period. This provides an overall picture of "high-PAN" vs "low-PAN" cities for this set of observations. Figure 2.1 ranks megacities by the mean detected tropospheric PAN during the TES megacity sampling period. During this period, the highest mean PAN was in Mexico City (average tropospheric PAN mixing ratio of 0.35 ppbv). Thus the MCMA serves as our first case study with new CrIS observations (described in Chapter 3) given the abundance of PAN, a long history of poor air quality, and the availability of complementary datasets.

2.2 CrIS OBSERVATIONS

The Cross-Track Infrared Sounder (CrIS) is a nadir viewing Fourier transform spectroradiometer measuring thermal infrared radiances with high spectral resolution (0.625 cm^{-1}). CrIS instruments are currently flying on the Suomi National Polar-Orbiting Partnership (S-NPP) satellite and on the National Oceanic and Atmospheric Administration (NOAA-20/JPSS-1) satellite as part of the Joint Polar Satellite System (JPSS). CrIS instruments are planned to be housed on future JPSS orbiters. Here we use CrIS on S-NPP. CrIS is one of five instruments aboard S-NPP which flies in a sun-synchronous polar orbit with equatorial overpass times at 01:30 and 13:30 LT. CrIS provides measurements at 30 crosstrack positions, each with a 3 x 3 array of fields of view (FOVs), where each field of view has a diameter of 15 km at nadir. Processed CrIS data provides calibrated and geolocated Level 1B spectra in three bands: $650\text{-}1095\text{ cm}^{-1}$ (longwave), $1210\text{-}1750\text{ cm}^{-1}$ (mid-wave), and $2155\text{-}2550\text{ cm}^{-1}$ (shortwave).

The PANs feature used in this analysis is located at 790 cm^{-1} . CrIS retrievals are processed using the MUlti-SpEctra, MUlti-SpEcies, MUlti-Sensors (MUSES) retrieval software (Fu et al., 2013; Fu et al., 2016; Fu et al., 2018; Worden et al., 2019) which builds on the optimal estimation algorithm developed for Aura-TES (Bowman et al., 2006; Beer et al., 2001). One difference from the TES PAN retrieval algorithm is that the retrievals are done in linear VMR (as opposed to log). Further details of the CrIS PANs retrieval can be found in Payne et al. [2022]. TES PAN could be biased high relative to CrIS PANs (Mahieu et al., 2021). In retrievals using ground-based FTIR measurements covering the spectral regions used by both instruments, Mahieu et al. [2021] showed that PAN values retrieved using the retrievals using the 790 cm^{-1} spectral feature utilized by CrIS were bias low relative to those using the 1150 cm^{-1} spectral feature used for the TES PAN retrievals.

This analysis used the free tropospheric column average volume mixing ratio between 825 and 215 hPa in the summary product files. CrIS sensitivity to PANs peaks in the free troposphere (roughly 680 hPa) and decreases rapidly near the surface. Payne et al. [2022] show validation of CrIS PANs observations against aircraft observations over the remote oceans. The validation suggests a single sounding uncertainty of around 0.08 ppbv that reduces with averaging to an approximate floor of 0.05 ppbv and demonstrates the ability of CrIS PANs retrievals to capture variation in the “background” PANs over remote regions.

CrIS-MUSES single-FOV retrievals of PANs, as well as temperature, water vapor (H_2O), deuterated water vapor (HDO), O_3 , carbon monoxide (CO), methane (CH_4) and ammonia (NH_3) are being processed routinely under the NASA Tropospheric Ozone and Precursors from Earth System Sounding (TROPESS) project and are publicly available via the GES DISC. The TROPESS datasets at the GES DISC include the forward stream, which incorporates both S-NPP and JPSS-1 CrIS data (Bowman, 2021a; Bowman, 2021b). There are also plans to release a “reprocessing” dataset, for which the long-term record will be processed with a uniform algorithm version. Due to constraints associated with algorithm speed and the volume of data from the CrIS meteorological sounder(s), the TROPESS project is not currently processing all available CrIS radiances. The

TROPESS CrIS forward stream data are subsampled using a grid sampling approach where the region is divided into 0.8 degree latitude x 0.8 degree longitude grid boxes and the single, center-most target within each box is selected to be included in the dataset. The forward stream dataset provides both day and night time coverage. The TROPESS datasets also include so-called “special collections” where the sampling may be tailored to address a particular scientific study (or studies). Data for this work were processed as part of a special collection, using the v1.12 of the MUSES algorithm, to provide retrievals for all S-NPP CrIS FOVs for the date range January 2016 to May 2021 in 2 degree by 2 degree latitude/longitude boxes centered on specific megacities. The list of cities was chosen to match those included in the TES megacity transect set. Note that since the S-NPP and JPSS-1 CrIS instruments are essentially identical, targeted processing of JPSS-1 CrIS over megacities is also possible, but has not yet been performed at the time of submission of this work.

CrIS CO data from the same special collection was also incorporated into this analysis as a supplementary dataset to contextualize CrIS PANs observations, as CO is an indicator of combustion (both fossil fuel and biomass burning) and it is an oxidation product of VOCs. For this analysis, we use a tropospheric average of CrIS CO data between 825 and 215 hPa. CrIS can be more sensitive to CO than to PANs in the lower troposphere (Juncosa Calahorrano et al., 2021). Details of the CrIS CO retrieval can be found in Fu et al. [2016] and CrIS CO validation against aircraft observations in Worden et al. [2022]. Note that the TROPESS CrIS CO forward stream is also available at the GES DISC (Bowman, 2021c; Bowman, 2021d).

This study used S-NPP CrIS data from January 2016 to May 2021. To be included in this analysis, CrIS retrievals have to be deemed “good” by the respective master quality flags (CO and PANs), and retrievals meet the additional following criteria as recommended by the developers of these data (Payne et al., 2022). The first four flags are standard quality flags, and the fifth checks whether the PANs spectral shape was fit:

1. Radiance Residual RMS (Root Mean Square of the standard deviation) < 5
2. Radiance Residual Mean < 2

3. Residual Norm Final < 5
4. Quality flag in water vapor files = 1
5. B - A > -0.15 (see Equations 2.1 and 2.2 below)

CrIS data was filtered based on the radiance files using the following equations to check if there is an improvement in the standard deviation, where NESR is the Noise Equivalent Spectral Radiance:

$$A = \frac{\text{StandardDeviation}(\text{RadianceFit} - \text{RadianceObserved})}{\text{NESR}} \quad (2.1)$$

$$B = \frac{\text{StandardDeviation}(\text{RadianceFitInitial} - \text{RadianceObserved})}{\text{NESR}} \quad (2.2)$$

There was a correction applied to CrIS PANs as suggested by Payne et al. [2022] to correct for a water vapor-dependent bias (Equation 2.3). Where c is the correction to be added to individual PANs retrievals and X is the column density of water vapor in units of molecules per cm^{-2} .

$$c = 0.05 + 0.035 \times 10^{-23} \times X \quad (2.3)$$

2.3 ADDITIONAL DATASETS

Given the complexity of PANs chemistry and the variety of sources that contribute to PANs abundances, we incorporate several other datasets into our analysis to contextualize the PANs observations.

2.3.1 OZONE MONITORING INSTRUMENT (OMI) OBSERVATIONS

We use Level 3 NO_2 tropospheric column measurements from OMI on the NASA Aura Satellite to find periods of anomalous NO_2 decline associated with COVID in 2020. We use the Quality Assurance for Essential Climate Variables (QA4ECV) NO_2 Level 3 product described in Boersma et al. [2018] as this is the most recent and improved data product. OMI NO_2 L3 monthly mean

data used in this study is provided on a global $0.125^\circ \times 0.125^\circ$ grid and can be found on the TEMIS database (Boersma et al., 2017a).

Level 3 HCHO tropospheric column measurements, also from OMI, are used to contextualize changes in VOC concentrations in megacities during the period of anomalous tropospheric NO_2 change. Space-based observations of HCHO have been used as an indicator of VOC emissions (De Smedt et al., 2008; Shen et al., 2019). HCHO is also processed using the QA4ECV algorithm consistently with the NO_2 data used in this study. HCHO L3 monthly mean data is also provided on a global $0.125^\circ \times 0.125^\circ$ grid and can also be found on the TEMIS database (De Smedt et al., 2017).

2.3.2 SURFACE O_3

Surface O_3 and (NO_x data) included here are from the environmental government network of Mexico City (Red Automática de Monitoreo Atmosférico; RAMA) (RAMA, 2020). We include monthly means of day time averages for all of the surface sites within the Mexico City Metropolitan Area (MCMA) in the analysis presented below.

2.3.3 MODIS AND VIIRS FIRE RADIATIVE POWER

We also use observations of fires from the Moderate Resolution Imaging Spectroradiometer (MODIS) on both the Terra and Aqua satellites for fire counts and fire radiative power (FRP) to assess the seasonal peak in local fire activity. The MODIS Active Fire product is provided by the Fire Information for Resource Management Systems (FIRMS) ([doi:10.5067/FIRMS/MODIS/MCD14ML](https://doi.org/10.5067/FIRMS/MODIS/MCD14ML)). The data is processed by MODIS Adaptive Processing System (MODAPS) using the enhanced contextual fire detection algorithm into the Collection 5 Active Fire product. Algorithm description for the MODIS Active Fire product can be found in Roy et al. [2008]. There are two MODIS instruments in orbit, one on the NASA Terra satellite and one on the NASA Aqua satellite. Aqua flies in the NASA A-train constellation with local overpass times of about 01:30 and 13:30. Terra has an overpass time of about 10:30 LT. MODIS fire data has 1 km resolution. MODIS active fire products are not available for May 2021 on the FIRMS archive, thus we also use observations

of fires from the S-NPP Visual Infrared Imaging Radiometer Suite (VIIRS) ([doi:10.5067/FIRMS/VIIRS/VNPI4IMGT_NRT.002](https://doi.org/10.5067/FIRMS/VIIRS/VNPI4IMGT_NRT.002)). A comparative strength of VIIRS is the ability to detect smaller fires (Li et al., 2018; Wei et al., 2018), leading to a consistently higher fire count than MODIS. MODIS and VIIRS FRP data were filtered using only retrievals with > 80 % confidence level.

2.3.4 CHEMICAL REANALYSIS PRODUCT

We used the global chemical transport model, MIROC-CHASER (Sudo et al., 2002; Watanabe et al., 2011; Sekiya et al., 2018), to explain the 3-dimensional distribution of PAN, including the relative contributions of different NO_x emission sources. The model calculates tracer transport (advection, cumulus convection, and vertical diffusion), emissions, dry and wet deposition, and chemical processes (92 species and 262 reactions) of chemical species in the troposphere and stratosphere at 1.125° horizontal resolution. Lightning NO_x sources were calculated in conjunction with the convection scheme of MIROC-atmospheric general circulation model (AGCM) (Watanabe et al., 2011) using the Price [1992] scheme. The meteorological fields were calculated using the MIROC-AGCM, in which the simulated meteorological fields were nudged to the six-hourly ERA-Interim reanalysis data.

NO_x emissions for 2016-2019 were obtained from an assimilation of multi-species satellite observations (ozone, CO, NO₂, HNO₃, and SO₂) in the Tropospheric Chemistry Reanalysis version 2 (TCR-2) framework (Miyazaki et al., 2020b; <https://doi.org/10.25966/9qgv-fe81>). The tropospheric NO₂ column retrievals from the QA4ECV version 1.1 level 2 products for OMI and GOME-2 (Boersma et al., 2017b, Boersma et al., 2017c) were used to constrain NO_x emissions. A priori emissions were obtained from HTAP version 2 for 2010 (Janssens-Maenhout et al., 2015), Global Fire Emissions Database (GFED) version 4 (Randerson et al., 2018), and the Global Emissions Inventory Activity (Graedel et al., 1993) emissions. The data assimilation optimizes only the combined total emission. After the data assimilation, the ratio of different emission categories within the a priori emissions was applied to the estimated emissions to obtain the a posteriori emissions for each sector separately. The quality of the reanalysis fields has been evaluated against independent observations for various chemical species on regional and global scales (Miyazaki

et al., 2020b). NO_x emissions for 2020 used in our analysis are estimated using business as usual (BAU) emissions added to the estimated COVID-19 emissions anomaly as described in Miyazaki et al. [2021].

Chapter 3

SPATIOTEMPORAL VARIABILITY OF PANs OVER AND AROUND MEXICO CITY

3.1 SPATIAL DISTRIBUTION OF PANs OVER MEXICO CITY

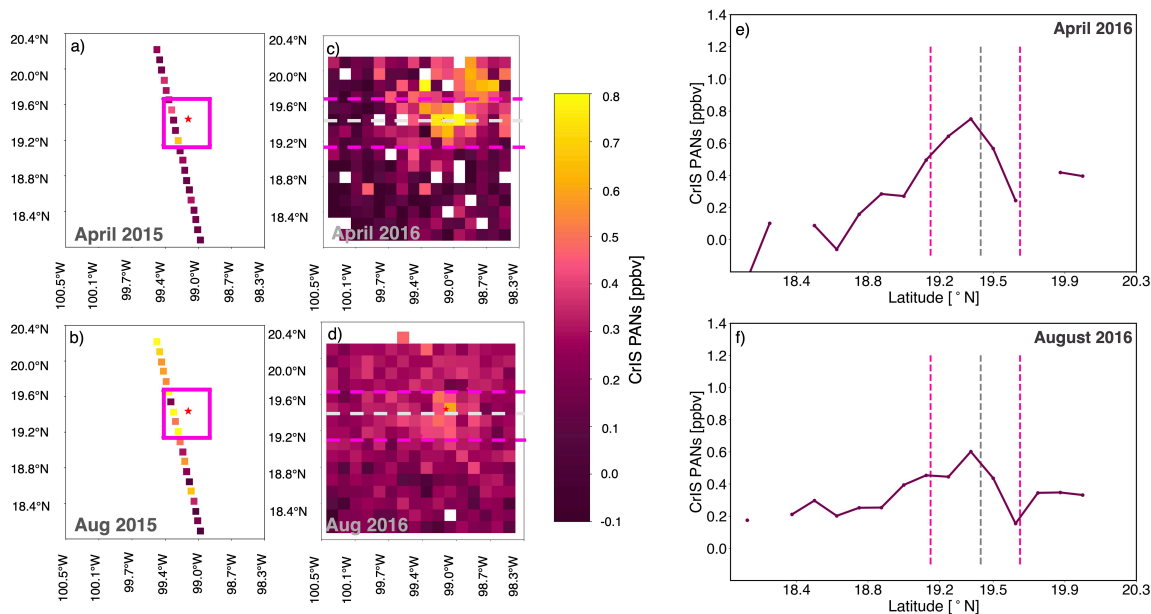


Figure 3.1: Maps demonstrating PANs enhancements around urban Mexico City. Monthly mean TES transects ($n = 2$) are shown for (a) April and (b) August 2015, and monthly averaged gridded CrIS PANs are shown for (c) April and (d) August 2016. CrIS PANs are plotted as a function of latitude for (e) April and (f) August. The latitude bounds of the urban Mexico City box shown in panels a-b and Fig. 1 are denoted by pink dashed lines in panels c-f. The Mexico City center is denoted by gray dashed lines. White pixels show grid boxes with data that has been filtered out.

Figure 3.1 presents¹ the spatial extent of the PANs enhancement around urban Mexico City. April and August are plotted because these are the two seasonal maxima in MCMA free tropospheric PAN from TES (not shown) and PANs from CrIS (see Figure 3.4 and later discussion). Figure 3.1a and 3b show the spatial extent of MCMA PAN from monthly averaged TES transects

¹Results from this chapter are published in the Journal of Atmospheric Chemistry and Physics, Shogrin et al. 2023

($n = 2$). The limited spatiotemporal and irregular temporal sampling by TES combined with the day-to-day variability in PAN limits the utility of monthly averages within the TES dataset for individual months. Figure 3.1c and 3d show clear PANs enhancements in monthly mean gridded CrIS data. Figure 3.1e and 3f show north-to-south slices of the data presented in Figure 3.1c and 3d. These panels show that the spatial extent of free tropospheric average PANs > 0.2 ppbv covers 0.5 degrees latitude (roughly 50 km) in April. This is less well-defined in August, but this distance is comparable to the diameter of the Mexico City basin (Molina et al., 2009). Thus Figure 3.1 demonstrates that the spatial resolution of CrIS is sufficient to determine the size of urban tropospheric PANs enhancements during specific seasons. Figure 3.1e and 3f also confirm that there is a localized peak in free tropospheric PANs collocated with the center of Mexico City, consistent with local production of PANs within the MCMA city limits.

The regional topography of the MCMA drives the meteorological transport patterns in the city. Previous studies show that thermally-driven mountain-valley flows contribute to most of the day-to-day variability in surface wind speed and direction, rather than circulations at the synoptic-scale (Fast and Zhong, 1998; Doran and Zhong, 2000; de Foy et al., 2005; 2006; 2008; Lei et al., 2007; Lei et al., 2008; Zavala et al., 2020). Intense vertical shear of these thermally-driven flows lead to recirculation of air within the MCMA basin. Near-surface convergence zones due to momentum down-mixing of thermally-driven wind and light synoptic winds aloft can lead to the accumulation of pollutants in the basin. However, the MCMA basin has relatively effective venting through the Chalcho passage to the southeast and northern plateau leading to little day-to-day pollutant accumulation (Zavala et al., 2020). Prior work has shown that on average the air quality "footprint" of MCMA is fairly local as air transported out of the basin is diluted quickly (e.g., Mena-Carrasco et al. [2009]; Emmons et al. [2010]). However, PANs are an exception because they can act as reservoirs and sources of NO_x to increase downwind O_3 production. For example, during March 2006 a plume containing elevated NO_y species was observed at about 900 km downwind in the northeast outflow direction (Mena-Carrasco et al., 2009). Next we explore PANs in the most common outflow regions around Mexico City.

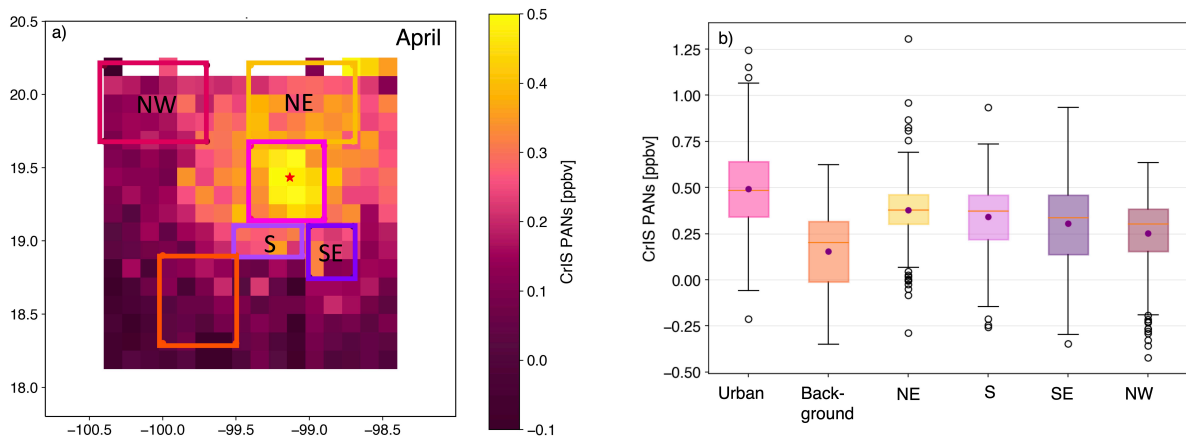


Figure 3.2: (a) Potential air pollutant outflow regions for the Mexico City basin (colored squares) plotted over monthly mean gridded CrIS PAN for April 2016-2021, (b) boxplots of daily CrIS free tropospheric PANs measurements within the boxes shown in (a). The orange lines and purple circles represent the median and mean respectively. The whiskers represent the standard deviation of daily CrIS free tropospheric PANs measurements.

Figure 3.2a denotes sub-regions within the CrIS data processing area around Mexico City. The regions denoted by NW, NE, S, and SE represent potential pollutant outflow regions for Mexico City, and our choice of regions is informed by the common patterns of pollutant outflow identified by de Foy et al. [2006] for the 2006 MILAGRO (Megacity Initiative: Local and Global Research Observations) field intensive. Figure 3.2b presents boxplots of daily CrIS free tropospheric PANs values within these regions. Together, these two panels show that there are more days with higher PANs in the region located to the northeast of Mexico City (yellow box) and in the region that encompasses the mountains south of the city (light purple box). These two regions appear to be the dominant directions of PANs outflow in MCMA in April. Our analysis implies that outflow of PANs to the northwest (magenta box) is infrequent, however, the lower values of PANs in the box could also be due to loss due to a longer transport area from the city center into this region. This box was chosen to represent the region to the NW of the urban area that is not influenced by the surrounding mountains (see Fig. 1). The largest spread in daily average PANs is over the southeast Chalco Passage (dark purple box). Figure 3.2 is largely consistent with the findings of de Foy et al. [2006]; [2008], and Emmons et al. [2010]. Pollutants can be transported out of Mexico City

to the northeast, channeled through the southeast, or vertically injected out over mountains to the southwest, depending on meteorological conditions present.

3.2 SEASONAL CYCLES OF PANs OVER MEXICO CITY

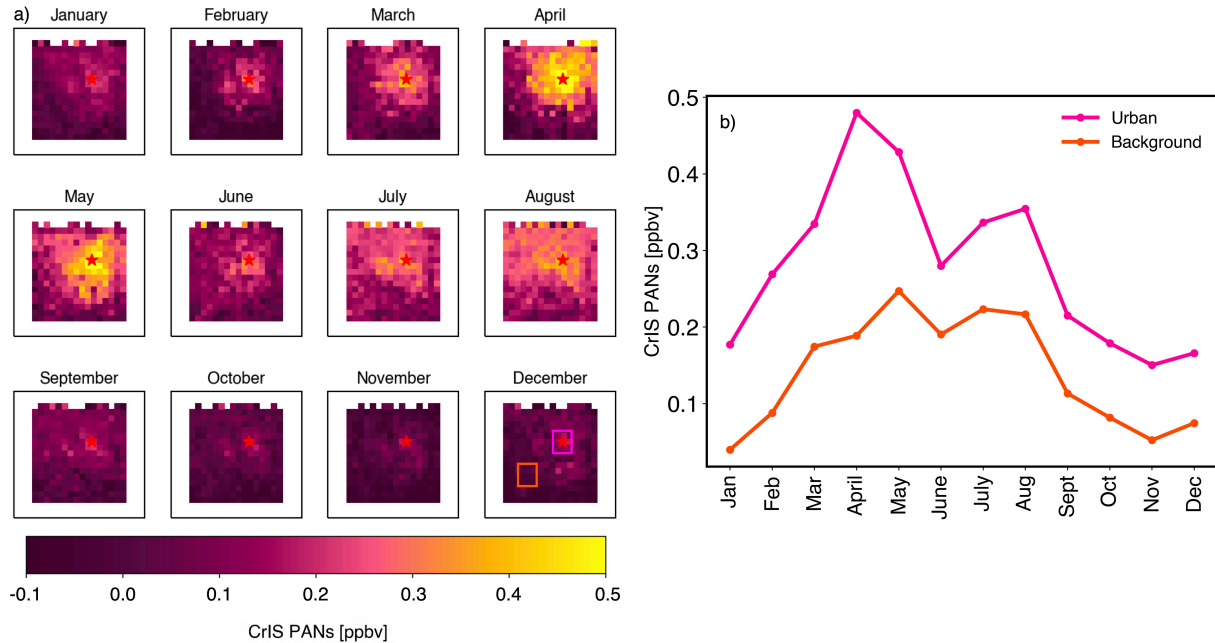


Figure 3.3: (a) Monthly mean gridded CrIS PANs over Mexico City. The boxes indicate the locations chosen to illustrate the urban Mexico City PANs (pink) enhancement compared to the “nearby background” (orange). The background box is confined by (18.99° N, 99.84° W, 18.49° N, 99.34° W) and the urban Mexico City box is confined by (19.15° N, 99.40° W, 19.65° N, 98.9° W). (b) Monthly mean urban and background mean CrIS free tropospheric PANs for the period January 2016 to May 2021.

Figure 3.3 contrasts PANs over a region only rarely impacted by direct outflow from Mexico City to the PANs observed directly over Mexico City. Figure 3.3a presents monthly gridded mean PANs for the period 2016-2021. The orange box in the “December” panel surrounds an area with consistently low free tropospheric PANs mixing ratios. We refer to this area as “nearby background” PANs conditions here. This is the same background region shown in Figure 3.2. Figure 3.3b presents a time series of monthly averaged CrIS PANs values within the two respective boxes shown in Figure 3.3a. Based on this Figure, PANs are always greater over the urban area than in the “nearby background”. On average, over the period 2016-2021, the difference between

urban and background free tropospheric PANs is greatest in April and reaches a minimum in the winter months of October, November, and December. During these winter months, the difference between urban and nearby background free tropospheric PANs is roughly 100 pptv. The nearby background PANs have a seasonal maximum in May, and this is consistent with the March-April-May peak in local fire activity (Yokelson et al., 2007; 2009; 2011). Background enhancements in July and August were not explored at the time of this work, however, model results included in the Supplemental Information (SI) indicate a seasonal enhancement in PANs aloft at this time that is associated with both natural and anthropogenic NO_x sources (Figures 3.5 and 3.6).

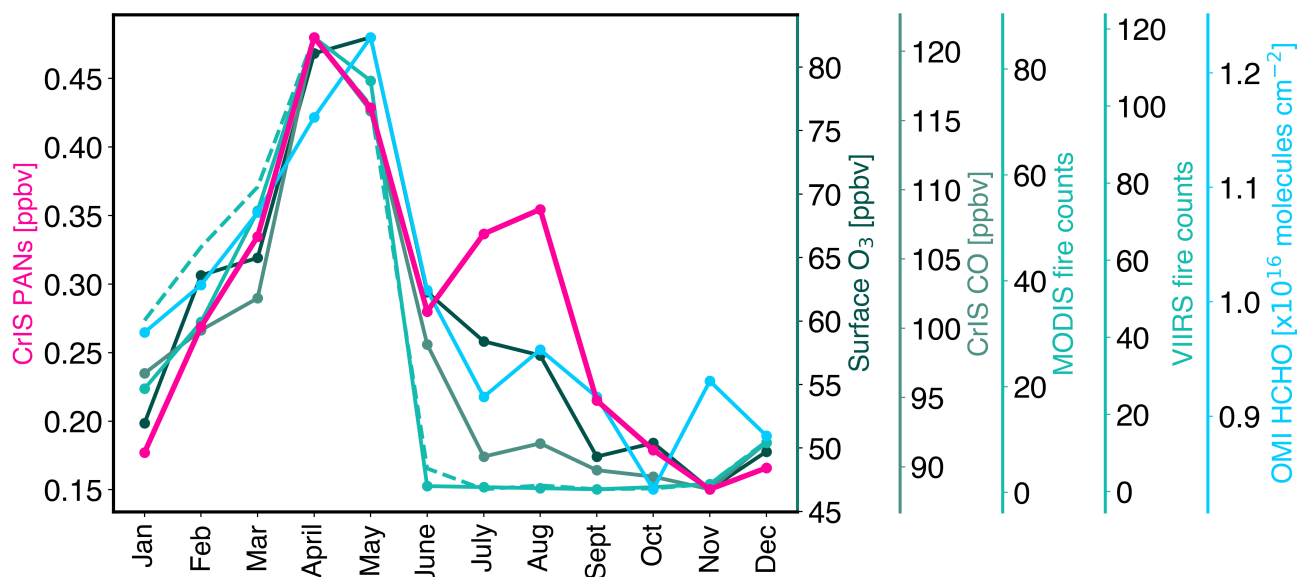


Figure 3.4: Seasonal cycle of CrIS free tropospheric PANs, RAMA surface O_3 , CrIS free tropospheric CO, MODIS fire counts (solid; 2016-2020), VIIRS fire counts (dashed) and OMI HCHO columns for urban Mexico City from 2016-2021. MODIS and VIIRS fire counts are constrained by (20.12° N , 100.40° W , 18.36° N , 98.44° W). All other species are constrained by the urban Mexico City box defined in Figure 3.3.

Figure 3.4 displays the seasonal cycle of PANs from 2016-2021. The maximum in PANs over urban Mexico City occurs in April. Surface O_3 , CrIS free tropospheric column mean CO, MODIS and VIIRS fire counts, and tropospheric column OMI HCHO have co-occurring peaks in March, April and May. Mexico City experiences a wet and a dry season. November through February is typically characterized by cool and dry conditions as anticyclonic westerly winds bring dry

air to the region. This is followed by a warm, dry season from March to May; followed by a rainy season that typically lasts from May through October (Molina et al., 2009). The warm, dry season is characterized by high pressure systems with clear skies, weak wind, and intense solar radiation promoting photochemical production of O_3 and other oxidants (Molina et al., 2019). Weak winds during the warm, dry season promote stagnation of pollutants near the southern area of the basin (Molina et al., 2019; Zavala et al., 2020). The observed seasonal maxima in surface O_3 and tropospheric column OMI HCHO occur during this period (Figure 3.4). Lei et al. [2009] show that secondary HCHO dominates the HCHO budget in the afternoon when the observations shown here were collected. Maxima in CrIS free tropospheric CO and MODIS fire counts occur in April and May. Local fire activity during these months contribute to increased local tropospheric CO abundances (Tzompa-Sosa et al., 2016; Yokelson et al., 2007; 2009; 2011). Note that the region included in Figure 3.4 may not encompass all the fires that impact the larger Mexico City region. It represents the local fire activity only. The rainy season is typically characterized by lower CO and O_3 mixing ratios; however, O_3 production continues throughout the year as intense photochemical reactions can occur prior to afternoon precipitation in the rainy season (Molina et al., 2019). Elevated O_3 mixing ratios can occur throughout the year in the MCMA due to its subtropical latitude and high elevation (Molina and Molina, 2002), though over 60 % of the O_3 episodes in Mexico City (i.e., exceedances to the 1-hour standard of 95 ppbv) occur during the warm, dry season (see Jaimes-Palomera et al. and references therein). Note that there is a secondary peak in PANs in July and August that is not associated with an similar increase in surface O_3 . This suggests that the PANs observed by CrIS over this region may not only be associated with local surface photochemistry but PANs aloft (Figure 3.5). Model results included in section 3.3 indicate that there are multiple NO_x sources, including anthropogenic, soil, biomass burning, and lightning, that contribute to this feature, and the PAN enhancement is located higher aloft (i.e. at 400 hPa versus 750 hPa).

The next section discusses results from model simulations of PAN over Mexico City in 2017. Model simulations were ran by co-author Dr. Kayuzaki Miyazaki.

3.3 SIMULATIONS OF PAN OVER MEXICO CITY

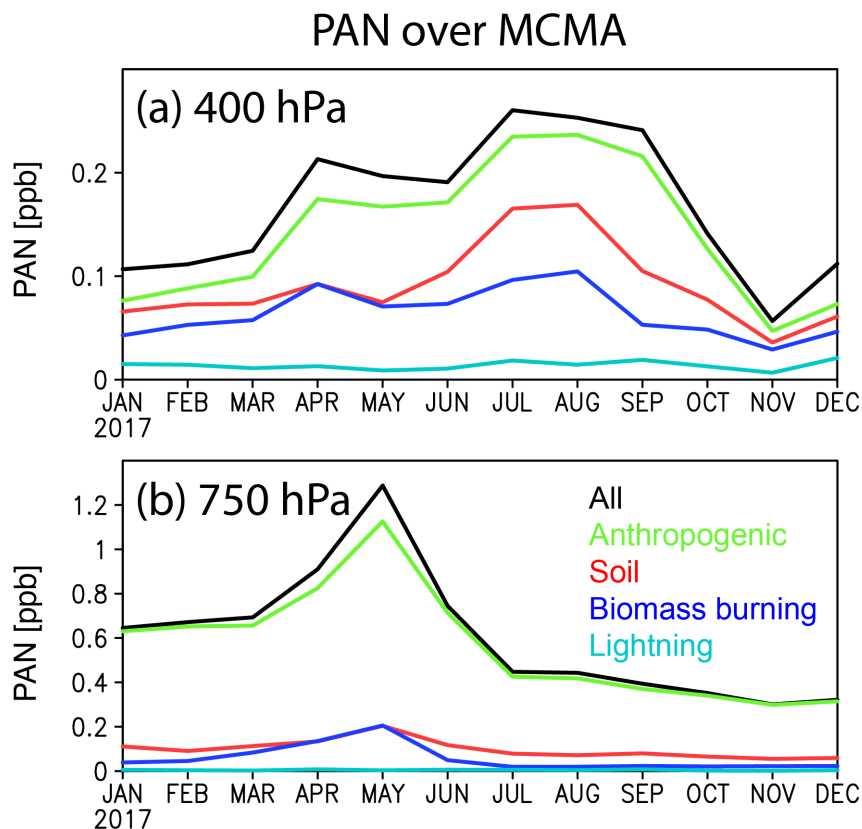


Figure 3.5: Seasonal changes of monthly mean PAN concentrations (in ppbv) at 750 (b) and 400 hPa (a) over MCMA in 2017 simulated by the CTM (black lines). Results from sensitivity calculations by using each NO_x emission separately are also shown by color lines.

The CTM model simulations were used to provide an extended picture of PAN variations over the MCMA region, including its vertical profiles and attributions to different emission sources. The general seasonal pattern of the simulated PAN in the troposphere, with a clear maximum in boreal spring in the lower troposphere (up to 1.2 ppb at 750 hPa) (Figure 3.5a), is generally consistent with the observed changes in average tropospheric PAN mixing ratio from CrIS (Figure 3.4). Meanwhile, the simulated PAN reveals different seasonal patterns between the lower and upper troposphere, with a maximum concentration of 0.25 ppb in July in the upper troposphere (at 400 hPa) (Figure 3.5b), due to atmospheric transports and chemical transformations. This confirms

that the observed average tropospheric PAN concentrations from satellites reflect complex vertical structures.

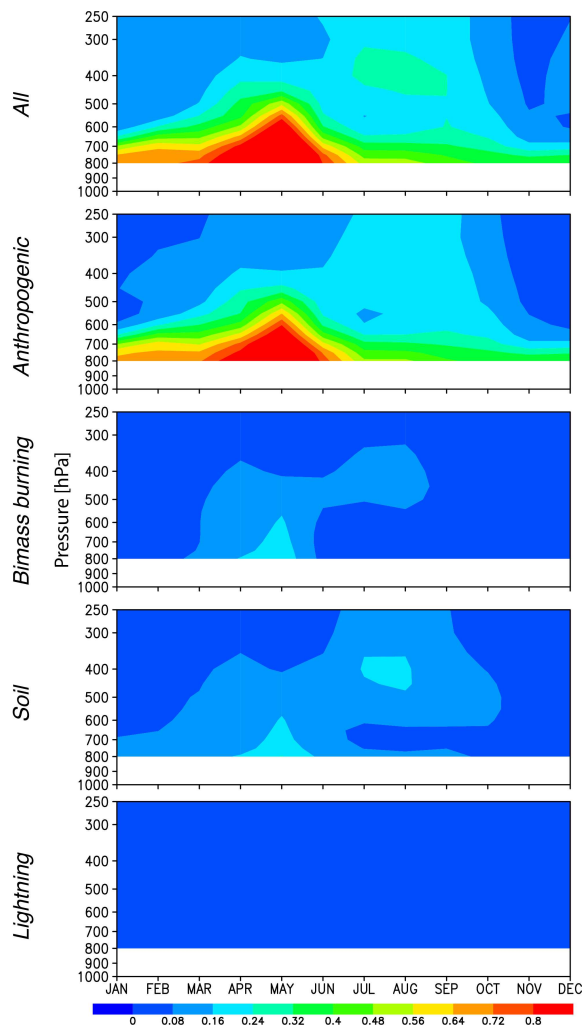


Figure 3.6: Latitude-pressure cross sections of monthly mean PAN concentrations (in ppbv) over MCMA in 2017 simulated by the CTM (first row). The relative contributions from each emission source separately are also shown (second through fifth row).

The model sensitivity calculations, by using each NO_x emission source separately, indicate that the enhanced PAN concentrations in the lower troposphere in boreal spring are mostly dominated (> 90 %) by anthropogenic sources (Figures 3.5 and 3.6). The continued enhancements from the surface through upper levels suggest the dominant effects from local anthropogenic sources. Biomass burning also increases PAN in April-May, but with smaller contributions than anthro-

pogenic emissions. Soil NO_x emissions also have non-negligible impacts. In particular, the local maximum in the upper troposphere during July-August produced by soil emissions demonstrates the importance of natural emissions from surrounding areas on urban PAN distributions. The contributions of lightning emissions are small over MCMA, while it has greater influences over the southern tropics (not shown). The natural emission sources reveal strong interannual variabilities, which could explain parts of the observed multi-year changes. Note that, because of the non-linear chemistry, the sum of each contribution in the sensitivity calculations does not match the total contribution. The model simulation also suggested a broader impact of anthropogenic NO_x emissions from Mexico City in the free troposphere horizontally (not shown). Further insights into the impacts of urban emissions on regional and global nitrogen cycles can be obtained by utilizing global satellite measurements of PAN combined with CTMs and chemical data assimilation (Miyazaki et al., 2020a) in following studies.

3.4 INTERANNUAL VARIABILITY IN PANs OVER MEXICO CITY

In addition to air pollution from the anthropogenic sources, air quality in the MCMA is impacted by local (Yokelson et al., 2007) and regional (Yokelson et al., 2009) biomass burning, as well as agricultural residue and trash fires (Yokelson et al., 2011; Christian et al., 2010). March-April-May is the seasonal peak in regional biomass burning (Tzompa-Sosa et al., 2016; Yokelson et al., 2007; 2009; 2011). Biomass burning in Mexico and urban emissions from the MCMA heavily influence the springtime air quality in much of Mexico and the United States (Yokelson et al., 2009). Fires can contribute to a quarter of the CO production within the MCMA (Yokelson et al., 2007). Figure 3.7 displays monthly averaged gridded CrIS PANs (panel a) and CO (panel d) for May 2016-2021 and corresponding fire-related products in Figure 3.7b and 3.7c. We focus on the month of May to demonstrate the interannual variability in free tropospheric PANs over Mexico City during this month and their relationship to local fires. The free tropospheric PAN enhancement in May 2017 located south of the urban enhancement is collocated with fires. There were 196 and 234 fires detected in the region during May 2019 by MODIS and VIIRS, respectively. S-NPP CrIS is missing data between 26 March 2019 and 24 June 2019. A hardware failure

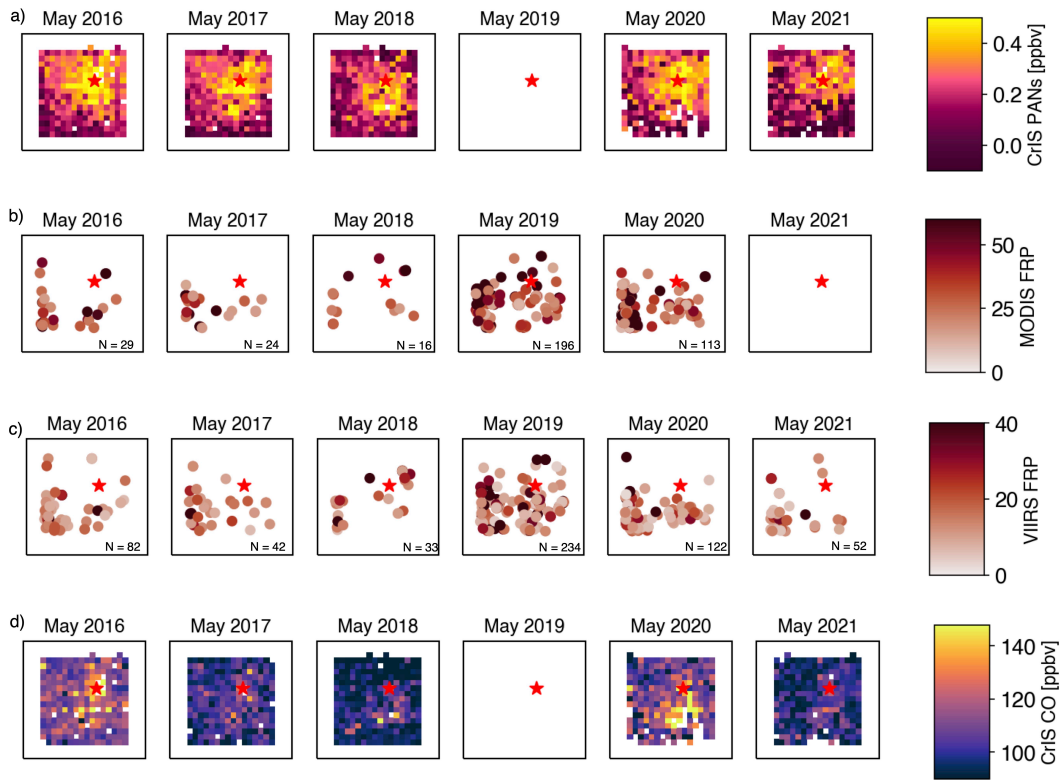


Figure 3.7: (a) Gridded average PANs for the month of May for the region surrounding Mexico City for multiple years. The center of Mexico City is denoted by a red star. (b) MODIS fire radiative power (FRP) for the Mexico City region, (c) VIIRS fire radiative power (FRP) for the Mexico City region, and (d) gridded free tropospheric average CrIS CO. This is the full region plotted in Fig. 1 (21° N, 100.9° W, 18° N, 97.1° W).

occurred in the S-NPP CrIS mid-wave signal processor, which led to a temporary halt in the L1b processing, but the issue was resolved by switching from the Side 1 electronics to the redundant Side 2 electronics. Note that JPSS-1 CrIS radiances are available over this time period, but targeted TROPES/MUSES CrIS processing over megacities has not been performed for JPSS-1 at this time. The smallest number of fires were detected in May 2018 ($N = 16$; 33), and the corresponding average free tropospheric PANs and CO are both also lower than other years, though small enhancements in both exist collocated with fires to the south of the city. The relationships between monthly mean CO and VIIRS ($R^2 = 0.87$) and MODIS fire counts ($R^2 = 0.60$) are strong (Figure A.1). We also found that total monthly fire counts (plotted in Figure 3.7b and 3.7c) explain

a substantial amount ($> 45\%$) of the variability in monthly mean PAN during May; MODIS fire counts, using only 4 months of data, explain more of the variability in monthly mean PAN ($R^2 = 0.69$; Figure 3.7b, Figure A.1) than VIIRS fire counts, which include all 5 months of available data ($R^2 = 0.47$; Figure 3.7c, A.1).

3.5 RECENT CHANGES PANs, NO_x, AND HCHO

In response to substantial air quality degradation the Mexican government developed and implemented successive air quality management programs that combined regulatory actions with technological advances (Molina et al., 2019; Molina, 2021). Reductions in O₃ were attributed to aggressive emission controls of O₃ precursor species, including improving fuels, adopting catalytic converters, removing an oil refinery and heavy industrial facilities, shifting to natural gas for power generation and other industrial needs, reformulating liquefied petroleum gas (LPG) for cooling and water heating, introducing vehicle inspection and maintenance programs, and introducing a “no driving day” (Hoy no Circula) rule (Zavala et al., 2020 and references therein). These control strategies led to reductions in all criteria pollutants (Zavala et al., 2020 and references therein); however, the MCMA basin still experiences elevated levels of many of the air pollutants listed above (Fast and Zhong, 1998; Gaffney, 1999; Velasco et al., 2007; Molina et al., 2010; Johansson et al., 2009; Jaimes-Palomera et al.; Zavala et al., 2020; Osibanjo et al., 2021; Cady-Pereira et al., 2017). There have been no substantial improvements in the concentration of O₃ (or PM_{2.5} and PM₁₀) since about 2006 (Molina et al., 2019; Zavala et al., 2020). The transport sector continues to have a large impact on VOC and NO_x emissions in the MCMA. Solvents, fuel evaporation and leaks, are large sources of VOCs, dominating over biogenic VOC emissions (Molina et al., 2010; Velasco et al., 2007). The distribution of sources are highly inhomogeneous throughout the MCMA (Zavala et al., 2020; Jaimes-Palomera et al.).

Figure 3.8 presents a time series and histograms of monthly averaged NO_x species, CrIS PANs, and tropospheric column OMI HCHO for the CrIS measurement record period (2016-2021) for urban Mexico City. There is a statistically significant decrease in MCMA OMI NO₂ between 2018 and 2019 (Mann-Whitney u-test, $p = 0.0001$). We separate the OMI NO₂ into two sample popula-

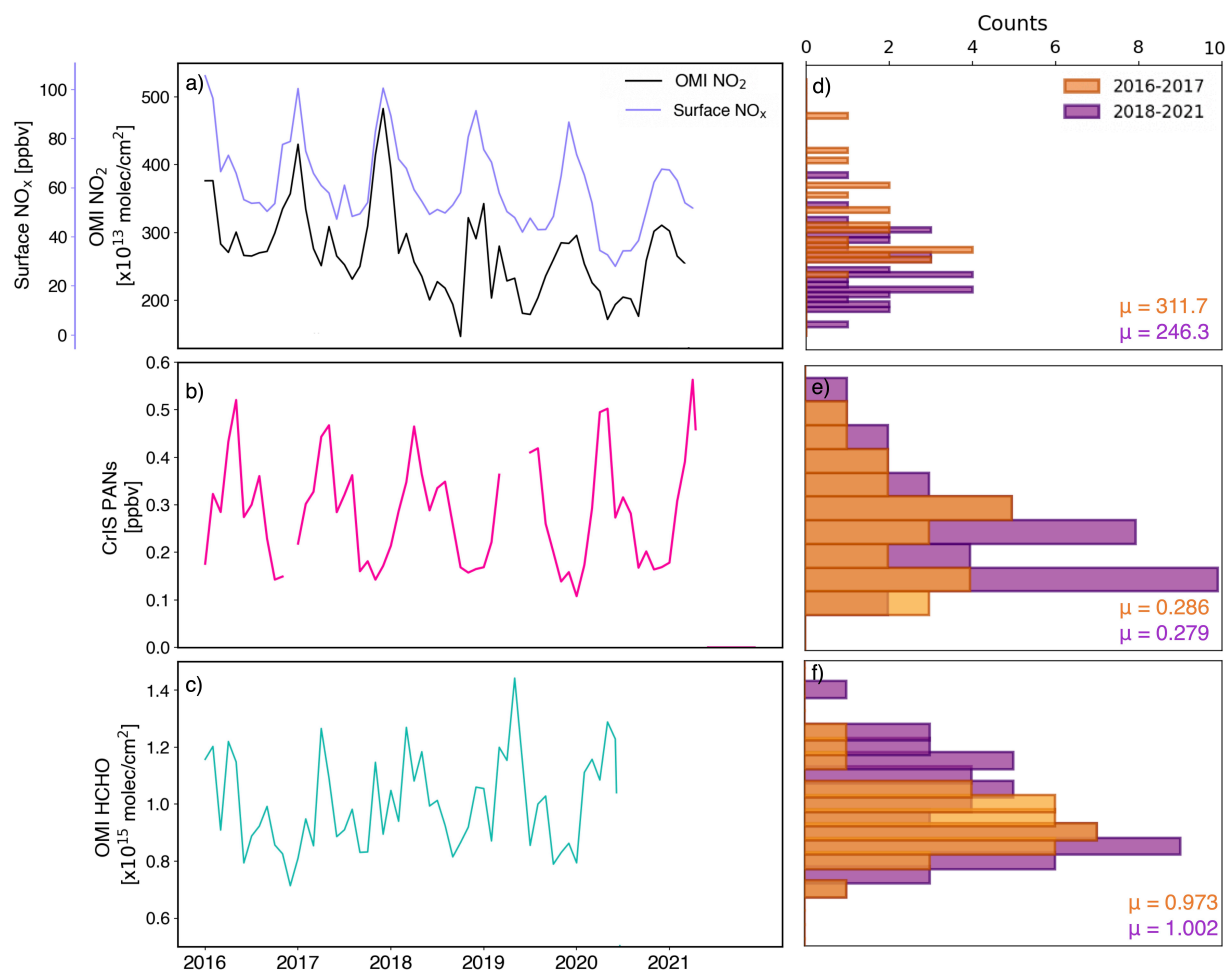


Figure 3.8: (a) Monthly average of OMI NO₂ (Dark Blue) and RAMA surface NO_x observations (light blue), (b) CrIS free tropospheric monthly average PANs, (c) OMI HCHO tropospheric columns for the period 2016-2021. Distribution of OMI NO₂ (d), CrIS PANs (e), and OMI HCHO (f) from two populations: 2016-2017 (orange) and 2018-2021 (purple). Sample means (μ) are provided in their respective colors and units. White grid cells in (a) and (d) represent areas where retrievals have been filtered out.

tions to represent the higher-value population (2018-2021; orange) and the lower-value population (2016-2017; purple). Figure 3.8d shows that the more recent data (purple) peaks towards lower values and the histogram representing the older population (orange) peaks towards higher values. This is further expressed in the sample means; the 2016-2017 and 2018-2021 means are 311×10^{13} and 246×10^{13} molecules cm^{-2} respectively (standard deviation: $63, 52 \times 10^{13}$ molecules cm^{-2} , re-

spectively). These are statistically different. However, there is no statistically significant difference in the mean free tropospheric PANs as observed by CrIS between 2016-2017 and 2018-2021. The sample means are 0.29 and 0.28 ppbv, respectively (standard deviation for both is 0.11 ppbv). We find there is also no significant difference in OMI HCHO between the two time periods. HCHO can be emitted directly and it is an intermediate product in the oxidation of many VOCs (Lei et al., 2009). MCMA has elevated levels of HCHO from both primary emissions and secondary photochemical formation (Baez et al., 1995; Garcia et al., 2006; Velasco et al., 2007; Lei et al., 2009). Lei et al. [2009] showed that secondary HCHO dominates the MCMA HCHO budget in the mid-morning and afternoon; coinciding with ascending satellite overpasses. HCHO is used as an indicator of VOC emissions (De Smedt et al., 2008; Shen et al., 2019) and changes in VOC emissions may not mirror changes in NO_x (Simon et al., 2015; Gao et al., 2017; Shen et al., 2019).

The lack of a change in PANs is not surprising. PAN can be more sensitive to NMVOCs than to NO_x emissions (Fischer et al., 2014), and the PANs observed by CrIS are not all formed from local anthropogenic NO_x emissions (see Figure 3.5 and 3.6). Surface PANs can also respond to changes in the environmental conditions that support photochemistry. For example, during the COVID-19 lockdown period, emissions of both NO_x and VOCs were reduced by 60 % and 30 %, respectively in the Beijing area, but Qiu et al. [2020b] showed enhanced levels of surface PAN in this region. They showed that this enhanced PAN (2-3 times the concentrations of the pre lockdown period) was the result of enhanced photochemistry, anomalous wind convergence leading to the accumulation of precursor species and accelerated VOC oxidation (i.e. further enhancing local photochemistry), and anomalously high temperatures to the area during the study period.

Chapter 4

CHANGES TO PANs ASSOCIATED WITH COVID-19

4.1 SEASONAL CYCLES OF PANs, CO, AND HCHO IN MEGACITIES

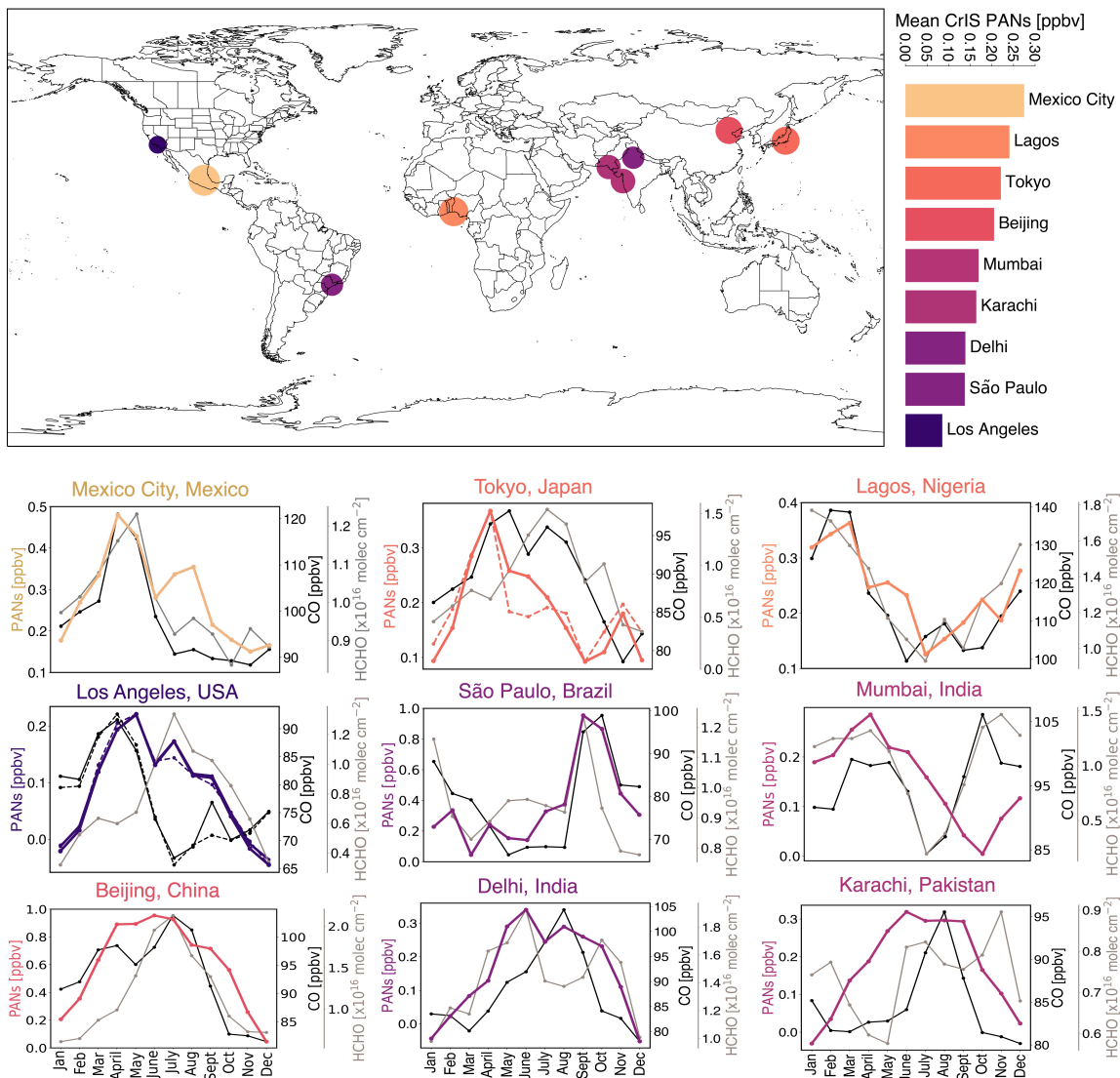


Figure 4.1: Seasonal cycles of CrIS PANs [ppbv] (respective colors shown on the map, dashed denotes median values), CrIS CO [ppbv] (black), and OMI HCHO tropospheric column average [$\times 10^{16}$ molecules cm^{-2}] (gray) for 9 megacities. Monthly means include data from January 2016 to May 2021. The scale to the right of the map ranks the cities using the mean CrIS PANs for the entire period. The dots on the map are sized based on mean detected PANs for the entire time period.

Figure 4.1 displays² the mean seasonal cycles for CrIS PANs, CrIS CO, and OMI tropospheric column HCHO for 9 different global megacities from 2016-2021. Cities are ranked based on average detected PANs from CrIS between 2016-2021. The highest mean PANs during this period were present over Mexico City, consistent with TES observations from 2013-2015 (Shogrin et al., 2023).

The seasonal springtime maximum in PAN is attributed to an increase in photochemical activity at a time when PAN has a relatively long lifetime against thermal decomposition (Penkett and Brice, 1986; Brice et al., 1988; Fischer et al., 2014). All but two selected megacities reflect this pattern of springtime maxima of PANs. Seasonal maxima occur in March, April, and/or May for northern hemisphere megacities (Mexico City, Los Angeles, Tokyo, Mumbai, Delhi, and Lagos), and in September for São Paulo (23.56 °S), the beginning of austral spring. In contrast, over Lagos (6.52 °N) and Mumbai (19.07 °N) PANs begin increasing towards the end of the calendar year and reach a maximum in March or April.

In addition to a springtime maxima, PANs over Beijing (39.92 °N) and Karachi (24.86 °N) remain elevated through the summer (April-September). Delhi (28.71 °N) has a comparably wide seasonal cycle in PANs, but reaches its seasonal maximum in the springtime, similar to other northern hemisphere megacities. Mexico City (19.43 °N), Los Angeles (34.05 °N), and Tokyo (35.68 °N) also show a springtime maximum, but with an additional period of elevated PANs later in the year. Mexico City has a secondary peak in July and August that may be associated with elevated PANs aloft (Shogrin et al., 2023). The extent of the published literature attributing air pollutants in each megacity differs widely. For example, there is a longstanding effort to attribute and control O₃ and other photochemical pollutants in Los Angeles (e.g., Langford et al., 2010; Pollack et al., 2013 and references therein; Nussbaumer and Cohen, 2020), and the literature base for Beijing is growing rapidly (e.g. Chen et al., 2015; Zhao et al., 2020; Zhao et al., 2022). Here

²Results from this chapter are to be submitted as the following manuscript: Shogrin, M. J., Payne, V. H., Kulawik, S. S., Miyazaki, K., and Fischer, E. V.: Changes to Peroxy Acyl Nitrates (PANs) associated with COVID-19 tropospheric NO₂ declines in megacities from CrIS satellite observations. *To be submitted*

we focus our discussion on Los Angeles, Beijing, and to a more limited extent, Tokyo, Mumbai, Lagos, and Delhi.

PAN was identified as an eye irritant in Los Angeles smog in the 1960s (Leighton, 1961; Grosjean, 2003). PAN abundances at the ground over this megacity have decreased much more rapidly than O₃ in response to emission controls in the Los Angeles Basin (Pollack et al., 2013). CrIS data indicate that free tropospheric PANs over LA have a different seasonal cycle than column HCHO (gray line) and surface O₃ (not shown); tropospheric column HCHO and O₃ have broad maxima extending from April through October and June through October respectively. Mean PANs are elevated in the spring and summer when conditions maximize photochemical activity. Increasing temperatures during the summer decrease the lifetime of PANs against thermal decomposition and decrease the PANs column to O₃ ratio during peak summertime photochemistry. The secondary and tertiary peak in monthly mean PANs over Los Angeles in July and September are likely driven by wildfires in 2018 and 2020, respectively (Liang et al., 2021). Wildfire impacts in September 2020 also drive the peak in September CO; note the difference between the mean and median as these peaks are not evident in the median (dashed) CO or PANs for these months.

Photochemically-produced species (surface O₃ and tropospheric column HCHO) have seasonal maximums in summer months (JJA), corresponding to the seasonal maximum in PANs over Beijing. Peak concentrations of PAN and PPN at the surface in Beijing also peak during summer (Zhang et al., 2015; Zhang et al., 2017), although more recent observations indicate that ground-level PAN is also elevated during winter haze events in Beijing (Zhang et al., 2015; Qiu et al., 2019; Zhang et al., 2020). CrIS observes elevated CO over Beijing in March and April, consistent with a seasonal peak in local fire activity in northeast China (Yin et al., 2019; Fang et al., 2021; Wang et al., 2020; Zhao et al., 2022). Biomass burning likely contributes to observed PANs during this period, as fires are large sources of NO_x and NMVOCs which serve as PAN precursors (Alvarado et al., 2011; Clarisse et al., 2011; Juncosa Calahorrano et al., 2021).

Tokyo has a seasonal spring maximum in photochemical species from both local and distant sources of precursors (i.e. China and Korea) (Ogawa and Miyata, 1985; Yoshitomi et al., 2011;

Lee et al., 2021a). Tokyo is a coastal megacity and local meteorology influences day to day photochemistry heavily (Kanaya et al., 2008). The typical daily land-sea breeze transports air masses with accumulated oxidants into the city center around midday (Kanaya et al., 2008), corresponding to satellite overpass time.

Delhi has a humid subtropical/semi-arid climate and is influenced by the Indian monsoon. The monsoon season lasts from July-September and the dry season is considered to be September-June. CrIS observes elevated PANs in Delhi from April to October; on average PAN remains elevated through the monsoon season, unlike Mumbai and Lagos. Surface O₃ drops in Delhi during the monsoon season, as a southwesterly wind flow brings clean marine air (Jain et al., 2005; Sahu et al., 2009). Crop residue burning in April-May and October-November can deteriorate air quality in the Delhi metropolitan area (Saxena et al., 2021). These periods correspond with periods of elevated PANs observed by CrIS, as well as mean tropospheric column HCHO observed by OMI. Lagos and Mumbai both have tropical wet and dry climates and thus experience strong wet and dry seasons. They are both coastal, tropical megacities and Mumbai is greatly influenced by the monsoon. O₃ increases seasonally during the dry season (Abdul Raheem et al., 2009; Sahu et al., 2009; Marathe and Murthy, 2015). This is consistent with CrIS observations of PANs, which increase and decrease with the respective dry and wet seasons.

The subsequent sections will explore changes in PANs during periods of anomalous NO₂ decreases in 2020. Figure 4.1 helps identify periods in the annual cycle that coincide with PAN production. For most cities, NO₂ changes from COVID overlapped with periods where PAN is above the CrIS detection limit and photochemically produced.

4.2 2020 NO₂ ANOMALIES

Major changes in NO_x emissions and tropospheric NO₂ column abundances have been documented worldwide for different periods of the COVID-19 pandemic (Bauwens et al., 2020; Berman and Ebisu, 2020; Zhang et al., 2022a). For the analysis presented here, we identify periods where:

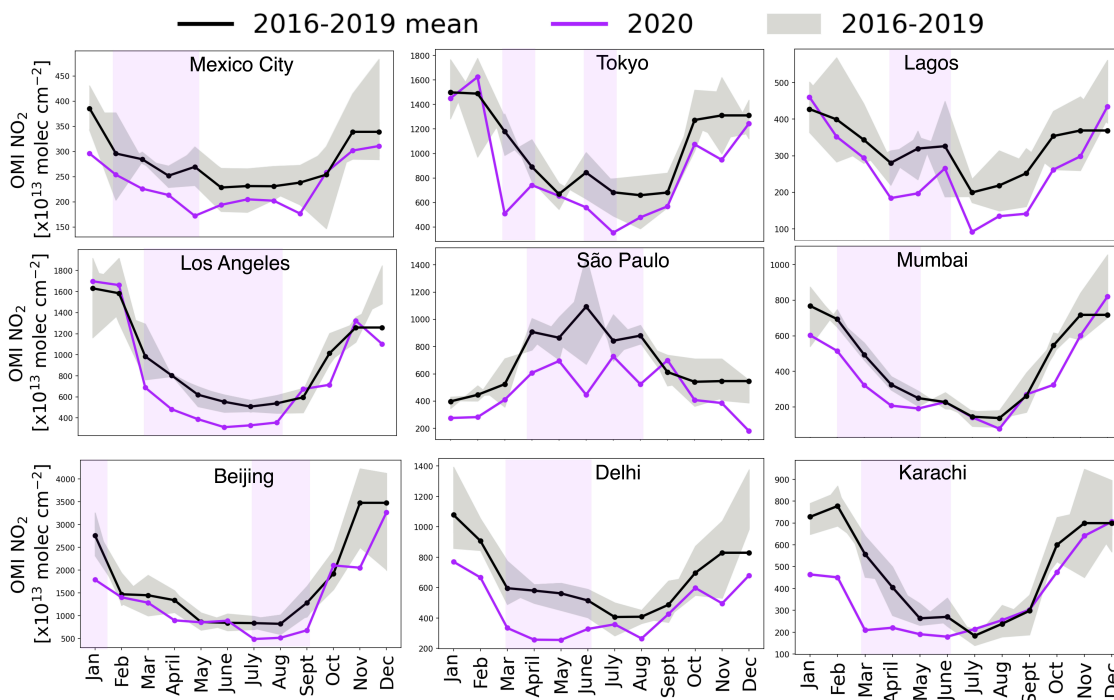


Figure 4.2: Trends of OMI NO₂ tropospheric column monthly means for 9 megacities. Area used for each city is the same small “urban box” area around the urban area of each city used for CrIS selection. 2020 is shown in purple. The mean of 2016-2019 is shown in bold black. Months with substantial NO₂ declines in 2020 have been highlighted in purple and these time frames are used in the subsequent analysis presented in Figure 4.3.

1. the monthly mean NO₂ column during 2020 was $\geq 15\%$ below the corresponding monthly mean for 2016-2019
2. the monthly mean PANs mixing ratio ≥ 0.05 ppbv

We only consider times in the seasonal cycle where PANs mixing ratios ≥ 0.05 ppbv because validation efforts for the CrIS PAN product suggest a single sounding uncertainty of around 0.08 ppbv that reduces with averaging to an approximate floor of 0.05 ppbv (Payne et al., 2021). Periods of observed NO₂ decline often do not exactly coincide with the COVID-19 government-enforced lockdowns, as reduced traffic was often observed prior to government-imposed stay-at-home orders. These months are highlighted by the light purple shading in Figure 4.2. The 2020 monthly mean NO₂ column density associated with these shaded periods are $> 20\%$ less than the mean of

| Changes to NO _x and PANs associated with COVID | | | | | | |
|---|------------------------|--------------------------------|--------------------------------|---------------------|--------------|---------------------|
| Megacity Name | months of perturbation | percent change NO ₂ | percent change NO _x | percent change PANs | p-value PANs | percent change HCHO |
| Mexico City | Feb-May | -22 % | -56 % | 1.8 % | 0.45 | 5.6 % |
| Beijing | January | -35 % | N/A | 80 % | 0.03 | 59 % |
| | July-Sept* | -40 % | N/A | -1.9 % | 0.31 | -7.6 % |
| Los Angeles | March-Aug* | -36 % | -80 % | -11 % | 0.06 | -10 % |
| Tokyo | March-April | -40 % | -5.1 % | 6.9 % | 0.11 | -26 % |
| | June-July* | -40 % | N/A | -0.9 % | 0.44 | -43 % |
| São Paulo | April-Aug* | -35 % | -64 % | 3.7 % | 0.33 | -1.7 % |
| Delhi | March-June | -48 % | -53 % | -20 % | 0.33 | -9.6 % |
| Mumbai | Feb-May | -30 % | N/A | N/A | N/A | -3.0 % |
| Lagos | April-June | -35 % | N/A | 11 % | 0.33 | -0.08 % |
| Karachi | March-June | -52 % | N/A | 12 % | 0.14 | 3.6 % |

Table 4.1: Periods of significant NO₂ decline based on OMI tropospheric column NO₂ monthly means shown in Figure 4.2. Percent change represents the change in 2020 values relative to the mean of 2016-2019 for the respective time periods. Percent change in PANs were calculated using daily means during the months of NO₂ anomaly. P-values for PANs from Mann-Whitney U-Test significance testing are shown. A negative percent change represents a decline in 2020, positive shows an increase. Locations with * denote that NO_x emissions are not representative of the entire time period. Locations with N/A represent absent data.

the corresponding months for the period 2016-2019. Mumbai was not included in the subsequent analysis as at the time of this work CrIS data was only available for 2020.

4.3 IMPACT OF COVID-19 NO_x REDUCTIONS ON PANs OVER SELECT MEGACITIES

Figure 4.3 presents the mean concentrations of tropospheric column NO₂, HCHO, free tropospheric PANs, and surface NO_x emissions for each megacity for the time periods listed in Table 4.1. The darker colored bars represent the mean of this time period for years 2016-2019 whereas the lighter colored bars represent the same period in 2020. We performed a Mann-Whitney U-Test to test the significance of changes to PANs during the respective time periods of COVID-19 NO₂ perturbations listed in Table 4.1. The population representing 2020 is compared to the population representing the means of the same time period from 2016-2019. We set our alpha at 0.1, so p values < 0.1 are considered significant and receive more discussion.

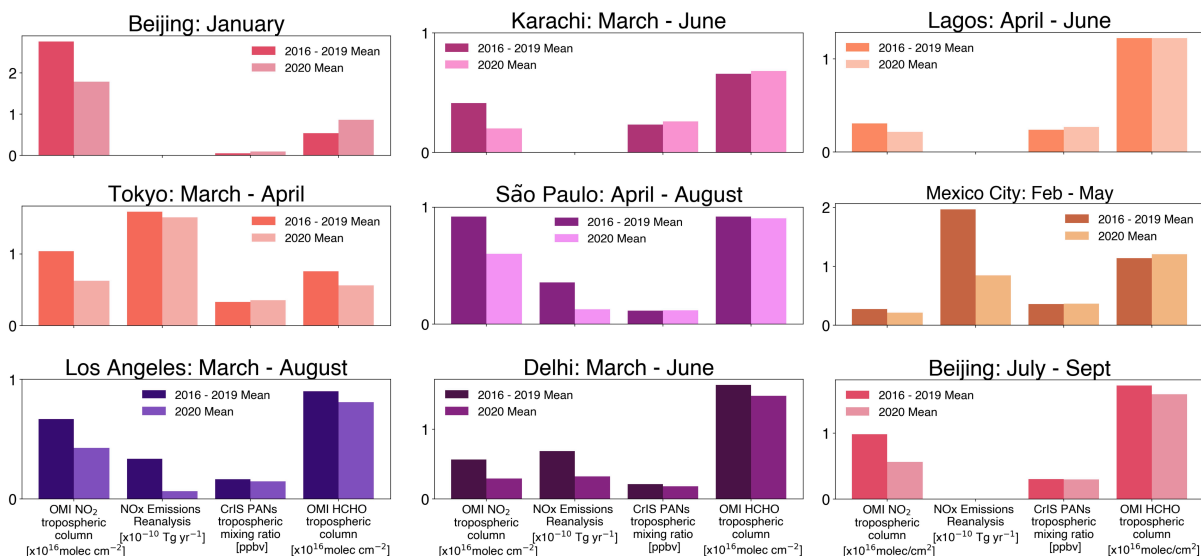


Figure 4.3: Histograms comparing monthly means for specified months of OMI NO₂ tropospheric column [$\times 10^{16}$ molecules cm⁻²], NO_x emissions from the Tropospheric Chemical Reanalysis [$\times 10^{-10}$ Tg yr⁻¹], CrIS free troposphere PANs [ppbv], and OMI HCHO tropospheric column [$\times 10^{16}$ molecules cm⁻²]. Means of monthly means for specified periods in 2020 are shown in the lighter colors and means of 2016, 2017, 2018, and 2019 are shown using the darker colors.

Figure 4.3 shows that while there were large NO₂ declines at some point in 2020, this did not yield a similarly large change in free tropospheric PANs for each region. Most megacities surveyed did not show a significant change in PAN at the 90 % confidence level, except for Los Angeles, which showed a significant decline ($p = 0.06$), and Beijing, which showed a significant increase ($p = 0.03$). The following paragraphs discuss these findings in the context of recent literature.

The COVID lockdown time period has been shown to correspond with increases in urban O₃ (Connerton et al., 2020; Le et al., 2020; Sicard et al., 2020; Venter et al., 2020; Qiu et al., 2020b; Khan, 2021; Miyazaki et al., 2021; Schroeder et al., 2022) and PANs (Qiu et al., 2020b) in some megacities, despite reductions in anthropogenic NO_x emissions due to transitions to a more NO_x limited O₃ production regime. For the period of decreased mean tropospheric column NO₂ during 2020, Beijing, Karachi, and Lagos exhibited increases in PANs; Los Angeles and Delhi display a decrease in PANs; São Paulo, Mexico City and Tokyo show less than a 10 % increase (Table 4.1).

The largest and only significant increase in free tropospheric PANs in our analysis are observed over urban Beijing (79.8 %, $p = 0.03$). Qiu et al. [2020b] reported a threefold increase in ground-level PAN measured in urban Beijing during the first lockdown period in late January through mid February, connected to enhanced local photochemistry and abnormal meteorological conditions, including anomalous wind convergence under higher temperatures. We find a similar change in free tropospheric PANs over Beijing, where mean urban CrIS PANs are 2.4 times higher during the lockdown period from 24 Jan 2020 through 15 Feb 2020. Beijing had a second period of NO_2 decline in July and August 2020, which was associated with a minor decrease in PANs (-1.96 %, $p = 0.31$), suggesting a seasonality in sensitivity to precursor emissions. Other recent studies have placed the Beijing region in the VOC-limited O_3 production regime, where sharp declines in NO_x lead to increases in O_3 (Le et al., 2020; Miyazaki et al., 2020c; Shi and Brasseur, 2020; Huang et al., 2021; Liu et al., 2021; Shi et al., 2021; Guo et al., 2021; Zhang et al., 2022b).

Los Angeles and Delhi displayed a decrease in all species shown in Figure 4.3, coinciding with reported decreases in surface O_3 in both cities during this period (Connerton et al., 2020; Sharma et al., 2020; Rathod et al., 2021; Vega et al., 2021; Shankar and Gadi, 2022; Schroeder et al., 2022). Daily mean PANs over Los Angeles and Delhi during the time period of lower NO_2 decreased by 11 % and 27 %, respectively, though only decreases in Los Angeles are statistically significant at the 90 % confidence interval ($p = 0.06$, $p = 0.33$). The underlying photochemical environment of Los Angeles has been transitioning from a VOC-limited regime to a NO_x -limited regime in recent years (Lee et al., 2021b; Schroeder et al., 2022), and spring 2020 was the first year on record to be NO_x -limited on average (Schroeder et al., 2022). This contributed to decreases in O_3 associated with decreases in NO_x , though these decreases are highly non-linear. O_3 production over Delhi is also considered to be NO_x -limited (Vega et al., 2021; Shankar and Gadi, 2022).

Karachi and Lagos show non-significant increases in PANs (27 %, $p = 0.14$; 12 %, $p = 0.33$) in Figure 4.3. Lagos and Karachi experienced increases in O_3 associated with COVID despite reductions in precursor emissions (Fuwape et al., 2021; Khan, 2021).

Mexico City and São Paulo had statistically insignificant increases in PANs (1.75 %, $p = 0.45$; 3.7 %, $p = 0.33$) Tokyo was on the cusp of significance ($p = 0.11$, 6.9 %) during the respective periods in Table 4.1. Prior work indicates that O_3 over Tokyo did not significantly change with COVID-19 lockdown measures (Ito et al., 2021; Wang and Li, 2021; Damiani et al., 2022). These studies attribute this to a shift in the underlying photochemical regime from VOC-limited towards the transition zone where O_3 production is expected to be equally sensitive to changes in both NO_x and VOCs. Peralta et al. [2021] reported that O_3 in Mexico City was statistically indistinguishable during periods of substantial precursor reduction in 2020 from that of other years. They showed that reductions in NO_x forced the underlying photochemical regime to move from VOC-limited towards a transition zone to more NO_x -limited, similar to Tokyo. São Paulo experienced an increase in O_3 attributable to reduction in vehicle emissions and relative humidity, as March is the end of the rainy season (Connerton et al., 2020). Free tropospheric PANs over Tokyo during the summer (June and July) of 2020 (not shown) were not significantly different from non-COVID years (-0.85 %, $p = 0.95$), suggesting a possible minor seasonal dependence in the sensitivity of PANs to precursors, similar to Beijing.

The response of PANs to a major change in precursor emissions is highly non-linear and depends on environmental factors. We analyzed possible changes in 2 meter air temperature and 500 hPa air temperature between the two respective periods over each of the megacities discussed above using MERRA-2 Reanalysis monthly mean product (GMAO, 2015; DOI:10.5067/AP1B0BA5PD2K). We find no significant change in mean temperature at either pressure levels between 2020 and corresponding months during the prior 3 years. Locations where temperatures did change, albeit insignificantly, the 2020 temperature difference would serve to diminish observed changes to PANs. For example, in Beijing, temperatures were slightly higher than the mean of previous years at both pressure levels (2-Meter temperature 2016-2019: 268 K; 2020: 270.5 K; 500 hPa temperature 2016-2019: 244 K; 2020: 246 K), which would decrease the lifetime of PANs. We find an overall significant increase in PANs in Beijing. Temperature was not likely not a significant factor influencing anomalies in PANs during the periods of NO_x perturbations.

Chapter 5

CONCLUSIONS AND FUTURE WORK

5.1 CONCLUSIONS

We use CrIS data from 2016-2021 to investigate the spatial and temporal variability of PANs over 9 megacities and identify periods of elevated production of PANs. We use this to inform our analysis in diagnosing the impact of NO_2 declines related to the COVID-19 pandemic on PANs in 8 locations. This is the first detailed analysis of satellite observations over multiple megacities.

1. We use a period with densely spaced TES observations of megacities from 2013-2015 to investigate the cities with the largest mean detected PANs from this period. The mean TES free tropospheric PAN mixing ratios for observations over Mexico City was 0.35 ppbv. Mexico City showed the highest mean PAN values of all the 19 megacities sampled by TES during this period.
2. S-NPP CrIS and TES observations show that PANs are enhanced around urban Mexico City with a strong seasonality. The largest difference between the urban enhancement and nearby background occurs in April and reaches a minimum in winter months (October, November, December). A seasonal maximum in PANs occurs in April and May. The seasonal peak in Mexico City PANs co-occurs with springtime seasonal maxima in surface O_3 , CrIS CO, MODIS fire counts, and tropospheric OMI HCHO. Seasonal maximums in local photochemistry and fire activity both contribute to the seasonal maxima in PANs.
3. We find that extreme fire years are associated with higher monthly mean PANs than low-fire years. However, missing observations in 2019, which was a severe fire year, make it difficult to fully quantify the effect of fires on the observed interannual variability of PANs over Mexico City during the month of May. JPSS-1 radiances are available for this time period

but the JPSS-1 CrIS PANs retrievals for dense sampling over MCMA are not available at the time of this submission.

4. We use S-NPP CrIS data to probe the spatial outflow pattern of PANs produced within urban Mexico City during April. We show that outflow occurs to the NE of Mexico City and over the mountains south of Mexico City. Outflow to the NW appears infrequently.
5. We see a secondary peak in PANs in July and August that is not associated with increase in surface O_3 . Analysis of model results indicate that there are multiple NO_x sources that contribute to this feature, and the PAN enhancement is located higher aloft (i.e. at 400 hPa versus 750 hPa).
6. We examine time series of surface NO_x measurements alongside OMI tropospheric NO_2 to analyze changes to Mexico City NO_2 during our study period. We find a statistically significant difference (decrease) in NO_2 between 2018 and 2019. CrIS PANs for the same period do not show the same significant decrease, nor does tropospheric OMI HCHO.
7. There are pronounced seasonal cycles in PANs over each megacity. Monthly mean PANs peak in the spring or summer (Beijing and Karachi), aligning with seasonal maximums in photochemical activity. Wildfire smoke can occasionally enhance monthly mean PANs.
8. Despite large changes in tropospheric NO_2 columns associated with the COVID-19 pandemic, we only identify two megacities over which PANs changed significantly: Beijing and Los Angeles. The relative response of PANs in these locations was smaller than the changes in NO_2 .
9. Sensitivity of free tropospheric PANs to the abundance of precursors appears to be seasonally dependent in Beijing and Tokyo. PANs over Beijing and Tokyo are more sensitive to NO_x reductions in winter and spring respectively.

The work presented here provides new information on the seasonality of PANs over 9 different megacities and the response of tropospheric PANs to major perturbations in NO_x emissions using

the natural experiment provided by the COVID-19 pandemic. We show that like O_3 , understanding the response of PANs to a major change in precursor emissions is highly non-linear. The analysis approach applied here has the potential to be applied to different megacities and regions of interest.

5.2 FUTURE WORK

A global dataset of CrIS PANs retrievals will eventually be routinely processed, but at the time of this work, selected regions and time periods were chosen for processing. In some megacities, this area with processed CrIS retrievals around an individual megacity was sufficient to explore regions of potential pollutant outflow from the urban center into the surrounding atmosphere, as was shown for Mexico City. However, for megacities that have strong influence from surrounding megacities, like the megacities of Eastern China, these current retrieval processing boxes are too small to provide information on outflow or regional enhancements. Figure 5.1 presents gridded monthly mean CrIS PANs data for the box surrounding Beijing. The entire box displays enhanced PANs from March-August without any localized enhancement around urban Beijing. The Beijing region is heavily influenced by emissions from Tianjin and cities in the Hebei Province (Streets et al., 2007; Zhang et al., 2017), making it difficult to extract enhancements with a box localized around only Beijing. Export of pollutants from Eastern Asia can influence pollutant concentrations in the United States via intercontinental transport (Lee et al., 2021a), making this an important region to understand primary pathways and seasonality of pollutant outflow. This analysis could be possible with a larger area of CrIS observations. CrIS observations across the Pacific would allow for further exploration of this intercontinental transport.

TES and CrIS observations used in this work were not directly comparable for a number of reasons. The two data records span different time periods (2013-2015 vs 2016-2021), use different spectral features (1150 cm^{-1} vs 790 cm^{-1}), and use different types of retrievals (linear vmr vs log vmr). The CrIS retrievals used in this work are done using NASA L1B full spectral resolution (FSR) radiances. The CrIS FSR L1B product is available beginning 2 November 2015, as prior to December 2014 the full amount of data needed to construct the FSR was not transmitted to the ground, so the radiances were reported at nominal spectral resolution (NSR). Additional points

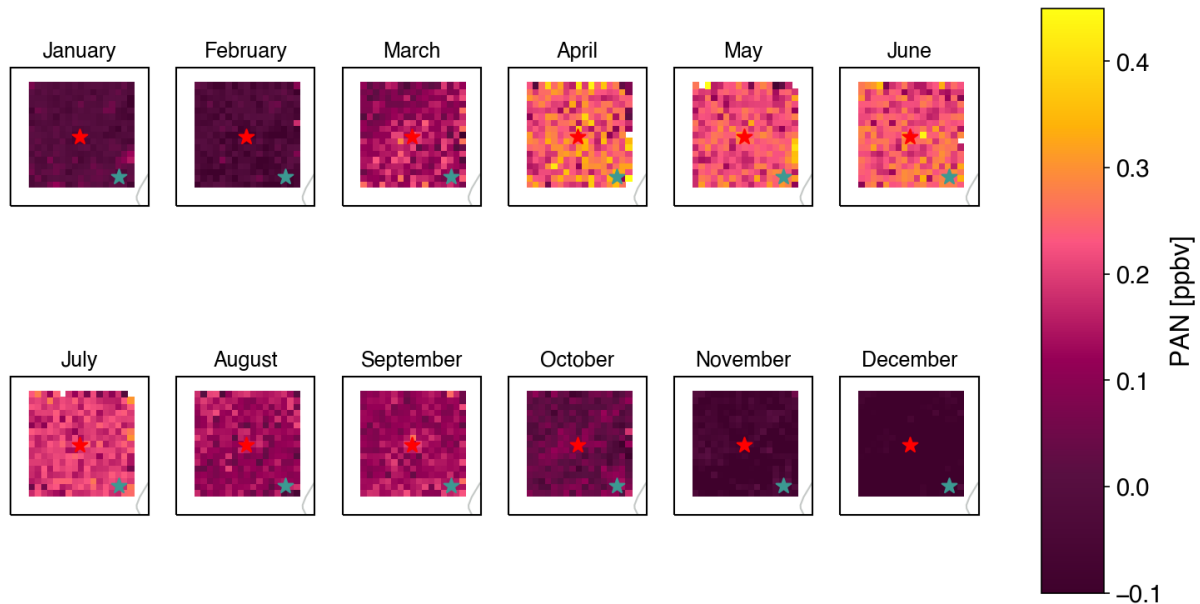


Figure 5.1: Monthly mean gridded CrIS data for January 2016-May 2021. Beijing is denoted by the red star and Tianjin is denoted by the teal star. Note that water vapor correction filtering was not applied to these retrievals.

were included at the ends of the longwave and shortwave interferograms to improve the quality of the calibration in November 2015 in order to be able to report at FSR. CrIS retrievals prior to November 2015 are reported at NSR, which overlaps with the TES megacity transect period. A more direct comparison between TES and CrIS could be possible with an overlapping time period (taking into account the differences in retrieval and spectral features) using the NSR retrievals. Additional work could be done with comparing the CrIS NSR and FSR retrievals in megacities to evaluate consistency for the time period where we have both.

An additional avenue for further work with this dataset would be to explore local vs regional enhancements in PANs over and around megacities. In our analysis determining local seasonal cycles of PANs and using monthly averaged gridded CrIS PANs for each city (A.5-A.15), we find some seasonal enhancements shown in Figure 4.1 to be regional and some to be very local around the urban center. For example, Figure 4.1 shows enhancements in PANs over urban Delhi in April-October. Figure A.10 displays the monthly mean for the CrIS box around Delhi, with non-localized enhancements over the entire box in May-June. However, October, displays a clear

localized enhancement over the Delhi/New Delhi megacity. These differences in local versus regional enhancements are not fully captured in Figure 4.1. Further exploration of extreme seasonal local enhancements around urban centers have the potential to inform decisions regarding emissions control for select time periods.

The megacities used in this study were chosen based on availability of processed CrIS megacity densely sampled data. This work has shown that the resolution of CrIS is sufficient to quantify urban enhancements and seasonal cycles of PANs in megacities. Understanding of the spatiotemporal variability of enhanced PANs in urban regions can be greatly increased using CrIS so further work could include applying these methods to other global megacities and regions of interest.

Bibliography

- B.R. Gurjar and J. Lelieveld. New Directions: Megacities and global change. *Atmospheric Environment*, 39(2):391–393, January 2005. ISSN 13522310. doi: 10.1016/j.atmosenv.2004.11.002. URL <https://linkinghub.elsevier.com/retrieve/pii/S1352231004010179>.
- UN/DESA. The World's Cities in 2018. Technical report, 2018. URL https://www.flickr.com/photos/thisisin%0Ahttps://www.un.org/en/events/citiesday/assets/pdf/the_worlds_cities_in_2018_data_booklet.pdf.
- D. Mage, G. Ozolins, P. Peterson, A. Webster, R. Orthofer, V. Vandeweerd, and M. Gwynne. Urban air pollution in megacities of the world. 30(5):681–868, 1996. doi: [https://doi.org/10.1016/1352-2310\(95\)00219-7](https://doi.org/10.1016/1352-2310(95)00219-7).
- Sasha Madronich. Chemical evolution of gaseous air pollutants down-wind of tropical megacities: Mexico City case study. *Atmospheric Environment*, 40(31):6012–6018, October 2006. ISSN 13522310. doi: 10.1016/j.atmosenv.2005.08.047. URL <https://linkinghub.elsevier.com/retrieve/pii/S1352231006000963>.
- M. G. Lawrence, T.M. Butler, J. Steinkamp, B.R. Gurjar, and J. Lelieveld. Regional pollution potentials of megacities and other major population centers. 7:3969–3987, 2007. doi: www.atmos-chem-phys.net/7/3969/2007/. OCLC: 77006337.
- Timothy M. Butler and Mark G. Lawrence. The influence of megacities on global atmospheric chemistry: a modelling study. *Environmental Chemistry*, 6(3):219, 2009. ISSN 1448-2517. doi: 10.1071/EN08110. URL <http://www.publish.csiro.au/?paper=EN08110>.
- Luisa T. Molina. Introductory lecture: air quality in megacities. *Faraday Discussions*, 226:9–52, 2021. ISSN 1359-6640, 1364-5498. doi: 10.1039/D0FD00123F. URL <http://xlink.rsc.org/?DOI=D0FD00123F>.
- Hanwant B. Singh and Philip L. Hanst. Peroxyacetyl nitrate (PAN) in the unpolluted atmosphere: An important reservoir for nitrogen oxides. *Geophysical Research Letters*, 8(8):941–944, August 1981. ISSN 00948276. doi: 10.1029/GL008i008p00941. URL <http://doi.wiley.com/10.1029/GL008i008p00941>.
- Hanwant B. Singh, Louis J. Salas, and William Viezee. Global distribution of peroxyacetyl nitrate. *Nature*, 321(6070):588–591, June 1986. ISSN 0028-0836, 1476-4687. doi: 10.1038/321588a0. URL <http://www.nature.com/articles/321588a0>.
- Jeffrey S Gaffney, Nancy A Marley, and Paul J Drayton. FAST GAS CHROMATOGRAPHY WITH LUMINOL DETECTION FOR MEASUREMENT OF NITROGEN DIOXIDE AND PANs. page 8, 1986.
- James M. Roberts. PAN and Related Compounds. In Ralf Koppmann, editor, *Volatile Organic Compounds in the Atmosphere*, pages 221–268. Blackwell Publishing Ltd, Oxford, UK, November 2007. ISBN 978-0-470-98865-7 978-1-4051-3115-5. doi: 10.1002/9780470988657.ch6. URL <https://onlinelibrary.wiley.com/doi/10.1002/9780470988657.ch6>.

- E. V. Fischer, D. J. Jacob, R. M. Yantosca, M. P. Sulprizio, D. B. Millet, J. Mao, F. Paulot, H. B. Singh, A. Roiger, L. Ries, R.W. Talbot, K. Dzepina, and S. Pandey Deolal. Atmospheric peroxyacetyl nitrate (PAN): a global budget and source attribution. *Atmospheric Chemistry and Physics*, 14(5):2679–2698, March 2014. ISSN 1680-7324. doi: 10.5194/acp-14-2679-2014. URL <https://acp.copernicus.org/articles/14/2679/2014/>.
- Leon E. Smith. Inhalation of the Photochemical Smog Compound Peroxyacetyl Nitrate. *American Journal of Public Health and the Nations Health*, 55(9):1460–1468, September 1965. ISSN 0002-9572. doi: 10.2105/AJPH.55.9.1460. URL <https://ajph.aphapublications.org/doi/full/10.2105/AJPH.55.9.1460>.
- A.P. Altshuller. Assessment of the Contribution of Chemical Species to The Eye Irritation Potential of Photochemical Smog. *Journal of the Air Pollution Control Association*, 28(6):594–598, June 1978. ISSN 0002-2470. doi: 10.1080/00022470.1978.10470634. URL <http://www.tandfonline.com/doi/abs/10.1080/00022470.1978.10470634>.
- A Vyskocil, C. Viau, and S. Lamy. Peroxyacetyl nitrate: review of toxicity. pages 212–220, 1998. doi: <https://doi.org/10.1177/096032719801700403>.
- O. C. Taylor. Importance of Peroxyacetyl Nitrate (PAN) as a Phytotoxic Air Pollutant. *Journal of the Air Pollution Control Association*, 19(5):347–351, May 1969. ISSN 0002-2470. doi: 10.1080/00022470.1969.10466498. URL <http://www.tandfonline.com/doi/abs/10.1080/00022470.1969.10466498>.
- Paul B. Shepson, Tadeusz E. Kleindienst, Edward O. Edney, Chris M. Nero, Larry T. Cupitt, and Larry D. Claxton. Acetaldehyde: the mutagenic activity of its photooxidation products. *Environmental Science & Technology*, 20(10):1008–1013, October 1986. ISSN 0013-936X, 1520-5851. doi: 10.1021/es00152a007. URL <https://pubs.acs.org/doi/abs/10.1021/es00152a007>.
- Tadeusz E. Kleindienst, Paul B. Shepson, D.F. Smith, E.E. Hudgens, Chris M. Nero, Larry T. Cupitt, J.J. Bufalini, L.D. Caxton, and F.R. Nestman. Comparison of mutagenic activities of several peroxyacetyl nitrates. 16(2):70–80, 1990. doi: <https://doi.org/10.1002/em.2850160204>.
- B Rappenglück, D Melas, and P Fabian. Evidence of the impact of urban plumes on remote sites in the Eastern Mediterranean. *Atmospheric Environment*, 37(13):1853–1864, April 2003. ISSN 13522310. doi: 10.1016/S1352-2310(03)00065-7. URL <https://linkinghub.elsevier.com/retrieve/pii/S1352231003000657>.
- Allison L. Steiner, Adam J. Davis, Sanford Sillman, Robert C. Owen, Anna M. Michalak, and Arlene M. Fiore. Observed suppression of ozone formation at extremely high temperatures due to chemical and biophysical feedbacks. *Proceedings of the National Academy of Sciences*, 107(46):19685–19690, November 2010. ISSN 0027-8424, 1091-6490. doi: 10.1073/pnas.1008336107. URL <https://pnas.org/doi/full/10.1073/pnas.1008336107>.
- S Sillman and J J West. Reactive nitrogen in Mexico City and its relation to ozone-precursor sensitivity: results from photochemical models. *Atmos. Chem. Phys.*, page 13, 2009.

- Richard E. Honrath, Amy J. Hamlin, and John T. Merrill. Transport of ozone precursors from the arctic troposphere to the north atlantic region. *Journal of Geophysical Research: Atmospheres*, 101(D22):29335–29351, 1996. doi: <https://doi.org/10.1029/95JD02673>. URL <https://agupubs.onlinelibrary.wiley.com/doi/abs/10.1029/95JD02673>.
- Rahul A. Zaveri. Ozone production efficiency and NO_x depletion in an urban plume: Interpretation of field observations and implications for evaluating O₃-NO_x-VOC sensitivity. *Journal of Geophysical Research*, 108(D14):4436, 2003. ISSN 0148-0227. doi: 10.1029/2002JD003144. URL <http://doi.wiley.com/10.1029/2002JD003144>.
- E. V. Fischer, D. A. Jaffe, D. R. Reidmiller, and L. Jaeglé. Meteorological controls on observed peroxyacetyl nitrate at Mount Bachelor during the spring of 2008. *Journal of Geophysical Research*, 115(D3):D03302, February 2010. ISSN 0148-0227. doi: 10.1029/2009JD012776. URL <http://doi.wiley.com/10.1029/2009JD012776>.
- M Mena-Carrasco, G R Carmichael, J E Campbell, D Zimmerman, Y Tang, B Adhikary, A D'allura, L T Molina, M Zavala, A Garcia, F Flocke, T Campos, A J Weinheimer, R Shetter, E Apel, D D Montzka, D J Knapp, and W Zheng. Assessing the regional impacts of Mexico City emissions on air quality and chemistry. *Atmos. Chem. Phys.*, page 13, 2009.
- Zhe Jiang, John R. Worden, Vivienne H. Payne, Liye Zhu, Emily Fischer, Thomas Walker, and Dylan B. A. Jones. Ozone export from East Asia: The role of PAN. *Journal of Geophysical Research: Atmospheres*, 121(11):6555–6563, June 2016. ISSN 2169-897X, 2169-8996. doi: 10.1002/2016JD024952. URL <https://onlinelibrary.wiley.com/doi/10.1002/2016JD024952>.
- P. Schneider, W. A. Lahoz, and R. van der A. Recent satellite-based trends of tropospheric nitrogen dioxide over large urban agglomerations worldwide. *Atmospheric Chemistry and Physics*, 15(3):1205–1220, February 2015. ISSN 1680-7324. doi: 10.5194/acp-15-1205-2015. URL <https://acp.copernicus.org/articles/15/1205/2015/>.
- Agnes Borbon, J. B. Gilman, W. C. Kuster, N. Grand, S. Chevaillier, A. Colomb, C. Dolgorouky, V. Gros, M. Lopez, R. Sarda-Esteve, J. Holloway, J. Stutz, H. Petetin, S. McKeen, M. Beekmann, C. Warneke, D. D. Parrish, and J. A. de Gouw. Emission ratios of anthropogenic volatile organic compounds in northern mid-latitude megacities: Observations versus emission inventories in Los Angeles and Paris: VOC EMISSION RATIOS IN MODERN MEGACITIES. *Journal of Geophysical Research: Atmospheres*, 118(4):2041–2057, February 2013. ISSN 2169897X. doi: 10.1002/jgrd.50059. URL <http://doi.wiley.com/10.1002/jgrd.50059>.
- A. Hilboll, A. Richter, and J. P. Burrows. Long-term changes of tropospheric NO₂ over megacities derived from multiple satellite instruments. *Atmospheric Chemistry and Physics*, 13(8):4145–4169, April 2013. ISSN 1680-7324. doi: 10.5194/acp-13-4145-2013. URL <https://acp.copernicus.org/articles/13/4145/2013/>.
- Aristeidis K. Georgoulias, Ronald J. van der A, Piet Stammes, K. Folkert Boersma, and Henk J. Eskes. Trends and trend reversal detection in 2 decades of tropospheric NO₂; satellite observations. *Atmospheric Chemistry and Physics*, 19(9):6269–6294, May 2019. ISSN 1680-7324. doi: 10.5194/acp-19-6269-2019. URL <https://acp.copernicus.org/articles/19/6269/2019/>.

- J S Gaffney. Peroxyacyl Nitrates (PANs): Their Physical and Chemical Properties. 1986.
- J S Gaffney. Measurements of peroxyacyl nitrates (PANS) in Mexico City: implications for megacity air quality impacts on regional scales. *Atmospheric Environment*, page 10, 1999.
- Gangwoong Lee, Yuwoon Jang, Heayoung Lee, Jin-Seok Han, Kyung-Ryul Kim, and Meehye Lee. Characteristic behavior of peroxyacetyl nitrate (PAN) in Seoul megacity, Korea. *Chemosphere*, 73(4):619–628, September 2008. ISSN 00456535. doi: 10.1016/j.chemosphere.2008.05.060. URL <https://linkinghub.elsevier.com/retrieve/pii/S0045653508006590>.
- Jun-Bok Lee, Joong-Sup Yoon, Kweon Jung, Seok-Won Eom, Young-Zoo Chae, Seog-Ju Cho, Shin-Do Kim, Jong Ryeul Sohn, and Ki-Hyun Kim. Peroxyacetyl nitrate (PAN) in the urban atmosphere. *Chemosphere*, 93(9):1796–1803, November 2013. ISSN 00456535. doi: 10.1016/j.chemosphere.2013.06.019. URL <https://linkinghub.elsevier.com/retrieve/pii/S0045653513008515>.
- Gen Zhang, Yujing Mu, Lingxi Zhou, Chenglong Zhang, Yuanyuan Zhang, Junfeng Liu, Shuangxi Fang, and Bo Yao. Summertime distributions of peroxyacetyl nitrate (PAN) and peroxypropionyl nitrate (PPN) in Beijing: Understanding the sources and major sink of PAN. *Atmospheric Environment*, 103:289–296, February 2015. ISSN 13522310. doi: 10.1016/j.atmosenv.2014.12.035. URL <https://linkinghub.elsevier.com/retrieve/pii/S1352231014009832>.
- Yulu Qiu, Zhiqiang Ma, and Ke Li. A modeling study of the peroxyacetyl nitrate (PAN) during a wintertime haze event in Beijing, China. *Science of The Total Environment*, 650:1944–1953, February 2019. ISSN 00489697. doi: 10.1016/j.scitotenv.2018.09.253. URL <https://linkinghub.elsevier.com/retrieve/pii/S0048969718336970>.
- Yulu Qiu, Zhiqiang Ma, Weili Lin, Weijun Quan, Weiwei Pu, Yingruo Li, Liyan Zhou, and Qingfeng Shi. A study of peroxyacetyl nitrate at a rural site in Beijing based on continuous observations from 2015 to 2019 and the WRF-Chem model. *Frontiers of Environmental Science & Engineering*, 14(4):71, August 2020a. ISSN 2095-2201, 2095-221X. doi: 10.1007/s11783-020-1250-0. URL <https://link.springer.com/10.1007/s11783-020-1250-0>.
- Yulu Qiu, Zhiqiang Ma, Ke Li, Mengyu Huang, Jiujiang Sheng, Ping Tian, Jia Zhu, Weiwei Pu, Yingxiao Tang, Tingting Han, Huaigang Zhou, and Hong Liao. Measurement report: Fast photochemical production of peroxyacetyl nitrate (PAN) over the rural North China Plain during cold-season haze events. preprint, Gases/Field Measurements/Troposphere/Chemistry (chemical composition and reactions), June 2021. URL <https://acp.copernicus.org/preprints/acp-2021-359/acp-2021-359.pdf>.
- J. M. Roberts, J. Williams, K. Baumann, M. P. Buhr, P. D. Goldan, J. Holloway, G. Hübler, W. C. Kuster, S. A. McKeen, T. B. Ryerson, M. Trainer, E. J. Williams, F. C. Fehsenfeld, S. B. Bertman, G. Nouaime, C. Seaver, G. Grodzinsky, M. Rodgers, , and V. L. Young. Measurements of pan, ppn, and mpan made during the 1994 and 1995 nashville intensives of the southern oxidant study: Implications for regional ozone production from biogenic hydrocarbons. *Journal of Geophysical Research*, 103:22473–22490, 1998. doi: doi:10.1029/98jd01637.

- J. M. Roberts, F. Flocke, C. A. Stroud, D. Hereid, E. Williams, F. Fehsenfeld, W. Brune, M. Martinez, and H. Harder. Ground-based measurements of peroxy-carboxylic nitric anhydrides (pans) during the 1999 southern oxidants study nashville intensive. *J. Geophys. Res.*, 107:ACH 1–1–ACH 1–10, 2002. doi: doi:10.1029/2001jd000947.
- G. M. Wolfe, J. A. Thornton, V. F. McNeill, D. A. Jaffe, D. Reidmiller, D. Chand, J. Smith, P. Swartzendruber, F. Flocke, and W. Zheng.
- N Glatthor, M Milz, T Steck, and G P Stiller. Global peroxyacetyl nitrate (PAN) retrieval in the upper troposphere from limb emission spectra of the Michelson Interferometer for Passive Atmospheric Sounding (MIPAS). *Atmos. Chem. Phys.*, page 13, 2007.
- D. P. Moore and J. J. Remedios. Seasonality of Peroxyacetyl nitrate (PAN) in the upper troposphere and lower stratosphere using the MIPAS-E instrument. *Atmospheric Chemistry and Physics*, 10 (13):6117–6128, July 2010. ISSN 1680-7324. doi: 10.5194/acp-10-6117-2010. URL <https://acp.copernicus.org/articles/10/6117/2010/>.
- A. Wiegele, N. Glatthor, M. Höpfner, U. Grabowski, S. Kellmann, A. Linden, G. Stiller, and T. von Clarmann. Global distributions of C_2H_6 , C_2H_2 , H_2 , HCN, and PAN retrieved from MIPAS reduced spectral resolution measurements. *Atmospheric Measurement Techniques*, 5(4):723–734, April 2012. ISSN 1867-8548. doi: 10.5194/amt-5-723-2012. URL <https://amt.copernicus.org/articles/5/723/2012/>.
- K. A. Tereszchuk, D. P. Moore, J. J. Harrison, C. D. Boone, M. Park, J. J. Remedios, W. J. Randel, and P. F. Bernath. Observations of peroxyacetyl nitrate (PAN) in the upper troposphere by the Atmospheric Chemistry Experiment-Fourier Transform Spectrometer (ACE-FTS). *Atmospheric Chemistry and Physics*, 13(11):5601–5613, June 2013. ISSN 1680-7324. doi: 10.5194/acp-13-5601-2013. URL <https://acp.copernicus.org/articles/13/5601/2013/>.
- Richard J. Pope, Nigel A. D. Richards, Martyn P. Chipperfield, David P. Moore, Sarah A. Monks, Stephen R. Arnold, Norbert Glatthor, Michael Kiefer, Tom J. Breider, Jeremy J. Harrison, John J. Remedios, Carsten Warneke, James M. Roberts, Glenn S. Diskin, Lewis G. Huey, Armin Wisthaler, Eric C. Apel, Peter F. Bernath, and Wuhu Feng. Intercomparison and evaluation of satellite peroxyacetyl nitrate observations in the upper troposphere–lower stratosphere. *Atmospheric Chemistry and Physics*, 16(21):13541–13559, November 2016. ISSN 1680-7324. doi: 10.5194/acp-16-13541-2016. URL <https://acp.copernicus.org/articles/16/13541/2016/>.
- Jörn Ungermann, Manfred Ern, Martin Kaufmann, Rolf Müller, Reinhold Spang, Felix Ploeger, Bärbel Vogel, and Martin Riese. Observations of PAN and its confinement in the Asian summer monsoon anticyclone in high spatial resolution. *Atmospheric Chemistry and Physics*, 16(13): 8389–8403, July 2016. ISSN 1680-7324. doi: 10.5194/acp-16-8389-2016. URL <https://acp.copernicus.org/articles/16/8389/2016/>.
- V. H. Payne, M. J. Alvarado, K. E. Cady-Pereira, J. R. Worden, S. S. Kulawik, and E. V. Fischer. Satellite observations of peroxyacetyl nitrate from the Aura Tropospheric Emission Spectrometer. *Atmospheric Measurement Techniques*, 7(11):3737–3749, November 2014. ISSN 1867-8548. doi: 10.5194/amt-7-3737-2014. URL <https://amt.copernicus.org/articles/7/3737/2014/>.

- B. Franco, L. Clarisse, T. Stavrou, J.-F. Müller, M. Van Damme, S. Whitburn, J. Hadji-Lazarou, D. Hurtmans, D. Taraborrelli, C. Clerbaux, and P.-F. Coheur. A General Framework for Global Retrievals of Trace Gases From IASI: Application to Methanol, Formic Acid, and PAN. *Journal of Geophysical Research: Atmospheres*, 123(24), December 2018. ISSN 2169-897X, 2169-8996. doi: 10.1029/2018JD029633. URL <https://onlinelibrary.wiley.com/doi/abs/10.1029/2018JD029633>.
- V. H. Payne, S. S. Kulawik, E. V. Fischer, J. F. Brewer, L. G. Huey, K. Miyazaki, J. R. Worden, K. W. Bowman, E. J. Hints, F. Moore, J. W. Elkins, and J. Juncosa Calahorrano. Satellite measurements of peroxyacetyl nitrate from the cross-track infrared sounder: comparison with atom aircraft measurements. *Atmospheric Measurement Techniques*, 15(11):3497–3511, 2022. doi: 10.5194/amt-15-3497-2022. URL <https://amt.copernicus.org/articles/15/3497/2022/>.
- Matthew J. Alvarado, Karen E. Cady-Pereira, Yaping Xiao, Dylan B. Millet, and Vivienne H. Payne. Emission Ratios for Ammonia and Formic Acid and Observations of Peroxy Acetyl Nitrate (PAN) and Ethylene in Biomass Burning Smoke as Seen by the Tropospheric Emission Spectrometer (TES). *Atmosphere*, 2(4):633–654, November 2011. ISSN 2073-4433. doi: 10.3390/atmos2040633. URL <http://www.mdpi.com/2073-4433/2/4/633>.
- Lieven Clarisse, Yasmina R'Honi, Pierre-François Coheur, Daniel Hurtmans, and Cathy Clerbaux. Thermal infrared nadir observations of 24 atmospheric gases: TRACE GAS OBSERVATIONS FROM IASI. *Geophysical Research Letters*, 38(10):n/a–n/a, May 2011. ISSN 00948276. doi: 10.1029/2011GL047271. URL <http://doi.wiley.com/10.1029/2011GL047271>.
- Julieta F. Juncosa Calahorrano, Vivienne H. Payne, Susan Kulawik, Bonne Ford, Frank Flocke, Teresa Campos, and Emily V. Fischer. Evolution of Acyl Peroxynitrates (PANs) in Wildfire Smoke Plumes Detected by the Cross-Track Infrared Sounder (CrIS) Over the Western U.S. During Summer 2018. *Geophysical Research Letters*, 48(23), December 2021. ISSN 0094-8276, 1944-8007. doi: 10.1029/2021GL093405. URL <https://onlinelibrary.wiley.com/doi/10.1029/2021GL093405>.
- Liye Zhu, Emily V. Fischer, Vivienne H. Payne, John R. Worden, and Zhe Jiang. TES observations of the interannual variability of PAN over Northern Eurasia and the relationship to springtime fires. *Geophysical Research Letters*, 42(17):7230–7237, September 2015. ISSN 0094-8276, 1944-8007. doi: 10.1002/2015GL065328. URL <https://onlinelibrary.wiley.com/doi/10.1002/2015GL065328>.
- Liye Zhu, Vivienne H. Payne, Thomas W. Walker, John R. Worden, Zhe Jiang, Susan S. Kulawik, and Emily V. Fischer. PAN in the eastern Pacific free troposphere: A satellite view of the sources, seasonality, interannual variability, and timeline for trend detection. *Journal of Geophysical Research: Atmospheres*, 122(6):3614–3629, March 2017. ISSN 2169-897X, 2169-8996. doi: 10.1002/2016JD025868. URL <https://onlinelibrary.wiley.com/doi/10.1002/2016JD025868>.
- Vivienne H. Payne, Emily V. Fischer, John R. Worden, Zhe Jiang, Liye Zhu, Thomas P. Kurosu, and Susan S. Kulawik. Spatial variability in tropospheric peroxyacetyl nitrate in the tropics from infrared satellite observations in 2005 and 2006. *Atmospheric Chemistry and Physics*, 17(10):6341–6351, May 2017. ISSN 1680-7324. doi: 10.5194/acp-17-6341-2017. URL <https://acp.copernicus.org/articles/17/6341/2017/>.

- Emily V. Fischer, Liye Zhu, Vivienne H. Payne, John R. Worden, Zhe Jiang, Susan S. Kulawik, Steven Brey, Arsineh Hecobian, Daniel Gombos, Karen Cady-Pereira, and Frank Flocke. Using TES retrievals to investigate PAN in North American biomass burning plumes. *Atmospheric Chemistry and Physics*, 18(8):5639–5653, April 2018. ISSN 1680-7324. doi: 10.5194/acp-18-5639-2018. URL <https://acp.copernicus.org/articles/18/5639/2018/>.
- Karen E. Cady-Pereira, Vivienne H. Payne, Jessica L. Neu, Kevin W. Bowman, Kazuyuki Miyazaki, Eloise A. Marais, Susan Kulawik, Zitely A. Tzompa-Sosa, and Jennifer D. Hegarty. Seasonal and spatial changes in trace gases over megacities from Aura TES observations: two case studies. *Atmospheric Chemistry and Physics*, 17(15):9379–9398, August 2017. ISSN 1680-7324. doi: 10.5194/acp-17-9379-2017. URL <https://acp.copernicus.org/articles/17/9379/2017/>.
- L T Molina and M. J. Molina. Air quality in the Mexico megacity: An integrated assessment. *EURE (Santiago)*, 32(96):141–145, 2002.
- L. T. Molina, C. E. Kolb, B. de Foy, B. K. Lamb, W. H. Brune, J. L. Jimenez, R. Ramos-Villegas, J. Sarmiento, V. H. Paramo-Figueroa, B. Cardenas, V. Gutierrez-Avedoy, and M. J. Molina. Air quality in North America’s most populous city – overview of the MCMA-2003 campaign. *Atmospheric Chemistry and Physics*, 7(10):2447–2473, May 2007. ISSN 1680-7324. doi: 10.5194/acp-7-2447-2007. URL <https://acp.copernicus.org/articles/7/2447/2007/>.
- UNEP and WHO. Urban Air Pollution in Megacities of the World. 84(1):117, 1992. doi: <https://doi.org/10.2307/215790>.
- L. T. Molina, S. Madronich, J. S. Gaffney, E. Apel, B. de Foy, J. Fast, R. Ferrare, S. Haddon, J. L. Jimenez, B. Lamb, A. R. Osornio-Vargas, P. Russell, J. J. Schauer, P. S. Stevens, R. Volkamer, and M. Zavala. An overview of the MILAGRO 2006 Campaign: Mexico City emissions and their transport and transformation. *Atmospheric Chemistry and Physics*, 10(18):8697–8760, September 2010. ISSN 1680-7324. doi: 10.5194/acp-10-8697-2010. URL <https://acp.copernicus.org/articles/10/8697/2010/>.
- W Lei, B de Foy, M Zavala, R Volkamer, and L T Molina. Characterizing ozone production in the Mexico City Metropolitan Area: a case study using a chemical transport model. *Atmos. Chem. Phys.*, page 20, 2007.
- W Lei, M Zavala, B de Foy, R Volkamer, and L T Molina. Characterizing ozone production and response under different meteorological conditions in Mexico City. *Atmos. Chem. Phys.*, page 11, 2008.
- Xuexi Tie, Sasha Madronich, GuoHui Li, Zhuming Ying, Renyi Zhang, Agustin R. Garcia, Julia Lee-Taylor, and Yubao Liu. Characterizations of chemical oxidants in Mexico City: A regional chemical dynamical model (WRF-Chem) study. *Atmospheric Environment*, 41(9):1989–2008, March 2007. ISSN 13522310. doi: 10.1016/j.atmosenv.2006.10.053. URL <https://linkinghub.elsevier.com/retrieve/pii/S1352231006010399>.
- J Song, W Lei, N Bei, M Zavala, B de Foy, R Volkamer, B Cardenas, J Zheng, R Zhang, and L T Molina. Ozone response to emission changes: a modeling study during the MCMA-2006/MILAGRO Campaign. *Atmos. Chem. Phys.*, page 20, 2010.

- H.A. Bravo, F.G. Perrin, R. E. Sosa, and Ricardo Torres-Jardón. Results of an air pollution strategy (lead reduction in gasoline) on the air quality of Mexico City. *Proceedings of the 8th Clean Air Congress, Man and his Ecosystem, Elsevier Science Publishers, BV The Hague.*, pages 31–37, 1989.
- MARI. MARI: Mexico City Air Quality Initiative. Technical Report Los Alamos Report #LA-12699, Los Alamos National Laboratory and the Mexican Petroleum Institute, 1994.
- Gerald E. Streit and Francisco Guzmán. Mexico City Air quality: Progress of an international collaborative project to define air quality management options. *Atmospheric Environment*, 30 (5):723–733, March 1996. ISSN 13522310. doi: 10.1016/1352-2310(95)00275-8. URL <https://linkinghub.elsevier.com/retrieve/pii/1352231095002758>.
- Jerome D. Fast and Shiyuan Zhong. Meteorological factors associated with inhomogeneous ozone concentrations within the Mexico City basin. *Journal of Geophysical Research: Atmospheres*, 103(D15):18927–18946, August 1998. ISSN 01480227. doi: 10.1029/98JD01725. URL <http://doi.wiley.com/10.1029/98JD01725>.
- N A Marley, J S Gaffney, R Ramos-Villegas, and B Cardenas Gonzalez. Comparison of measurements of peroxyacyl nitrates and primary carbonaceous aerosol concentrations in Mexico City determined in 1997 and 2003. *Atmos. Chem. Phys.*, page 9, 2007.
- L. K. Emmons, E. C. Apel, J.-F. Lamarque, P. G. Hess, M. Avery, D. Blake, W. Brune, T. Campos, J. Crawford, P. F. DeCarlo, S. Hall, B. Heikes, J. Holloway, J. L. Jimenez, D. J. Knapp, G. Kok, M. Mena-Carrasco, J. Olson, D. O’Sullivan, G. Sachse, J. Walega, P. Weibring, A. Weinheimer, and C. Wiedinmyer. Impact of Mexico City emissions on regional air quality from MOZART-4 simulations. *Atmospheric Chemistry and Physics*, 10(13):6195–6212, July 2010. ISSN 1680-7324. doi: 10.5194/acp-10-6195-2010. URL <https://acp.copernicus.org/articles/10/6195/2010/>.
- Miguel Zavala, William H. Brune, Erik Velasco, Armando Retama, Luis Adrian Cruz-Alavez, and Luisa T. Molina. Changes in ozone production and VOC reactivity in the atmosphere of the Mexico City Metropolitan Area. *Atmospheric Environment*, 238:117747, October 2020. ISSN 13522310. doi: 10.1016/j.atmosenv.2020.117747. URL <https://linkinghub.elsevier.com/retrieve/pii/S1352231020304799>.
- Matteo Chinazzi, Jessica T. Davis, Marco Ajelli, Corrado Gioannini, Maria Litvinova, Stefano Merler, Ana Pastore y Piontti, Kunpeng Mu, Luca Rossi, Kaiyuan Sun, Cécile Viboud, Xinyue Xiong, Hongjie Yu, M. Elizabeth Halloran, Ira M. Longini, and Alessandro Vespignani. The effect of travel restrictions on the spread of the 2019 novel coronavirus (COVID-19) outbreak. *Science*, 368(6489):395–400, April 2020. ISSN 0036-8075, 1095-9203. doi: 10.1126/science.aba9757. URL <https://www.science.org/doi/10.1126/science.aba9757>.
- WHO. Coronavirus disease 2019 (COVID-19): Situation Report – 43. Technical report, 2020. URL www.who.int/docs/default-source/coronaviruse/situation-reports/20200303-sitrep-43-covid-19.pdf?sfvrsn=2c21c09c_2.
- M. Bauwens, S. Compennolle, T. Stavrou, J.-F. Müller, J. Gent, H. Eskes, P. F. Levelt, R. A. J. P. Veefkind, J. Vlietinck, H. Yu, and C. Zehner. Impact of Coronavirus Outbreak on NO₂

- Pollution Assessed Using TROPOMI and OMI Observations. *Geophysical Research Letters*, 47(11), June 2020. ISSN 0094-8276, 1944-8007. doi: 10.1029/2020GL087978. URL <https://onlinelibrary.wiley.com/doi/10.1029/2020GL087978>.
- Kazuyuki Miyazaki, Kevin Bowman, Takashi Sekiya, Henk Eskes, Folkert Boersma, Helen Worden, Nathaniel Livesey, Vivienne H. Payne, Kengo Sudo, Yugo Kanaya, Masayuki Takigawa, and Koji Ogochi. Updated tropospheric chemistry reanalysis and emission estimates, TCR-2, for 2005–2018. *Earth System Science Data*, 12(3):2223–2259, September 2020a. ISSN 1866-3516. doi: 10.5194/essd-12-2223-2020. URL <https://essd.copernicus.org/articles/12/2223/2020/>.
- Shubham Sharma, Mengyuan Zhang, Anshika, Jingsi Gao, Hongliang Zhang, and Sri Harsha Kota. Effect of restricted emissions during COVID-19 on air quality in India. *Science of The Total Environment*, 728:138878, August 2020. ISSN 00489697. doi: 10.1016/j.scitotenv.2020.138878. URL <https://linkinghub.elsevier.com/retrieve/pii/S0048969720323950>.
- Xiaoqin Shi and Guy P. Brasseur. The Response in Air Quality to the Reduction of Chinese Economic Activities During the COVID-19 Outbreak. *Geophysical Research Letters*, 47(11), June 2020. ISSN 0094-8276, 1944-8007. doi: 10.1029/2020GL088070. URL <https://onlinelibrary.wiley.com/doi/10.1029/2020GL088070>.
- Zander S. Venter, Kristin Aunan, Sourangsu Chowdhury, and Jos Lelieveld. COVID-19 lockdowns cause global air pollution declines. *Proceedings of the National Academy of Sciences*, 117(32): 18984–18990, August 2020. ISSN 0027-8424, 1091-6490. doi: 10.1073/pnas.2006853117. URL <https://pnas.org/doi/full/10.1073/pnas.2006853117>.
- Shanshan Liu, Cheng Liu, Qihou Hu, Wenjing Su, Xian Yang, Jinan Lin, Chengxin Zhang, Chengzhi Xing, Xiangguang Ji, Wei Tan, Haoran Liu, and Meng Gao. Distinct Regimes of O₃ Response to COVID-19 Lockdown in China. *Atmosphere*, 12(2):184, January 2021. ISSN 2073-4433. doi: 10.3390/atmos12020184. URL <https://www.mdpi.com/2073-4433/12/2/184>.
- K. Miyazaki, K. Bowman, T. Sekiya, Masayuki Takigawa, Jessica L. Neu, K. Sudo, G. Osterman, and H. Eskes. Global tropospheric ozone responses to reduced NO_x emissions linked to the COVID-19 worldwide lockdowns. *SCIENCE ADVANCES*, page 15, 2021.
- William A. Gough and Vidya Anderson. Changing Air Quality and the Ozone Weekend Effect during the COVID-19 Pandemic in Toronto, Ontario, Canada. *Climate*, 10(3):41, March 2022. ISSN 2225-1154. doi: 10.3390/cli10030041. URL <https://www.mdpi.com/2225-1154/10/3/41>.
- E.L. Odekanle, B.S. Fakinle, O.J. Odejobi, O.E. Akangbe, J.A. Sonibare, F.A. Akeredolu, and O.M. Oladoja. COVID-19 induced restriction in developing countries and its impacts on pollution load: case study of Lagos mega city. *Heliyon*, 8(8):e10402, August 2022. ISSN 24058440. doi: 10.1016/j.heliyon.2022.e10402. URL <https://linkinghub.elsevier.com/retrieve/pii/S2405844022016905>.
- Jiawei Zhang, Youn-Hee Lim, Zorana Jovanovic Andersen, George Napolitano, Seyed Mahmood Taghavi Shahri, Rina So, Maude Plucker, Mahdieh Danesh-Yazdi, Thomas Cole-Hunter, Jeanette Therming Jørgensen, Shuo Liu, Marie Bergmann, Amar Jayant Mehta, Laust H. Mortensen, Weeberb Requia, Theis Lange, Steffen Loft, Nino Kuenzli, Joel Schwartz, and

- Heresh Amini. Stringency of COVID-19 Containment Response Policies and Air Quality Changes: A Global Analysis across 1851 Cities. *Environmental Science & Technology*, 56(17): 12086–12096, September 2022a. ISSN 0013-936X, 1520-5851. doi: 10.1021/acs.est.2c04303. URL <https://pubs.acs.org/doi/10.1021/acs.est.2c04303>.
- Tianhao Le, Yuan Wang, Lang Liu, Jiani Yang, Yuk L. Yung, Guohui Li, and John H. Seinfeld. Unexpected air pollution with marked emission reductions during the COVID-19 outbreak in China. *Science*, 369(6504):702–706, August 2020. ISSN 0036-8075, 1095-9203. doi: 10.1126/science.abb7431. URL <https://www.science.org/doi/10.1126/science.abb7431>.
- Pierre Sicard, Alessandra De Marco, Evgenios Agathokleous, Zhaozhong Feng, Xiaobin Xu, Elena Paoletti, José Jaime Diéguez Rodríguez, and Vicent Calatayud. Amplified ozone pollution in cities during the COVID-19 lockdown. *Science of The Total Environment*, 735: 139542, September 2020. ISSN 00489697. doi: 10.1016/j.scitotenv.2020.139542. URL <https://linkinghub.elsevier.com/retrieve/pii/S004896972033059X>.
- Yulu Qiu, Zhiqiang Ma, Ke Li, Weili Lin, Yingxiao Tang, Fan Dong, and Hong Liao. Markedly Enhanced Levels of Peroxyacetyl Nitrate (PAN) During COVID-19 in Beijing. *Geophysical Research Letters*, 47(19), October 2020b. ISSN 0094-8276, 1944-8007. doi: 10.1029/2020GL089623. URL <https://onlinelibrary.wiley.com/doi/10.1029/2020GL089623>.
- M. J. Shogrin, V. H. Payne, S. S. Kulawik, K. Miyazaki, and E. V. Fischer. Measurement report: Spatiotemporal variability of peroxy acyl nitrates (pans) over Mexico City from TES and CRIS satellite measurements. *Atmos. Chem. Phys.*, 2023.
- D. Fu, J. R. Worden, X. Liu, S. S. Kulawik, K. W. Bowman, and V. Natraj. Characterization of ozone profiles derived from Aura TES and OMI radiances. *Atmospheric Chemistry and Physics*, 13(6):3445–3462, March 2013. ISSN 1680-7324. doi: 10.5194/acp-13-3445-2013. URL <https://acp.copernicus.org/articles/13/3445/2013/>.
- Dejian Fu, Kevin W. Bowman, Helen M. Worden, Vijay Natraj, John R. Worden, Shanshan Yu, Pepijn Veefkind, Ilse Aben, Jochen Landgraf, Larrabee Strow, and Yong Han. High-resolution tropospheric carbon monoxide profiles retrieved from CrIS and TROPOMI. *Atmospheric Measurement Techniques*, 9(6):2567–2579, June 2016. ISSN 1867-8548. doi: 10.5194/amt-9-2567-2016. URL <https://amt.copernicus.org/articles/9/2567/2016/>.
- Dejian Fu, Susan S. Kulawik, Kazuyuki Miyazaki, Kevin W. Bowman, John R. Worden, Annmarie Eldering, Nathaniel J. Livesey, Joao Teixeira, Fredrick W. Irion, Robert L. Herman, Gregory B. Osterman, Xiong Liu, Pieter F. Levelt, Anne M. Thompson, and Ming Luo. Retrievals of tropospheric ozone profiles from the synergism of AIRS and OMI: methodology and validation. *Atmospheric Measurement Techniques*, 11(10):5587–5605, October 2018. ISSN 1867-8548. doi: 10.5194/amt-11-5587-2018. URL <https://amt.copernicus.org/articles/11/5587/2018/>.
- John R. Worden, Susan S. Kulawik, Dejian Fu, Vivienne H. Payne, Alan E. Lipton, Igor Polonsky, Yuguang He, Karen Cady-Pereira, Jean-Luc Moncet, Robert L. Herman, Fredrick W. Irion, and Kevin W. Bowman. Characterization and evaluation of AIRS-based estimates of the deuterium content of water vapor. *Atmospheric Measurement Techniques*, 12(4):2331–2339, April 2019.

ISSN 1867-8548. doi: 10.5194/amt-12-2331-2019. URL <https://amt.copernicus.org/articles/12/2331/2019/>.

K.W. Bowman, C.D. Rodgers, S.S. Kulawik, J. Worden, E. Sarkissian, G. Osterman, T. Steck, Ming Lou, A. Eldering, M. Shephard, H. Worden, M. Lampel, S. Clough, P. Brown, C. Rinsland, M. Gunson, and R. Beer. Tropospheric emission spectrometer: retrieval method and error analysis. *IEEE Transactions on Geoscience and Remote Sensing*, 44(5):1297–1307, May 2006. ISSN 0196-2892. doi: 10.1109/TGRS.2006.871234. URL <http://ieeexplore.ieee.org/document/1624609/>.

R. Beer, T. Glavich, and D.M. Rider. Tropospheric emission spectrometer for the Earth Observing System’s Aura satellite. 40:2356–2367, 2001.

Emmanuel Mahieu, Emily V. Fischer, Bruno Franco, Mathias Palm, Tyler Wizenberg, Dan Smale, Lieven Clarisse, Cathy Clerbaux, Pierre-François Coheur, James W. Hannigan, Erik Lutsch, Justus Notholt, Irene Pardo Cantos, Maxime Prignon, Christian Servais, and Kimberley Strong. First retrievals of peroxyacetyl nitrate (PAN) from ground-based FTIR solar spectra recorded at remote sites, comparison with model and satellite data. *Elementa: Science of the Anthropocene*, 9(1):00027, September 2021. ISSN 2325-1026. doi: 10.1525/elementa.2021.00027. URL <https://online.ucpress.edu/elementa/article/9/1/00027/118497/First-retrievals-of-peroxyacetyl-nitrate-PAN-from>.

K. W. Bowman. TROPES CrIS-SNPP L2 Peroxyacetyl Nitrate for Forward Stream, Summary Product V1, 2021a.

K. W. Bowman. TROPES CrIS-JPSS1 L2 Peroxyacetyl Nitrate for Forward Stream, Standard Product V1, 2021b.

Helen M. Worden, Gene L. Francis, Susan S. Kulawik, Kevin W. Bowman, Karen Cady-Pereira, Dejian Fu, Jennifer D. Hegarty, Valentin Kantchev, Ming Luo, Vivienne H. Payne, John R. Worden, Róisín Commane, and Kathryn McKain. TROPES/CrIS carbon monoxide profile validation with NOAA GML and ATom in situ aircraft observations. preprint, Gases/Remote Sensing/Validation and Intercomparisons, April 2022. URL <https://amt.copernicus.org/preprints/amt-2022-128/amt-2022-128.pdf>.

K. W. Bowman. TROPES CrIS-SNPP L2 Carbon Monoxide for Forward Stream, Standard Product V1, 2021c.

K. W. Bowman. TROPES CrIS-JPSS1 L2 Carbon Monoxide for Forward Stream, Summary Product V1, 2021d.

K. Folkert Boersma, Henk J. Eskes, Andreas Richter, Isabelle De Smedt, Alba Lorente, Steffen Beirle, Jos H. G. M. van Geffen, Marina Zara, Enno Peters, Michel Van Roozendaal, Thomas Wagner, Joannes D. Maasackers, Ronald J. van der A, Joanne Nightingale, Anne De Rudder, Hitoshi Irie, Gaia Pinardi, Jean-Christopher Lambert, and Steven C. Compernelle. Improving algorithms and uncertainty estimates for satellite NO₂ retrievals: results from the quality assurance for the essential climate variables (QA4ECV) project. *Atmospheric Measurement Techniques*, 11(12):6651–6678, December 2018. ISSN 1867-8548. doi: 10.5194/amt-11-6651-2018. URL <https://amt.copernicus.org/articles/11/6651/2018/>.

- K.F. Boersma, H. Eskes, A. Richter, I. De Smedt, Alba Lorente, Steffen Beirle, Jos H. G. M. van Geffen, Enno Peters, M. Van Roozendael, and Thomas Wagner. QA4ECV NO₂ tropospheric and stratospheric vertical column data from OMI (Version 1.1) [L3 Monthly Means], 2017a. URL <http://doi.org/10.21944/qa4ecv-no2-omi-v1.1>.
- I. De Smedt, J.-F. Müller, T. Stavrou, R. van der A, H. Eskes, and M. Van Roozendael. Twelve years of global observations of formaldehyde in the troposphere using GOME and SCIAMACHY sensors. *Atmospheric Chemistry and Physics*, 8(16):4947–4963, August 2008. ISSN 1680-7324. doi: 10.5194/acp-8-4947-2008. URL <https://acp.copernicus.org/articles/8/4947/2008/>.
- Lu Shen, Daniel J. Jacob, Lei Zhu, Qiang Zhang, Bo Zheng, Melissa P. Sulprizio, Ke Li, Isabelle De Smedt, Gonzalo González Abad, Hansen Cao, Tzung-May Fu, and Hong Liao. The 2005–2016 Trends of Formaldehyde Columns Over China Observed by Satellites: Increasing Anthropogenic Emissions of Volatile Organic Compounds and Decreasing Agricultural Fire Emissions. *Geophysical Research Letters*, 46(8):4468–4475, April 2019. ISSN 0094-8276, 1944-8007. doi: 10.1029/2019GL082172. URL <https://onlinelibrary.wiley.com/doi/10.1029/2019GL082172>.
- I. De Smedt, H. Yu, A. Richter, Steffen Beirle, H. Eskes, Folkert Boersma, M. Van Roozendael, Jos H. G. M. van Geffen, Alba Lorente, and Enno Peters. QA4ECV HCHO tropospheric column data from OMI (Version 1.1) [L3 Monthly Means], 2017. URL <http://doi.org/10.18758/71021031>.
- RAMA. Secretaría de Medio Ambiente; Gobierno de la Ciudad de México: 2020., 2020. URL <http://www.aire.cdmx.gob.mx/>.
- D.P. Roy, L. Boschetti, C.O. Justice, and J. Ju. The collection 5 MODIS burned area product — Global evaluation by comparison with the MODIS active fire product. *Remote Sensing of Environment*, 112(9):3690–3707, September 2008. ISSN 00344257. doi: 10.1016/j.rse.2008.05.013. URL <https://linkinghub.elsevier.com/retrieve/pii/S0034425708001752>.
- Fangjun Li, Xiaoyang Zhang, Shobha Kondragunta, and Ivan Csiszar. Comparison of Fire Radiative Power Estimates From VIIRS and MODIS Observations. *Journal of Geophysical Research: Atmospheres*, 123(9):4545–4563, May 2018. ISSN 2169-897X, 2169-8996. doi: 10.1029/2017JD027823. URL <https://onlinelibrary.wiley.com/doi/10.1029/2017JD027823>.
- Jing Wei, Lin Sun, Bo Huang, Muhammad Bilal, Zhaoyang Zhang, and Lunche Wang. Verification, improvement and application of aerosol optical depths in China Part 1: Inter-comparison of NPP-VIIRS and Aqua-MODIS. *Atmospheric Environment*, 175:221–233, February 2018. ISSN 13522310. doi: 10.1016/j.atmosenv.2017.11.048. URL <https://linkinghub.elsevier.com/retrieve/pii/S1352231017308099>.
- Kengo Sudo, Masaaki Takahashi, Jun-ichi Kurokawa, and Hajime Akimoto. CHASER: A global chemical model of the troposphere 1. Model description: CHASER 1. MODEL DESCRIPTION. *Journal of Geophysical Research: Atmospheres*, 107(D17):ACH 7–1–ACH 7–20, September 2002. ISSN 01480227. doi: 10.1029/2001JD001113. URL <http://doi.wiley.com/10.1029/2001JD001113>.

- S. Watanabe, T. Hajima, K. Sudo, T. Nagashima, T. Takemura, H. Okajima, T. Nozawa, H. Kawase, M. Abe, T. Yokohata, T. Ise, H. Sato, E. Kato, K. Takata, S. Emori, and M. Kawamiya. MIROC-ESM 2010: model description and basic results of CMIP5-20c3m experiments. *Geoscientific Model Development*, 4(4):845–872, October 2011. ISSN 1991-9603. doi: 10.5194/gmd-4-845-2011. URL <https://gmd.copernicus.org/articles/4/845/2011/>.
- Takashi Sekiya, Kazuyuki Miyazaki, Koji Ogochi, Kengo Sudo, and Masayuki Takigawa. Global high-resolution simulations of tropospheric nitrogen dioxide using CHASER V4.0. *Geoscientific Model Development*, 11(3):959–988, March 2018. ISSN 1991-9603. doi: 10.5194/gmd-11-959-2018. URL <https://gmd.copernicus.org/articles/11/959/2018/>.
- D. Price, C. and Rind. A simple lightning parameterization for calculating global lightning distributions. 97:9919–9933, 1992.
- Kazuyuki Miyazaki, Kevin Bowman, Takashi Sekiya, Henk Eskes, Folkert Boersma, Helen Worden, Nathaniel Livesey, Vivienne H. Payne, Kengo Sudo, Yugo Kanaya, Masayuki Takigawa, and Koji Ogochi. Updated tropospheric chemistry reanalysis and emission estimates, TCR-2, for 2005–2018. *Earth System Science Data*, 12(3):2223–2259, September 2020b. ISSN 1866-3516. doi: 10.5194/essd-12-2223-2020. URL <https://essd.copernicus.org/articles/12/2223/2020/>.
- K.F. Boersma, H. Eskes, A. Richter, I. De Smedt, Alba Lorente, Steffen Beirle, Jos H. G. M. van Geffen, Enno Peters, M. Van Roozendaal, and Thomas Wagner. QA4ECV NO₂ tropospheric and stratospheric vertical column data from OMI (Version 1.1) [Data set], 2017b. URL <http://doi.org/10.21944/qa4ecv-no2-omi-v1.1>.
- K.F. Boersma, H. Eskes, A. Richter, I. De Smedt, Alba Lorente, Steffen Beirle, Jos H. G. M. van Geffen, Enno Peters, M. Van Roozendaal, and Thomas Wagner. QA4ECV NO₂ tropospheric and stratospheric vertical column data from GOME-2A (Version 1.1) [Data set], 2017c. URL <http://doi.org/10.21944/qa4ecv-no2-gome2a-v1.1>.
- G. Janssens-Maenhout, M. Crippa, D. Guizzardi, F. Dentener, M. Muntean, G. Pouliot, T. Keating, Q. Zhang, J. Kurokawa, R. Wankmüller, H. Denier van der Gon, J. J. P. Kuenen, Z. Klimont, G. Frost, S. Darras, B. Koffi, and M. Li. HTAP_v2.2: a mosaic of regional and global emission grid maps for 2008 and 2010 to study hemispheric transport of air pollution. *Atmospheric Chemistry and Physics*, 15(19):11411–11432, October 2015. ISSN 1680-7324. doi: 10.5194/acp-15-11411-2015. URL <https://acp.copernicus.org/articles/15/11411/2015/>.
- J. Randerson, G. van der verf, L. Gilglio, G. Collatz, and P. Kasibhatla. Global Fire Emissions Database, Version 4, (GFEDv4), ORNL DAAC. *Oak Ridge, Tennessee, USA*, 2018.
- T. E. Graedel, T. S. Bates, A. F. Bouwman, D. Cunnold, J. Dignon, I. Fung, D. J. Jacob, B. K. Lamb, J. A. Logan, G. Marland, P. Middleton, J. M. Pacyna, M. Placet, and C. Veldt. A compilation of inventories of emissions to the atmosphere. *Global Biogeochemical Cycles*, 7(1):1–26, March 1993. ISSN 08866236. doi: 10.1029/92GB02793. URL <http://doi.wiley.com/10.1029/92GB02793>.
- L T Molina, B. de Foy, O Vazquez Martinez, V Hugo, and P Figueroa. Air quality, weather and climate in Mexico City. *WMO Bulletin*, 8(581):48–53, 2009.

- J. C. Doran and S. Zhong. Thermally Driven Gap Winds into the Mexico City Basin. *Journal of Applied Meteorology*, 39(8):1330–1340, August 2000. ISSN 0894-8763, 1520-0450. doi: 10.1175/1520-0450(2000)039<1330:TDGWIT>2.0.CO;2. URL [http://journals.ametsoc.org/doi/10.1175/1520-0450\(2000\)039<1330:TDGWIT>2.0.CO;2](http://journals.ametsoc.org/doi/10.1175/1520-0450(2000)039<1330:TDGWIT>2.0.CO;2).
- B de Foy, E Caetano, and M J Molina. Mexico City basin wind circulation during the MCMA-2003 field campaign. *Atmos. Chem. Phys.*, page 22, 2005.
- B de Foy, J R Varela, L T Molina, and M J Molina. Rapid ventilation of the Mexico City basin and regional fate of the urban plume. *Atmos. Chem. Phys.*, page 15, 2006.
- B de Foy, J D Fast, S J Paech, D Phillips, J T Walters, R L Coulter, T J Martin, M S Pekour, W J Shaw, P P Kastendeuch, N A Marley, A Retama, and L T Molina. Basin-scale wind transport during the MILAGRO field campaign and comparison to climatology using cluster analysis. *Atmos. Chem. Phys.*, page 16, 2008.
- R J Yokelson, S P Urbanski, E L Atlas, D W Toohey, E C Alvarado, J D Crouse, P O Wennberg, M E Fisher, C E Wold, T L Campos, K Adachi, P R Buseck, and W M Hao. Emissions from forest fires near Mexico City. *Atmos. Chem. Phys.*, page 16, 2007.
- R J Yokelson, J D Crouse, P F DeCarlo, T Karl, S Urbanski, E Atlas, T Campos, Y Shinozuka, V Kapustin, A D Clarke, A Weinheimer, D J Knapp, D D Montzka, J Holloway, P Weibring, F Flocke, W Zheng, D Toohey, P O Wennberg, C Wiedinmyer, L Mauldin, A Fried, D Richter, J Walega, J L Jimenez, K Adachi, P R Buseck, S R Hall, and R Shetter. Emissions from biomass burning in the Yucatan. *Atmos. Chem. Phys.*, page 28, 2009.
- R. J. Yokelson, I. R. Burling, S. P. Urbanski, E. L. Atlas, K. Adachi, P. R. Buseck, C. Wiedinmyer, S. K. Akagi, D. W. Toohey, and C. E. Wold. Trace gas and particle emissions from open biomass burning in Mexico. *Atmospheric Chemistry and Physics*, 11(14):6787–6808, July 2011. ISSN 1680-7324. doi: 10.5194/acp-11-6787-2011. URL <https://acp.copernicus.org/articles/11/6787/2011/>.
- Molina, Velasco, Retama, and Zavala. Experience from Integrated Air Quality Management in the Mexico City Metropolitan Area and Singapore. *Atmosphere*, 10(9):512, August 2019. ISSN 2073-4433. doi: 10.3390/atmos10090512. URL <https://www.mdpi.com/2073-4433/10/9/512>.
- W Lei, M Zavala, B de Foy, R Volkamer, M J Molina, and L T Molina. Impact of primary formaldehyde on air pollution in the Mexico City Metropolitan Area. *Atmos. Chem. Phys.*, page 12, 2009.
- Zitely A. Tzompa-Sosa, Amy P. Sullivan, Armando Retama, and Sonia M. Kreidenweis. Contribution of Biomass Burning to Carbonaceous Aerosols in Mexico City during May 2013. *Aerosol and Air Quality Research*, 16(1):114–124, 2016. ISSN 16808584, 20711409. doi: 10.4209/aaqr.2015.01.0030. URL <https://aaqr.org/articles/aaqr-15-01-0a-0030>.
- M. Jaimes-Palomera, A. Retama, G. Elias-Castro, A. Neria-Hernández, O. Rivera-Hernández, and E. Velasco. Non-methane hydrocarbons in the atmosphere of Mexico City: Results of the 2012 ozone-season campaign. 132:258–275. doi: <https://doi.org/10.1016/j.atmosenv.2016.02.047>.

- T J Christian, R J Yokelson, B Cardenas, L T Molina, and G Engling. Trace gas and particle emissions from domestic and industrial biofuel use and garbage burning in central Mexico. *Atmos. Chem. Phys.*, page 20, 2010.
- E. Velasco, B. Lamb, H. Westberg, E. Allwine, G. Sosa, J. L. Arriaga-Colina, B. T. Jobson, M. L. Alexander, P. Prazeller, W. B. Knighton, T. M. Rogers, M. Grutter, S. C. Herndon, C. E. Kolb, M. Zavala, B. de Foy, R. Volkamer, L. T. Molina, and M. J. Molina. Distribution, magnitudes, reactivities, ratios and diurnal patterns of volatile organic compounds in the Valley of Mexico during the MCMA 2002 & 2003 field campaigns. *Atmospheric Chemistry and Physics*, 7(2):329–353, January 2007. ISSN 1680-7324. doi: 10.5194/acp-7-329-2007. URL <https://acp.copernicus.org/articles/7/329/2007/>.
- M. Johansson, C. Rivera, B. de Foy, W. Lei, J. Song, Y. Zhang, B. Galle, and L. Molina. Mobile mini-DOAS measurement of the outflow of NO₂ and HCHO from Mexico City. *Atmospheric Chemistry and Physics*, 9(15):5647–5653, August 2009. ISSN 1680-7324. doi: 10.5194/acp-9-5647-2009. URL <https://acp.copernicus.org/articles/9/5647/2009/>.
- O.O. Osibanjo, B. Rappenglück, and A. Retama. Anatomy of the March 2016 severe ozone smog episode in Mexico-City. *Atmospheric Environment*, 244:117945, January 2021. ISSN 13522310. doi: 10.1016/j.atmosenv.2020.117945. URL <https://linkinghub.elsevier.com/retrieve/pii/S1352231020306798>.
- A.P. Baez, R. Belmont, and H. Padilla. Measurements of formaldehyde and acetaldehyde in the atmosphere of Mexico City. *Environmental Pollution*, 89(2):163–167, 1995. ISSN 02697491. doi: 10.1016/0269-7491(94)00059-M. URL <https://linkinghub.elsevier.com/retrieve/pii/026974919400059M>.
- A R Garcia, R Volkamer, L T Molina, M J Molina, J Samuelson, J Mellqvist, B Galle, S C Herndon, and C E Kolb. Separation of emitted and photochemical formaldehyde in Mexico City using a statistical analysis and a new pair of gas-phase tracers. *Atmos. Chem. Phys.*, page 13, 2006.
- Heather Simon, Adam Reff, Benjamin Wells, Jia Xing, and Neil Frank. Ozone Trends Across the United States over a Period of Decreasing NO_x and VOC Emissions. *Environmental Science & Technology*, 49(1):186–195, January 2015. ISSN 0013-936X, 1520-5851. doi: 10.1021/es504514z. URL <https://pubs.acs.org/doi/10.1021/es504514z>.
- Wei Gao, Xuexi Tie, Jianming Xu, Rujin Huang, Xiaoqing Mao, Guangqiang Zhou, and Luyu Chang. Long-term trend of O₃ in a mega City (Shanghai), China: Characteristics, causes, and interactions with precursors. *Science of The Total Environment*, 603-604:425–433, December 2017. ISSN 00489697. doi: 10.1016/j.scitotenv.2017.06.099. URL <https://linkinghub.elsevier.com/retrieve/pii/S0048969717315036>.
- S. A. Penkett and K. A. Brice. The spring maximum in photo-oxidants in the Northern Hemisphere troposphere. *Nature*, 319(6055):655–657, February 1986. ISSN 0028-0836, 1476-4687. doi: 10.1038/319655a0. URL <http://www.nature.com/articles/319655a0>.

- K. A. Brice, J. W. Bottenheim, K. G. Anlauf, and H. A. Wiebe. Long-term measurements of atmospheric peroxyacetyl nitrate (PAN) at rural sites in Ontario and Nova Scotia; seasonal variations and long-range transport. *Tellus B*, 40B(5):408–425, November 1988. ISSN 02806509, 16000889. doi: 10.1111/j.1600-0889.1988.tb00113.x. URL <http://www.tellusb.net/index.php/tellusb/article/view/16007>.
- A. O. Langford, C. J. Senff, R. J. Alvarez, R. M. Banta, and R. M. Hardesty. Long-range transport of ozone from the Los Angeles Basin: A case study: LONG-RANGE TRANSPORT OF OZONE. *Geophysical Research Letters*, 37(6):n/a–n/a, March 2010. ISSN 00948276. doi: 10.1029/2010GL042507. URL <http://doi.wiley.com/10.1029/2010GL042507>.
- Ilana B. Pollack, Thomas B. Ryerson, Michael Trainer, J. A. Neuman, James M. Roberts, and David D. Parrish. Trends in ozone, its precursors, and related secondary oxidation products in Los Angeles, California: A synthesis of measurements from 1960 to 2010: OZONE TRENDS IN LA FROM 1960 TO 2010. *Journal of Geophysical Research: Atmospheres*, 118(11):5893–5911, June 2013. ISSN 2169897X. doi: 10.1002/jgrd.50472. URL <http://doi.wiley.com/10.1002/jgrd.50472>.
- Clara M. Nussbaumer and Ronald C. Cohen. The Role of Temperature and NO_x in Ozone Trends in the Los Angeles Basin. *Environmental Science & Technology*, 54(24):15652–15659, December 2020. ISSN 0013-936X, 1520-5851. doi: 10.1021/acs.est.0c04910. URL <https://pubs.acs.org/doi/10.1021/acs.est.0c04910>.
- Wei Chen, Lei Yan, and Haimeng Zhao. Seasonal Variations of Atmospheric Pollution and Air Quality in Beijing. *Atmosphere*, 6(11):1753–1770, November 2015. ISSN 2073-4433. doi: 10.3390/atmos6111753. URL <http://www.mdpi.com/2073-4433/6/11/1753>.
- Fengjun Zhao, Yongqiang Liu, Lifu Shu, and Qi Zhang. Wildfire Smoke Transport and Air Quality Impacts in Different Regions of China. *Atmosphere*, 11(9):941, September 2020. ISSN 2073-4433. doi: 10.3390/atmos11090941. URL <https://www.mdpi.com/2073-4433/11/9/941>.
- Yifei Zhao, Ruiguang Xu, Zhiguang Xu, Litao Wang, and Pu Wang. Temporal and Spatial Patterns of Biomass Burning Fire Counts and Carbon Emissions in the Beijing–Tianjin–Hebei (BTH) Region during 2003–2020 Based on GFED4. *Atmosphere*, 13(3):459, March 2022. ISSN 2073-4433. doi: 10.3390/atmos13030459. URL <https://www.mdpi.com/2073-4433/13/3/459>.
- P.A. Leighton. Photochemistry of Air Pollution. 1961.
- Daniel Grosjean. Ambient PAN and PPN in southern California from 1960 to the SCOS97-NARSTO. *Atmospheric Environment*, 37:221–238, January 2003. ISSN 13522310. doi: 10.1016/S1352-2310(03)00392-3. URL <https://linkinghub.elsevier.com/retrieve/pii/S1352231003003923>.
- Yutong Liang, Deep Sengupta, Mark J. Campmier, David M. Lunderberg, Joshua S. Apte, and Allen H. Goldstein. Wildfire smoke impacts on indoor air quality assessed using crowdsourced data in California. *Proceedings of the National Academy of Sciences*, 118(36):e2106478118, September 2021. ISSN 0027-8424, 1091-6490. doi: 10.1073/pnas.2106478118. URL <https://pnas.org/doi/full/10.1073/pnas.2106478118>.

- Boya Zhang, Bu Zhao, Peng Zuo, Zhi Huang, and Jianbo Zhang. Ambient peroxyacyl nitrate concentration and regional transportation in Beijing. *Atmospheric Environment*, 166:543–550, October 2017. ISSN 13522310. doi: 10.1016/j.atmosenv.2017.07.053. URL <https://linkinghub.elsevier.com/retrieve/pii/S1352231017305022>.
- Gen Zhang, Lingjun Xia, Kunpeng Zang, Wanyun Xu, Fang Zhang, Linlin Liang, Bo Yao, Weili Lin, and Yujing Mu. The abundance and inter-relationship of atmospheric peroxyacetyl nitrate (PAN), peroxypropionyl nitrate (PPN), O₃, and NO_y during the wintertime in Beijing, China. *Science of The Total Environment*, 718:137388, May 2020. ISSN 00489697. doi: 10.1016/j.scitotenv.2020.137388. URL <https://linkinghub.elsevier.com/retrieve/pii/S0048969720308986>.
- Lifei Yin, Pin Du, Minsi Zhang, Mingxu Liu, Tingting Xu, and Yu Song. Estimation of emissions from biomass burning in China (2003–2017) based on MODIS fire radiative energy data. *Biogeosciences*, 16(7):1629–1640, April 2019. ISSN 1726-4189. doi: 10.5194/bg-16-1629-2019. URL <https://bg.copernicus.org/articles/16/1629/2019/>.
- Keyan Fang, Qichao Yao, Zhengtang Guo, Ben Zheng, Jianhua Du, Fangzhong Qi, Ping Yan, Jie Li, Tinghai Ou, Jane Liu, Maosheng He, and Valerie Trouet. ENSO modulates wildfire activity in China. *Nature Communications*, 12(1):1764, March 2021. ISSN 2041-1723. doi: 10.1038/s41467-021-21988-6. URL <https://www.nature.com/articles/s41467-021-21988-6>.
- Lili Wang, Xin Jin, Qinglu Wang, Huiqin Mao, Qiyang Liu, Guoqing Weng, and Yuesi Wang. Spatial and temporal variability of open biomass burning in Northeast China from 2003 to 2017. *Atmospheric and Oceanic Science Letters*, 13(3):240–247, May 2020. ISSN 1674-2834, 2376-6123. doi: 10.1080/16742834.2020.1742574. URL <https://www.tandfonline.com/doi/full/10.1080/16742834.2020.1742574>.
- T. Ogawa and A. Miyata. Seasonal Behavior of the Tropospheric Ozone in Japan. In *Atmospheric Ozone*. Springer, Dordrecht, 1985. URL https://doi.org/10.1007/978-94-009-5313-0_148.
- M. Yoshitomi, O. Wild, and H. Akimoto. Contributions of regional and intercontinental transport to surface ozone in Tokyo. preprint, Gases/Atmospheric Modelling/Troposphere/Chemistry (chemical composition and reactions), April 2011. URL <https://acp.copernicus.org/preprints/11/10403/2011/acpd-11-10403-2011.pdf>.
- Y. Lee, L. G. Huey, Y. Wang, H. Qu, R. Zhang, Y. Ji, D. J. Tanner, X. Wang, J. Tang, W. Song, W. Hu, and Y. Zhang. Photochemistry of Volatile Organic Compounds in the Yellow River Delta, China: Formation of O₃ and Peroxyacyl Nitrates. *Journal of Geophysical Research: Atmospheres*, 126(23), December 2021a. ISSN 2169-897X, 2169-8996. doi: 10.1029/2021JD035296. URL <https://onlinelibrary.wiley.com/doi/10.1029/2021JD035296>.
- Yugo Kanaya, Masato Fukuda, Hajime Akimoto, Nobuyuki Takegawa, Yuichi Komazaki, Yoko Yokouchi, Makoto Koike, and Yutaka Kondo. Urban photochemistry in central Tokyo: 2. Rates and regimes of oxidant (O₃ + NO₂) production. *Journal of Geophysical Research*, 113(D6): D06301, March 2008. ISSN 0148-0227. doi: 10.1029/2007JD008671. URL <http://doi.wiley.com/10.1029/2007JD008671>.

S. L. Jain, B. C. Arya, Arun Kumar, Sachin D. Ghude, and P. S. Kulkarni. Observational study of surface ozone at New Delhi, India. *International Journal of Remote Sensing*, 26(16):3515–3524, August 2005. ISSN 0143-1161, 1366-5901. doi: 10.1080/01431160500076616. URL <https://www.tandfonline.com/doi/full/10.1080/01431160500076616>.

Lokesh K. Sahu, Shyam Lal, Valérie Thouret, and Herman G. Smit. Seasonality of tropospheric ozone and water vapor over Delhi, India: a study based on MOZAIC measurement data. *Journal of Atmospheric Chemistry*, 62(2):151–174, March 2009. ISSN 0167-7764, 1573-0662. doi: 10.1007/s10874-010-9146-1. URL <http://link.springer.com/10.1007/s10874-010-9146-1>.

Pallavi Saxena, Saurabh Sonwani, Ananya Srivastava, Madhavi Jain, Anju Srivastava, Akash Bharti, Deepali Rangra, Nancy Mongia, Shweta Tejan, and Shreshtha Bhardwaj. Impact of crop residue burning in Haryana on the air quality of Delhi, India. *Heliyon*, 7(5):e06973, May 2021. ISSN 24058440. doi: 10.1016/j.heliyon.2021.e06973. URL <https://linkinghub.elsevier.com/retrieve/pii/S2405844021010768>.

A. M. O. Abdul Raheem, F. A. Adekola, and I. O. Obioh. The Seasonal Variation of the Concentrations of Ozone, Sulfur Dioxide, and Nitrogen Oxides in Two Nigerian Cities. *Environmental Modeling & Assessment*, 14(4):497–509, August 2009. ISSN 1420-2026, 1573-2967. doi: 10.1007/s10666-008-9142-x. URL <http://link.springer.com/10.1007/s10666-008-9142-x>.

Sagar Marathe and Shankar Murthy. Seasonal Variation in Surface Ozone Concentrations, Meteorology and Primary Pollutants in Coastal Mega City of Mumbai, India. *Journal of Climatology & Weather Forecasting*, 03(03), 2015. ISSN 23322594. doi: 10.4172/2332-2594.1000149. URL <http://www.esciencecentral.org/journals/seasonal-variation-in-surface-ozone-concentrations-meteorology-andprimary-pollutants-in-coastal-mega-city.php?aid=65537>.

Jesse D. Berman and Keita Ebisu. Changes in U.S. air pollution during the COVID-19 pandemic. *Science of The Total Environment*, 739:139864, October 2020. ISSN 00489697. doi: 10.1016/j.scitotenv.2020.139864. URL <https://linkinghub.elsevier.com/retrieve/pii/S0048969720333842>.

Vivienne H. Payne, Susan S. Kulawik, Emily V. Fischer, Jared F. Brewer, L. Gregory Huey, Kazuyuki Miyazaki, John R. Worden, Kevin W. Bowman, Eric J. Hints, Fred Moore, James W. Elkins, and Julieta Juncosa Calahorrano. Satellite measurements of peroxyacetyl nitrate from the Cross-Track Infrared Sounder: Comparison with ATom aircraft measurements. preprint, Gases/Remote Sensing/Validation and Intercomparisons, November 2021. URL <https://amt.copernicus.org/preprints/amt-2021-353/amt-2021-353.pdf>.

Patrick Connerton, João Vicente de Assunção, Regina Maura de Miranda, Anne Dorothée Slovic, Pedro José Pérez-Martínez, and Helena Ribeiro. Air Quality during COVID-19 in Four Megacities: Lessons and Challenges for Public Health. *International Journal of Environmental Research and Public Health*, 17(14):5067, July 2020. ISSN 1660-4601. doi: 10.3390/ijerph17145067. URL <https://www.mdpi.com/1660-4601/17/14/5067>.

Yousaf Ali Khan. The COVID-19 pandemic and its impact on environment: the case of the major cities in Pakistan. *Environmental Science and Pollution Research*, 28(39):54728–54743,

- October 2021. ISSN 0944-1344, 1614-7499. doi: 10.1007/s11356-021-13851-4. URL <https://link.springer.com/10.1007/s11356-021-13851-4>.
- Jason R. Schroeder, Chenxia Cai, Jin Xu, David Ridley, Jin Lu, Nancy Bui, Fang Yan, and Jeremy Avice. Changing ozone sensitivity in the South Coast Air Basin during the COVID-19 period. *Atmospheric Chemistry and Physics*, 22(19):12985–13000, October 2022. ISSN 1680-7324. doi: 10.5194/acp-22-12985-2022. URL <https://acp.copernicus.org/articles/22/12985/2022/>.
- K. Miyazaki, K. Bowman, T. Sekiya, Z. Jiang, X. Chen, H. Eskes, M. Ru, Y. Zhang, and D. Shindell. Air Quality Response in China Linked to the 2019 Novel Coronavirus (COVID-19) Lockdown. *Geophysical Research Letters*, 47(19), October 2020c. ISSN 0094-8276, 1944-8007. doi: 10.1029/2020GL089252. URL <https://onlinelibrary.wiley.com/doi/10.1029/2020GL089252>.
- Xin Huang, Aijun Ding, Jian Gao, Bo Zheng, Derong Zhou, Ximeng Qi, Rong Tang, Jiaping Wang, Chuanhua Ren, Wei Nie, Xuguang Chi, Zheng Xu, Liangduo Chen, Yuanyuan Li, Fei Che, Nini Pang, Haikun Wang, Dan Tong, Wei Qin, Wei Cheng, Weijing Liu, Qingyan Fu, Baoxian Liu, Fahe Chai, Steven J Davis, Qiang Zhang, and Kebin He. Enhanced secondary pollution offset reduction of primary emissions during COVID-19 lockdown in China. *National Science Review*, 8(2):nwaa137, February 2021. ISSN 2095-5138, 2053-714X. doi: 10.1093/nsr/nwaa137. URL <https://academic.oup.com/nsr/article/doi/10.1093/nsr/nwaa137/5859289>.
- Zongbo Shi, Congbo Song, Bowen Liu, Gongda Lu, Jingsha Xu, Tuan Van Vu, Robert J. R. Elliott, Weijun Li, William J. Bloss, and Roy M. Harrison. Abrupt but smaller than expected changes in surface air quality attributable to COVID-19 lockdowns. *Science Advances*, 7(3):eabd6696, January 2021. ISSN 2375-2548. doi: 10.1126/sciadv.abd6696. URL <https://www.science.org/doi/10.1126/sciadv.abd6696>.
- Qingchun Guo, Zhaosheng Wang, Zhenfang He, Xinzhou Li, Jingjing Meng, Zhanfang Hou, and Jiaoxue Yang. Changes in Air Quality from the COVID to the Post-COVID Era in the Beijing-Tianjin-Tangshan Region in China. *Aerosol and Air Quality Research*, 21(12):210270, 2021. ISSN 16808584, 20711409. doi: 10.4209/aaqr.210270. URL <https://aaqr.org/articles/aaqr-21-10-covid2-0270>.
- Kun Zhang, Zhiqiang Liu, Xiaojuan Zhang, Qing Li, Andrew Jensen, Wen Tan, Ling Huang, Yangjun Wang, Joost de Gouw, and Li Li. Insights into the significant increase in ozone during COVID-19 in a typical urban city of China. *Atmospheric Chemistry and Physics*, 22(7):4853–4866, April 2022b. ISSN 1680-7324. doi: 10.5194/acp-22-4853-2022. URL <https://acp.copernicus.org/articles/22/4853/2022/>.
- A. Rathod, S.K. Sahu, S. Singh, and G. Beig. Anomalous behaviour of ozone under COVID-19 and explicit diagnosis of O₃-NO_x-VOCs mechanism. *Heliyon*, 7(2):e06142, February 2021. ISSN 24058440. doi: 10.1016/j.heliyon.2021.e06142. URL <https://linkinghub.elsevier.com/retrieve/pii/S2405844021002474>.
- E. Vega, A. Namdeo, L. Bramwell, Y. Miquelajauregui, C.G. Resendiz-Martinez, M. Jaimes-Palomera, F. Luna-Falfan, A. Terrazas-Ahumada, K.J. Maji, J. Entwistle, J.C. Núñez Enríquez, J.M. Mejia, A. Portas, L. Hayes, and R. McNally. Changes in air quality in Mexico City, London and Delhi in response to various stages and levels of lockdowns and easing of restrictions

- during COVID-19 pandemic. *Environmental Pollution*, 285:117664, September 2021. ISSN 02697491. doi: 10.1016/j.envpol.2021.117664. URL <https://linkinghub.elsevier.com/retrieve/pii/S026974912101246X>.
- Shobhna Shankar and Ranu Gadi. Variation in Air Quality over Delhi Region: A Comparative Study for 2019 and 2020. *Aerosol Science and Engineering*, 6(3):278–295, September 2022. ISSN 2510-375X, 2510-3768. doi: 10.1007/s41810-022-00144-7. URL <https://link.springer.com/10.1007/s41810-022-00144-7>.
- Hyo-Jung Lee, Lim-Seok Chang, Daniel A. Jaffe, Juseon Bak, Xiong Liu, Gonzalo González Abad, Hyun-Young Jo, Yu-Jin Jo, Jae-Bum Lee, and Cheol-Hee Kim. Ozone Continues to Increase in East Asia Despite Decreasing NO₂: Causes and Abatements. *Remote Sensing*, 13(11):2177, June 2021b. ISSN 2072-4292. doi: 10.3390/rs13112177. URL <https://www.mdpi.com/2072-4292/13/11/2177>.
- I. A. Fuwape, C. T. Okpalaonwuka, and S. T. Ogunjo. Impact of COVID -19 pandemic lockdown on distribution of inorganic pollutants in selected cities of Nigeria. *Air Quality, Atmosphere & Health*, 14(2):149–155, February 2021. ISSN 1873-9318, 1873-9326. doi: 10.1007/s11869-020-00921-8. URL <https://link.springer.com/10.1007/s11869-020-00921-8>.
- Akiyoshi Ito, Shinji Wakamatsu, Tazuko Morikawa, and Shinji Kobayashi. 30 Years of Air Quality Trends in Japan. *Atmosphere*, 12(8):1072, August 2021. ISSN 2073-4433. doi: 10.3390/atmos12081072. URL <https://www.mdpi.com/2073-4433/12/8/1072>.
- Qiang Wang and Shuyu Li. Nonlinear impact of COVID-19 on pollutions – Evidence from Wuhan, New York, Milan, Madrid, Bandra, London, Tokyo and Mexico City. *Sustainable Cities and Society*, 65:102629, February 2021. ISSN 22106707. doi: 10.1016/j.scs.2020.102629. URL <https://linkinghub.elsevier.com/retrieve/pii/S2210670720308465>.
- Alessandro Damiani, Hitoshi Irie, Dmitry A. Belikov, Shuei Kaizuka, Hossain Mohammed Syedul Hoque, and Raul R. Cordero. Peculiar COVID-19 effects in the Greater Tokyo Area revealed by spatiotemporal variabilities of tropospheric gases and light-absorbing aerosols. *Atmospheric Chemistry and Physics*, 22(18):12705–12726, September 2022. ISSN 1680-7324. doi: 10.5194/acp-22-12705-2022. URL <https://acp.copernicus.org/articles/22/12705/2022/>.
- Oscar Peralta, Abraham Ortínez-Alvarez, Ricardo Torres-Jardón, Manuel Suárez-Lastra, Telma Castro, and Luis Gerardo Ruíz-Suárez. Ozone over Mexico City during the COVID-19 pandemic. *Science of The Total Environment*, 761:143183, March 2021. ISSN 00489697. doi: 10.1016/j.scitotenv.2020.143183. URL <https://linkinghub.elsevier.com/retrieve/pii/S0048969720367139>.
- GMAO. MERRA-2 tavgM_2d_slv_nx: 2d,Monthly mean,Time-Averaged,Single-Level,Assimilation,Single-Level Diagnostics V5.12.4, 2015. URL [10.5067/AP1B0BA5PD2K](https://doi.org/10.5067/AP1B0BA5PD2K).
- David G. Streets, Joshua S. Fu, Carey J. Jang, Jiming Hao, Kebin He, Xiaoyan Tang, Yuanhang Zhang, Zifa Wang, Zuopan Li, Qiang Zhang, Litao Wang, Binyu Wang, andCarolyn Yu. Air quality during the 2008 Beijing Olympic Games. *Atmospheric Environment*, 41(3):480–492, January 2007. ISSN 13522310. doi: 10.1016/j.atmosenv.2006.08.046. URL <https://linkinghub.elsevier.com/retrieve/pii/S135223100600865X>.

Appendix A

ADDITIONAL FIGURES FOR MEGACITIES

This appendix contains additional figures for each megacity. Please note that values of CrIS PANs in these figures do not have the water vapor correction applied (Equation 2.3). With the addition of the water vapor correction, we can expect all values of CrIS PANs to increase by roughly 0.05-0.1 ppbv.

A.1 MEXICO CITY

Additional figures for Mexico City are below.

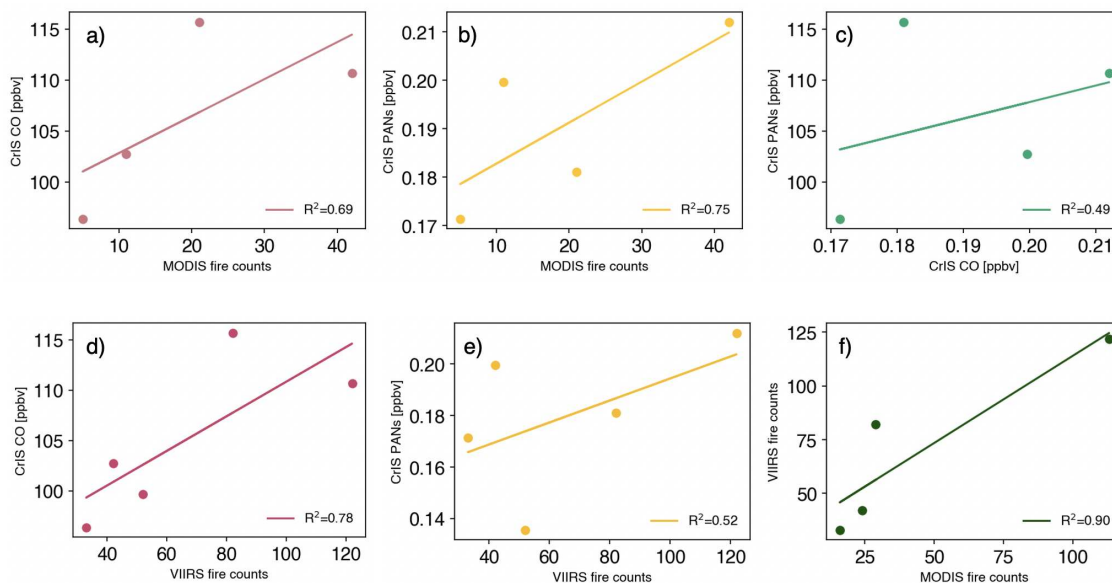


Figure A.1: Correlations between monthly means presented in Figure 3.7. (a) CrIS CO and MODIS fire counts (b)CrIS PANs and MODIS fire counts (c) CrIS PANs and CrIS CO (d) CrIS CO and VIIRS fire counts (e) CrIS PANs and VIIRS fire counts (f) VIIRS and MODIS fire counts

A.2 BEIJING

Additional figures for Beijing are below.

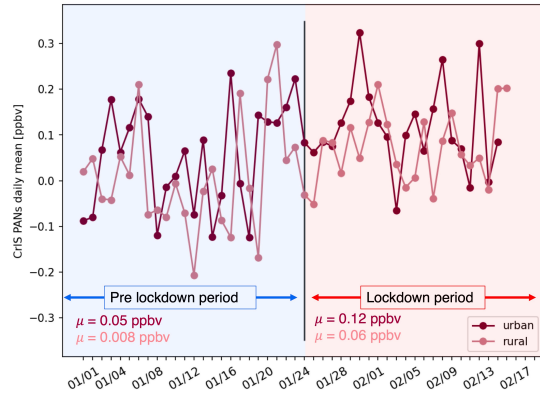


Figure A.2: Daily means of CrIS PANs during January and February for urban (dark red) and rural (light red) boxes. Pre lockdown time period highlighted in blue and lockdown time period highlighted in red. Respective sample means printed in bottom left of time boxes.

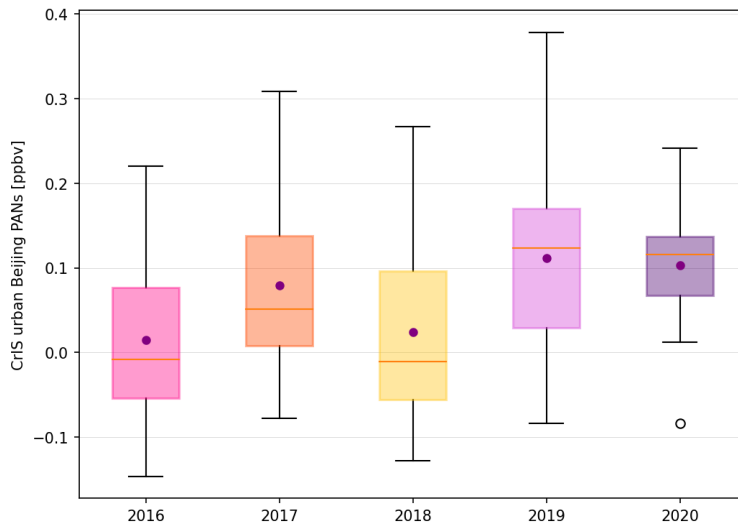


Figure A.3: Daily means of CrIS PANs within the urban box around Beijing for the time period of COVID-19 lockdown (24 January 2020 through 14 February 2020) for respective years. Purple dot represents mean of values and orange bar shows the medians. Whiskers show standard deviation and dots outside show outliers.

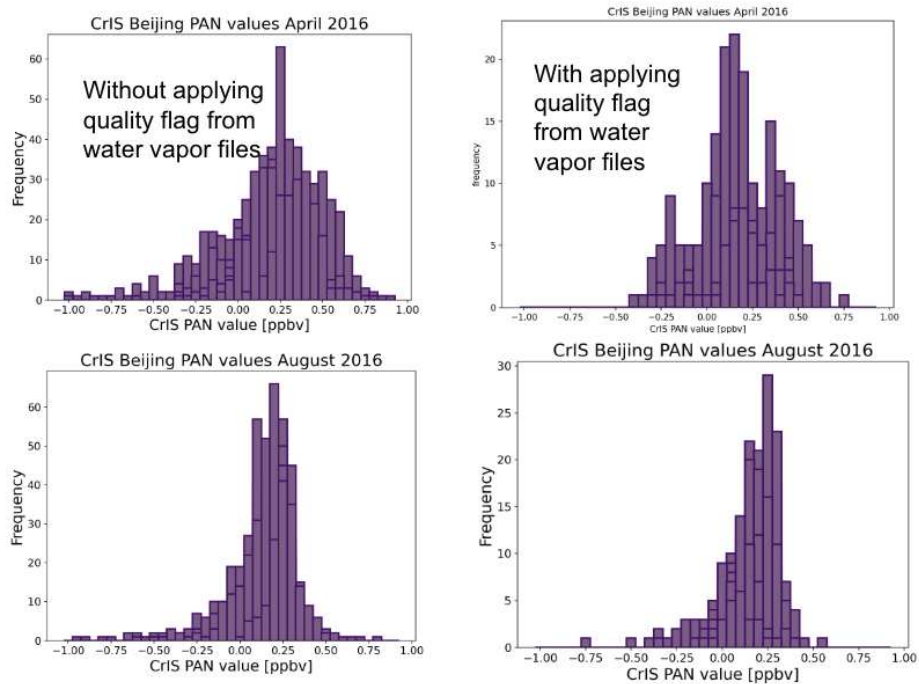


Figure A.4: Example of values of CrIS PANs over the entire CrIS Beijing "box" for April (top) and August (bottom). Left column shows retrieval values without applying the water vapor quality flag. Right column shows retrieval values with applying water vapor quality flag. This cuts negative retrievals significantly in April (top).

A.3 LOS ANGELES

Additional figures for Los Angeles are below.

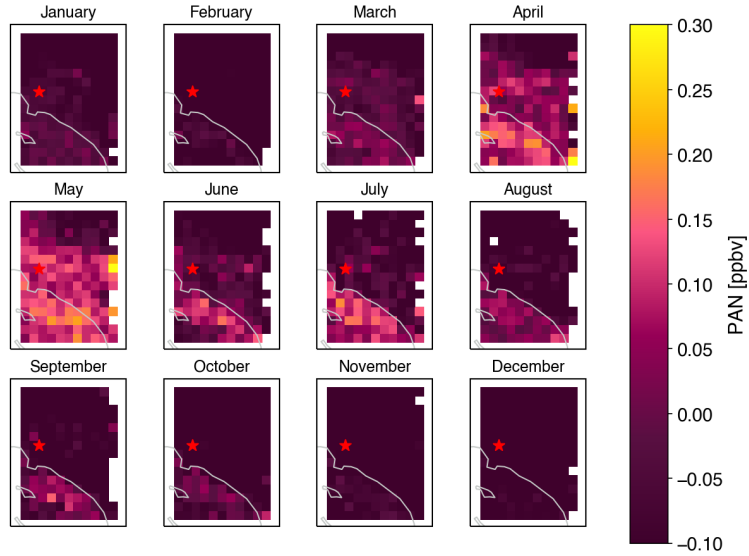


Figure A.5: Average 2016-2021 monthly mean gridded CrIS PANs. City is shown by colored star in middle.

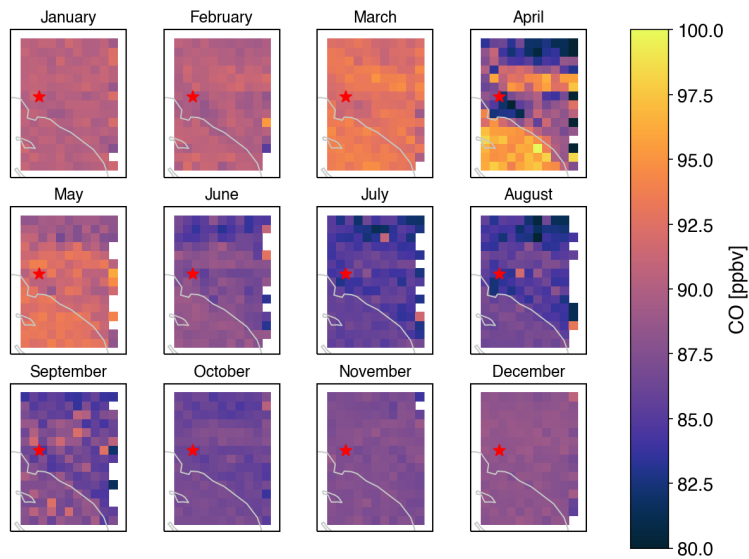


Figure A.6: Average 2016-2021 monthly mean gridded tropospheric CrIS CO. City is shown by colored star in middle.

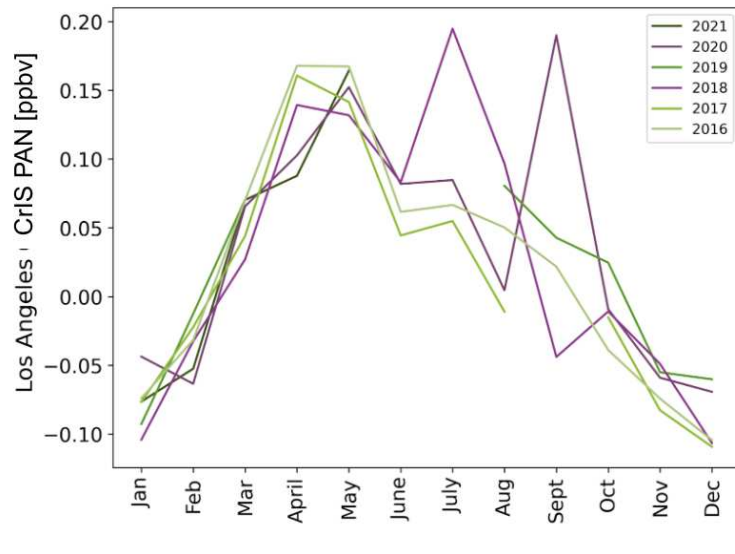


Figure A.7: CrIS PANs over urban LA for each year. Years impacted by fire activity are highlighted in purple (2018 and 2020).

A.4 TOKYO

Additional figures for Tokyo are below.

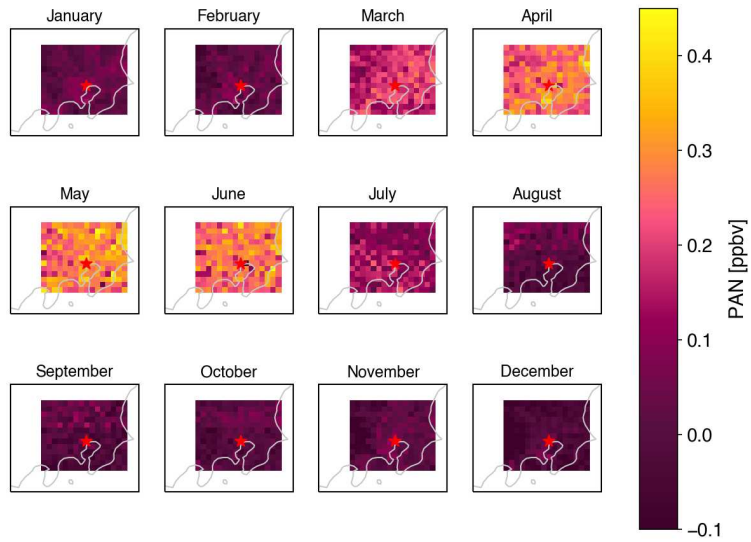


Figure A.8: Average 2016-2021 monthly mean gridded CrIS PANs. City is shown by colored star in middle.

A.5 SÃO PAULO

Additional figures for São Paulo are below.

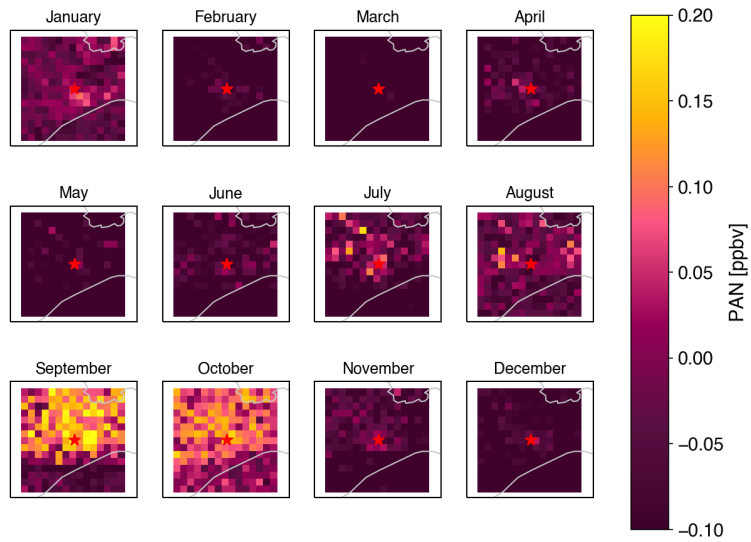


Figure A.9: Average 2016-2021 monthly mean gridded CrIS PANs. City is shown by colored star in middle.

A.6 DELHI

Additional figures for Delhi are below.

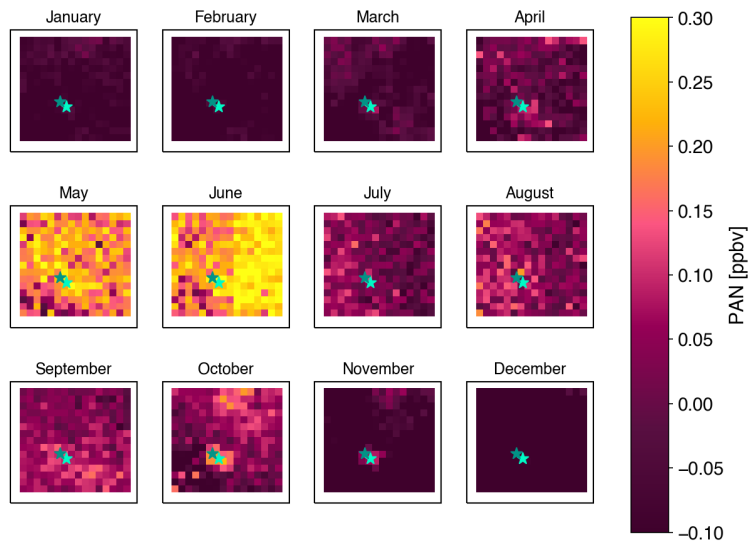


Figure A.10: Average 2016-2021 monthly mean gridded CrIS PANs. Delhi is shown by darker blue star, New Delhi is shown by light blue star.

A.7 MUMBAI

Additional figures for Mumbai are below.

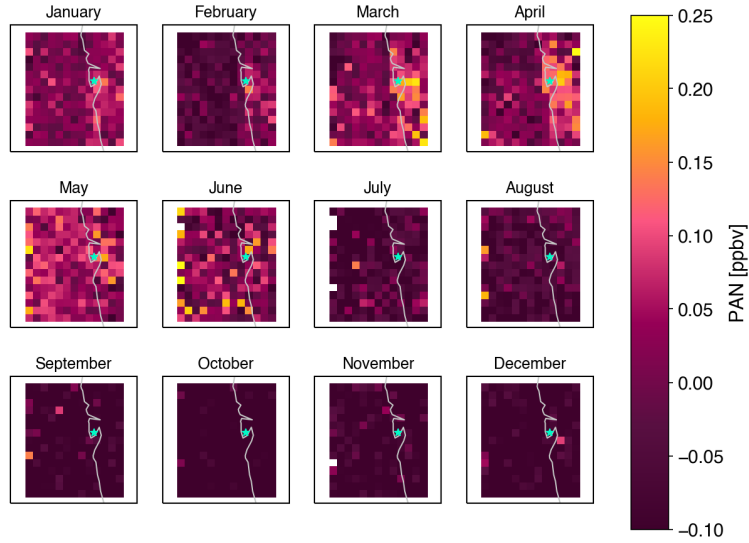


Figure A.11: Average 2016-2021 monthly mean gridded CrIS PANs. City is shown by colored star in middle.

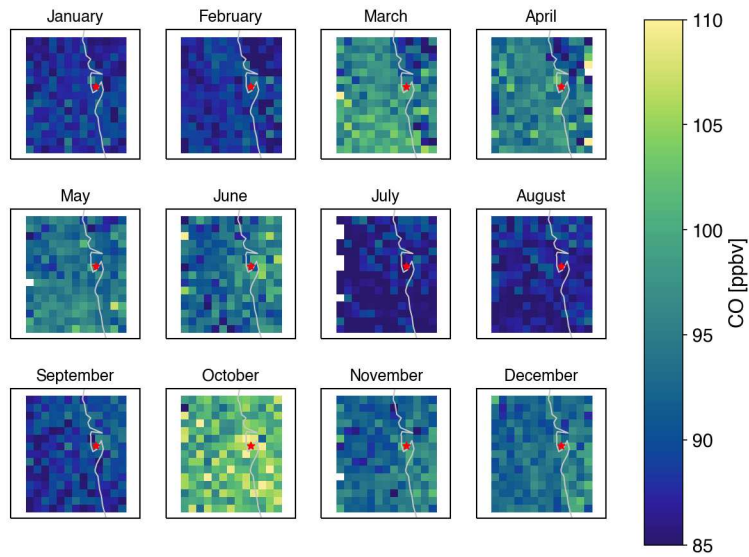


Figure A.12: Average 2016-2021 monthly mean gridded tropospheric CrIS CO. City is shown by colored star in middle.

A.8 LAGOS

Additional figures for Lagos are below.

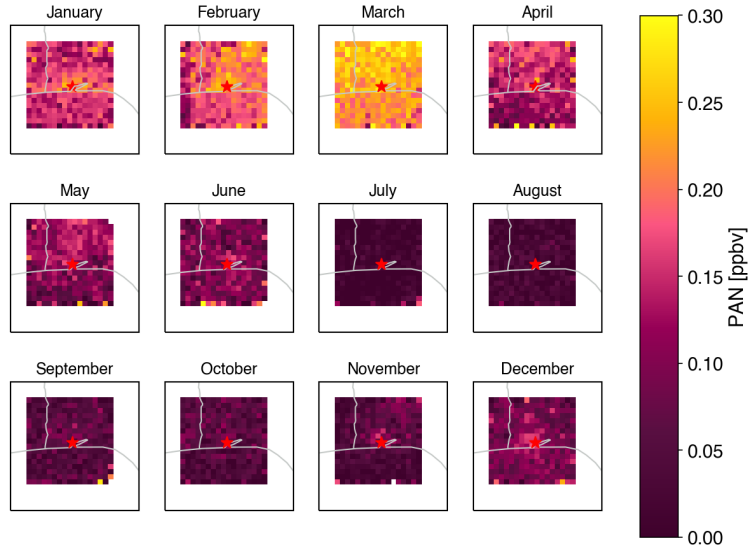


Figure A.13: Average 2016-2021 monthly mean gridded CrIS PANs. City is shown by colored star in middle.

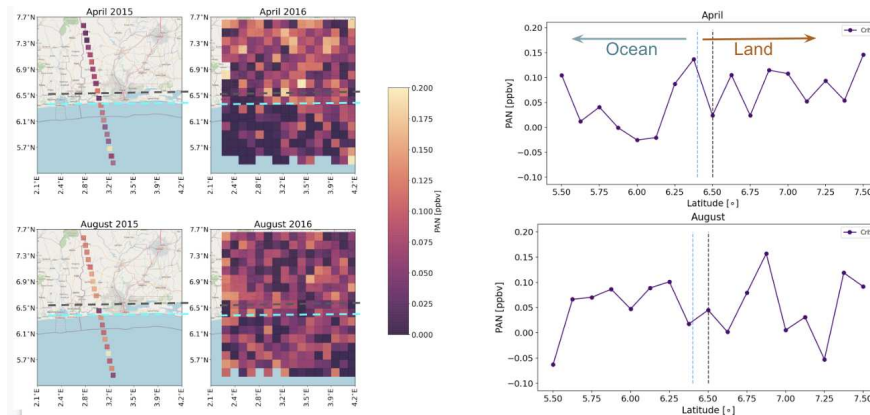


Figure A.14: (left) TES transects over Lagos for April and August 2015. (middle) Monthly mean gridded CrIS PANs for April and August 2016. (right) latitudinal mean of PANs over longitude of city center. Blue dashed line shows latitude of coastline, grey dashed line shows latitude of city center.

A.9 KARACHI

Additional figures for Karachi are below.

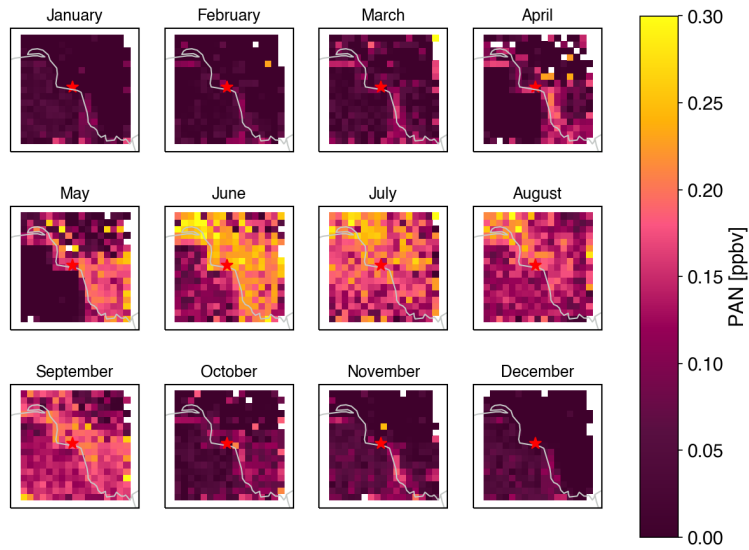


Figure A.15: Average 2016-2021 monthly mean gridded CrIS PANs. City is shown by colored star in middle.

Appendix B

SPATIAL EXTENTS FOR MEGACITIES

The following tables presents the bounds for each megacity. The small box refers to the urban box around the defined urban area of each city. The CrIS box refers to the rough spatial extents of the box used for CrIS megacity dense sampling and the box used to grid CrIS data.

S

| Spatial extents | | | |
|-----------------|-------------------|-------------------------------------|---|
| Megacity Name | city center | CrIS box | small box |
| Mexico City | 19.43°N, 99.13°W | 18°N, 100.9°W, 21°N, 97.1°W | 19.15°N, 98.9°W, 19.65°N, 99.40°W |
| Beijing | 39.90°N, 116.41°E | 38.5°N, 115°E, 41.5°N, 118°E | 39.6°N, 116.09°E, 40.22°N, 116.77°E |
| Los Angeles | 35.05°N, 118.24°W | 33.0°N, 118.5°W, 35.0°N, 117.0°W | 34.1826°N, 118.4937°W, 33.8022°N, 117.9937°W |
| Tokyo | 35.68°N, 139.77°E | 35.0°N, 138.6°E, 36.7°N, 140.8°E | 35.59604°N, 139.6365°E, 35.76494°N, 139.9067°E |

| Spatial extents | | | |
|-----------------|------------------|---|---|
| Megacity Name | city center | CrIS box | small box |
| São Paulo | 23.56°S, 46.64°W | 24.5°S, 47.6°W, 22.507°S, 36.7°W, | 23.689°S, 46.80453°W, 23.39838°S, 46.361575°W |
| Delhi | 28.71°N, 77.10°E | 28.0°N, 76.0°E, 30.0°N, 78.5°E | 28.416498°N, 76.86656°E, 28.853845°N, 77.331748°E |
| Mumbai | 19.08°N, 72.88°E | 18.0°N, 71.0°E, 20.0°N, 73.5°E | 19.020075°N, 72.797566°E, 19.163379°N, 72.964448°E |
| Lagos | 6.52°N, 3.38°E | 5.0°N, 2.0°E, 8.0°N, 5.0°E | 6.451°N, 3.23°E, 6.64°N, 3.41°E |
| Karachi | 24.86°N, 67.01°E | 23.0°N, 65.5°E, 26.0°N, 68.5°E | 24.802739°N, 66.938695°E, 25.033907°N, 67.230026°E |